
**PROPERTIES OF AUSTENITIC
STAINLESS STEELS AND
THEIR WELD METALS**

(Influence of Slight Chemistry Variations)

Brinkman / Garvin

editors

ASTM STP 679

**AMERICAN SOCIETY FOR
TESTING AND MATERIALS**

PROPERTIES OF AUSTENITIC STAINLESS STEELS AND THEIR WELD METALS (Influence of Slight Chemistry Variations)

A symposium
sponsored by ASTM
Committee A-1 on Steel,
Stainless Steel, and
Related Alloys
AMERICAN SOCIETY FOR
TESTING AND MATERIALS
Atlanta, Ga., 14 Nov. 1977

ASTM SPECIAL TECHNICAL PUBLICATION 679
C. R. Brinkman, Oak Ridge National Laboratory
H. W. Garvin, Armco Steel
editors

List price \$13.50
04-679000-02



AMERICAN SOCIETY FOR TESTING AND MATERIALS
1916 Race Street, Philadelphia, Pa. 19103

Copyright © by AMERICAN SOCIETY FOR TESTING AND MATERIALS 1979
Library of Congress Catalog Card Number: 78-74566

NOTE

The Society is not responsible, as a body,
for the statements and opinions
advanced in this publication.

Foreword

This publication, *Properties of Austenitic Stainless Steels and Their Weld Metals (Influence of Slight Chemistry Variations)*, contains papers presented at the Symposium on Influence of Carbon, Nitrogen, and Residual Element Chemistry on the Behavior of Austenitic Stainless Steels Used in Construction which was held in Atlanta, Ga., 14 Nov. 1977. The symposium was sponsored by Committee A-1 on Steel, Stainless Steel, and Related Alloys, American Society for Testing and Materials. C. R. Brinkman, Oak Ridge National Laboratory, and H. W. Garvin, Armco Steel, presided as symposium chairmen and editors of this publication.

Related ASTM Publications

Fatigue Testing of Weldments, STP 648 (1978), \$28.50, 04-648000-30

Intergranular Corrosion of Stainless Alloys, STP 656 (1978), \$24.00,
04-656000-27

Unified Numbering System for Metals and Alloys, DS 56A (1977), 05-
056001-01

A Note of Appreciation to Reviewers

This publication is made possible by the authors and, also, the unheralded efforts of the reviewers. This body of technical experts whose dedication, sacrifice of time and effort, and collective wisdom in reviewing the papers must be acknowledged. The quality level of ASTM publications is a direct function of their respected opinions. On behalf of ASTM we acknowledge with appreciation their contribution.

ASTM Committee on Publications

Editorial Staff

Jane B. Wheeler, *Managing Editor*
Helen M. Hoersch, *Associate Editor*
Ellen J. McGlinchey, *Senior Assistant Editor*
Helen Mahy, *Assistant Editor*

Contents

Introduction	1
Effect of Heat-to-Heat and Melt Practice Variations upon Fatigue Crack Growth in Two Austenitic Steels—L. A. JAMES	3
Discussion	16
Effect of Nitrogen on the Sensitization, Corrosion, and Mechanical Properties of 18Cr-8Ni Stainless Steels—J. J. ECKENROD AND C. W. KOVACH	17
Discussion	40
Effect of Electrode Coating on the High-Temperature Mechanical Properties of AISI 316 Austenitic Weld Metals—R. G. THOMAS	42
Residual Elements Have Significant Effects on the Elevated-Temperature Properties of Austenitic Stainless Steel Welds—	
D. P. EDMONDS, R. T. KING, AND G. M. GOODWIN	56
Discussion	68
Influence of Small Amounts of Niobium on Mechanical and Corrosion Properties of Type 304 Stainless Steel—V. K. SIKKA, A. J. MOORHEAD, AND C. R. BRINKMAN	69
Effect of Small Additions of Niobium on the Welding Behavior of an Austenitic Stainless Steel—A. J. MOORHEAD, V. K. SIKKA, AND R. W. REED	103
Development of Austenitic Stainless Steels with Controlled Residual Nitrogen Content; Application to Nuclear Energy—P. RABBE AND J. HERITIER	123
Discussion	141
Summary	142
Index	145

Introduction

In 1967 the American Society for Testing and Materials published *ASTM STP 418, Effects of Residual Elements on Properties of Austenitic Stainless Steels*. This was followed in 1973 by *ASTM STP 522, Elevated Temperature Properties as Influenced by Nitrogen Additions to Types 304 and 316 Austenitic Stainless Steels*. During the intervening years considerable emphasis had been placed on obtaining mechanical and physical properties of AISI Types 304 and 316 stainless steel and associated weld metals in the nuclear industry in support of worldwide liquid metal fast breeder reactor development for power generation applications. Accordingly, it was thought appropriate by ASTM's Committee A-1 on Steels, Stainless Steel, and Related Alloys to organize another symposium as a follow-on activity to the aforementioned publications in order to present new data and conclusions.

The objective of this effort was to solicit papers that dealt with the influence of carbon, nitrogen, and other residual elements on the heat-to-heat variability of the austenitic stainless steels and their weldments or weld metals used in construction. Specifically, reports or investigations were sought that dealt with the effects of melting practice on chemical variability and differences in fabricability, weldability, and resultant physical and mechanical properties (at both low and high temperature) due to variations in these elements.

The symposium contained seven papers, four of which dealt with the influence of such elements as nitrogen and niobium on primarily elevated-temperature behavior of AISI stainless steel Types 304, 304L, 316, and 316H. The remaining three papers dealt with effects of intentionally added or controlled as well as residual element content on weldability and subsequent mechanical properties of weld metal. It was particularly gratifying to see the increased effort directed toward understanding the beneficial and harmful effects of many of the normally considered residual elements in weld metal, since this was an area recommended in *STP 418* as needing additional attention.

It is expected that the results of this symposium will be of particular interest to the designers, metallurgists, and suppliers of these materials who must concern themselves with heat-to-heat variability and ways of improving properties.

Special acknowledgments and thanks are made to the authors as well as to the reviewers of the papers. Appreciation is also due to A. Van Echo, chairman of ASTM's Committee A-1 on Steels, Stainless Steel, and Related Alloys.

C. R. Brinkman

Oak Ridge National Laboratory, Oak Ridge,
Tenn, 37830; symposium chairman and
coeditor.

L. A. James¹

Effect of Heat-to-Heat and Melt Practice Variations upon Fatigue Crack Growth in Two Austenitic Steels

REFERENCE: James, L. A., "Effect of Heat-to-Heat and Melt Practice Variations upon Fatigue Crack Growth in Two Austenitic Steels," *Properties of Austenitic Stainless Steels and Their Weld Metals (Influence of Slight Chemistry Variations)*, ASTM STP 679, C. R. Brinkman and H. W. Garvin, Eds., American Society for Testing and Materials, 1979, pp. 3-16.

ABSTRACT: Linear-elastic fracture mechanics techniques were employed to characterize the fatigue-crack growth behavior of five heats of annealed Type 304 (including one heat of Type 304L) and three heats of annealed Type 316 (including one heat of Type 316H) stainless steels at 538°C (1000°F). Specimens were tested under conditions of continuous cycling at 40 cpm, or under tensile hold-time (10.8 min) conditions, producing transgranular or intergranular cracking, respectively. In general, no heat-to-heat variations were noted in the crack growth behavior of either alloy or under the different cycling conditions. Also, the three heats of Type 316 represented three different melt practices, and again there was no apparent effect due to melt practice.

KEY WORDS: fatigue-crack growth, fracture mechanics, austenitic stainless steels, heat-to-heat variations, melt practice variations

The austenitic stainless steels are employed extensively in pressure vessel, piping, and other structural applications in both the nuclear and petrochemical industries. Such structural components are often subject to cyclic loading fluctuations in service, and the possibility therefore exists for subcritical extension of cracks or crack-like flaws, should such defects be present with the appropriate size, shape, and location. The analysis techniques of linear-elastic fracture mechanics (LEFM) are particularly useful for estimating the in-service extension of such defects [1].² Crack-

¹Fellow engineer, Westinghouse Hanford Co., Richland, Wash.

²The italic numbers in brackets refer to the list of references appended to this paper.

growth rate data appropriate for use in such analyses can be found in sources such as the *Nuclear Systems Materials Handbook* [2], as well as in a recent review paper [3]. However, due to the large number of material heats and various product forms employed incorporating different melt practices as well as alloy compositional variations, it is necessary to assess the potential for the effect of heat-to-heat or melt practice variations or both upon fatigue-crack growth behavior in these alloys. Hence, the objective of this paper is to examine the effect of heat-to-heat variations upon fatigue-crack growth behavior in annealed Types 304 and 316 stainless steels using LEFM techniques.

Experimental Procedure

Five heats of annealed Type 304 (including one heat of Type 304L), designated as Heats A-E, and three heats of annealed Type 316 (including one heat of Type 316H), designated as Heats F-H, were employed in this study. The heat identifications, chemical compositions, and room temperature mechanical properties are given in Tables 1-3, respectively.

ASTM "compact-type" specimens [see ASTM Test for Plane-Strain Fracture Toughness of Metallic Materials] (E 399-74) having nominal dimensions of width $W = 50.8$ mm (2.00 in.) and thickness $B = 12.7$ mm (0.5 in.) were employed in this study. The specimens were all tested on servo-controlled electrohydraulic machines employing load as the control parameter. "Sawtooth" waveforms (see Ref 4) at 40 cpm (0.667 Hz) were employed throughout the study except for one series of tests, where a "square" waveform (see Ref 4) at 0.083 cpm (0.00138 Hz) incorporating a 10.8-min tensile hold-time was used. The stress ratio ($R = K_{\min}/K_{\max}$) was 0.05 for all tests.

The specimens were tested within an air-circulating furnace. All of the tests reported in the present study were conducted in an air environment at 538°C (1000°). This test temperature was selected because it represents one of the temperatures of interest in fast breeder reactor applications.

Crack lengths were obtained periodically throughout each test using a traveling microscope. Fatigue-crack growth rates (da/dN) were calculated using the "secant method" (Ref 5), and the stress intensity factor (K) was calculated using the relationship of Ref 6. The results were then plotted as $\log(da/dN)$ as a function of $\log(\Delta K)$, where ΔK is the stress intensity factor range, $\Delta K = K_{\max} - K_{\min}$.

Results and Discussion

Before examining the results for different material heats to determine possible heat-to-heat variations, it is appropriate to review the results obtained for a number of specimens from a single heat tested under identical

TABLE 1—Identification of heats investigated.

Heat Identification	Material	Producer	Heat No.	Melt Practice	Condition
Heat A	Type 304	Allegheny Ludlum	55697	air-melt	annealed 1 h @ 1093°C (2000°F), water quenched
Heat B	Type 304L	Eastern Stainless Steel Co.	V50035	unknown	annealed 1/2 h @ 1066°C (1950°F), water quenched
Heat C ^b	Type 304	G. O. Carlson Co.	600414-1A	air-melt	annealed 2 h-23 min @ 1093 to 1121°C (2000 to 2050°F), water quenched
Heat D	Type 304	Allegheny Ludlum	335074	air-melt	^a
Heat E	Type 304	Republic	8043813	unknown	ASTM A-240
Heat F	Type 316	Allegheny Ludlum	65808	air-melt	annealed 1/2 h @ 1093°C (2000°F) water quenched
Heat G ^c	Type 316H	Cameron Iron Works	55320	vacuum-arc remelt	annealed 3/4 h @ 1010°C (1850°F), forced air cooled
Heat H	Type 316	Carpenter Technology	89335	double-vacuum melt	annealed 1 h @ 1066°C (1950°F), water quenched

^aMaterial was annealed, but exact annealing conditions are unknown.

^bFast Flux Test Facility pressure vessel material.

^cFast Flux Test Facility hot-leg piping material.

TABLE 2—Chemical composition (percent by weight).

Heat Identification	C	Mn	P	S	Si	Cr	Ni	Cu	Mo	Pb	Ca
Heat A	0.053	0.87	0.019	0.010	0.49	18.25	9.51	0.21	0.18	<0.001	0.11
Heat B	0.024	1.70	0.020	0.014	0.61	18.00	9.32	0.17	0.44
Heat C	0.064	1.42	0.019	0.015	0.68	18.79	9.48
Heat D	0.05	1.80	0.027	0.022	0.50	18.58	9.13
Heat E	0.063	1.79	0.036	0.007	0.50	18.24	9.10
Heat F	0.060	1.72	0.012	0.007	0.40	17.30	13.30	0.065	2.33	0.0014	...
Heat G	0.075	1.55	0.02	0.018	0.25	16.75	12.80	...	2.30
Heat H	0.05	1.61	0.017	0.010	0.50	16.63	13.63	0.15	2.52

Heat Identification	Sn	Ti	Al	Ta	Co	Fe	B	Ce	Nb	N ₂	Total Rare Earths
Heat A	0.006	<0.01	balance	0.003	0.030	0.001
Heat B	0.15	balance
Heat C	...	0.015	...	0.004	0.077	balance	0.008	0.054	...
Heat D	0.13	balance
Heat E	balance	0.0009	...	0.02	0.033	...
Heat F	0.013	0.003	0.012	...	0.030	balance	0.005	0.0006	...	0.048	0.0010
Heat G	...	<0.02	...	<0.01 ^b	...	balance	<0.01 ^b	0.116	...
Heat H	0.21	balance	0.0006	0.028	...

^aNot determined.^bNiobium + tantalum.

TABLE 3—Room temperature mechanical properties.

Heat Identification	0.2% Yield Strength, MPa (lb./in. ²)	Tensile Strength, MPa (lb./in. ²)	Percent Elongation	Reduction of Area, %	Hardness	Grain Size, ASTM
Heat A	(39 600) 273 MPa	(77 050) 531 MPa	65.0	60.7	$R_B = 73.2$	4 to 5
Heat B	(39 300) 271 MPa	(90 750) 626 MPa	67.4	... ^a	$R_B = 82.5$... ^a
Heat C	(37 000) 255 MPa	(82 000) 565 MPa	57.0	... ^a	$R_B = 85.3$... ^a
Heat D	(39 350) 271 MPa	(77 000) 531 MPa	65.5	72.2	$HB^b = 160$	3 to 4
Heat E	(36 300) 250 MPa	(80 800) 557 MPa	66.0	... ^a	$R_B = 77.8$	3 to 5
Heat F	(44 100) 304 MPa	(82 100) 566 MPa	68.0	63.4	$HB = 163$	4
Heat G	(47 100) 325 MPa	(90 400) 623 MPa	52.0	65.9	$R_B = 83.3$	5 to 6
Heat H	(43 000) 296 MPa	(81 500) 562 MPa	54.3	72.5	$HB = 143$	7 to 8

^aNot determined.
^bHB = Brinell hardness number.

conditions. In this way the scatter inherent in this type of testing can be evaluated, and this will aid in establishing whether possible trends observed in multiheat companions are significant, or whether they fall within normal scatter.

The heat chosen for such a series of tests is Heat A. This particularly well-characterized heat was procured a number of years ago for use as a reference heat for Atomic Energy Commission/Energy Research and Development Administration (AEC/ERDA) programs, and, as a result, over the years numerous studies on various properties have been conducted on this heat by a number of different laboratories around the country. A detailed thermomechanical processing history for this heat is given in Ref 7.

The results for six fatigue-crack growth specimens from Heat A tested under identical conditions are shown in Fig. 1. The results of a least-squares regression analysis for all of the data points (a few of which were not plotted because of overlap) are also given in Fig. 1. Scatter bands drawn through the data at the same slope as the regression line show a total scatter on da/dN of about a factor of 2.75. The coefficient of determination of the regression results is 0.931 (a "perfect" fit would have a coefficient of determination of unity).

The total scatter of 2.75 can be compared with the results of an extensive interlaboratory round-robin test program conducted by ASTM Committee E24.04 [5]. These tests were all conducted on a single well-behaved, well-characterized heat of material at room temperature, and the results showed a total scatter of a factor of 2 to be "normal" for intralaboratory tests, and a factor of 3 to be "normal" for interlaboratory tests. Hence, the factor of 2.75 observed in Fig. 1 is in reasonable agreement with the findings of Ref 5, and, although somewhat higher than the factor of 2 for intralaboratory tests, the difference is attributed to the increased difficulties associated with elevated-temperature testing.

The results for several heats of Type 304 may now be reviewed, keeping in mind the foregoing discussion on scatter associated with a single heat. These data are shown in Fig. 2, along with the results of a regression analysis through the data. One specimen from each of the five heats was analyzed, and only one specimen from Heat A (Specimen 61) was included so as not to bias the results in favor of Heat A. Comparing the results of Figs. 1 and 2, it will be noted that the overall total scatter bands are almost exactly the same. There is, however, slightly more scatter in the results for the five different heats, as evidenced by their slightly lower coefficient of determination. Although not plotted in Fig. 2, the results [8] for ASME SA-351, Grade CF8 (a cast version of Type 304 stainless steel), tested under identical conditions of temperature, frequency, and stress ratio, would have also generally fit within the scatter bands of Fig. 2.

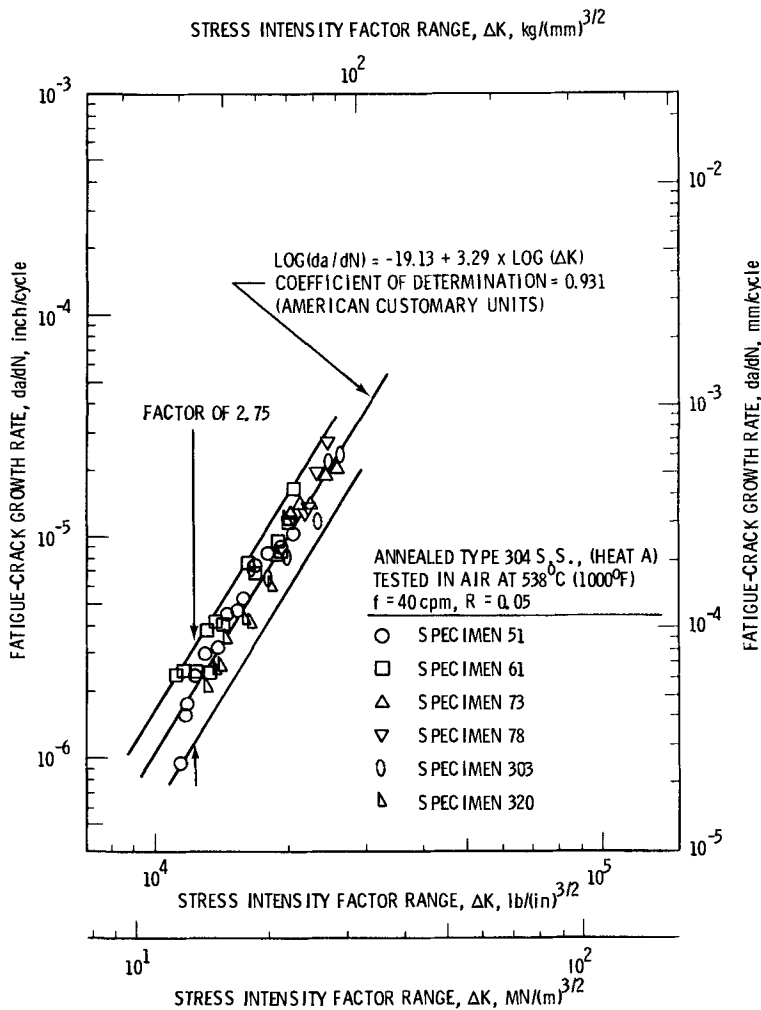


FIG. 1—Fatigue-crack growth behavior of six specimens from a single heat of Type 304 (Heat A) tested under identical conditions at 538° (1000°F).

Hence, it is apparent that there is little or no effect of heat-to-heat variation upon the fatigue-crack propagation behavior of annealed Type 304 as represented by these five heats and as tested under the conditions stated in Fig. 2. This is in agreement with observations of Brinkman and Korth [9] that there was little or no effect of heat-to-heat variations in the low-cycle fatigue (LCF) behavior of four heats of Type 304 tested under continuous cycling (no hold-time) conditions in air at 593°C (1100°F). (Heats A, C, and E of the present study were also included in the study by Brinkman and Korth.)

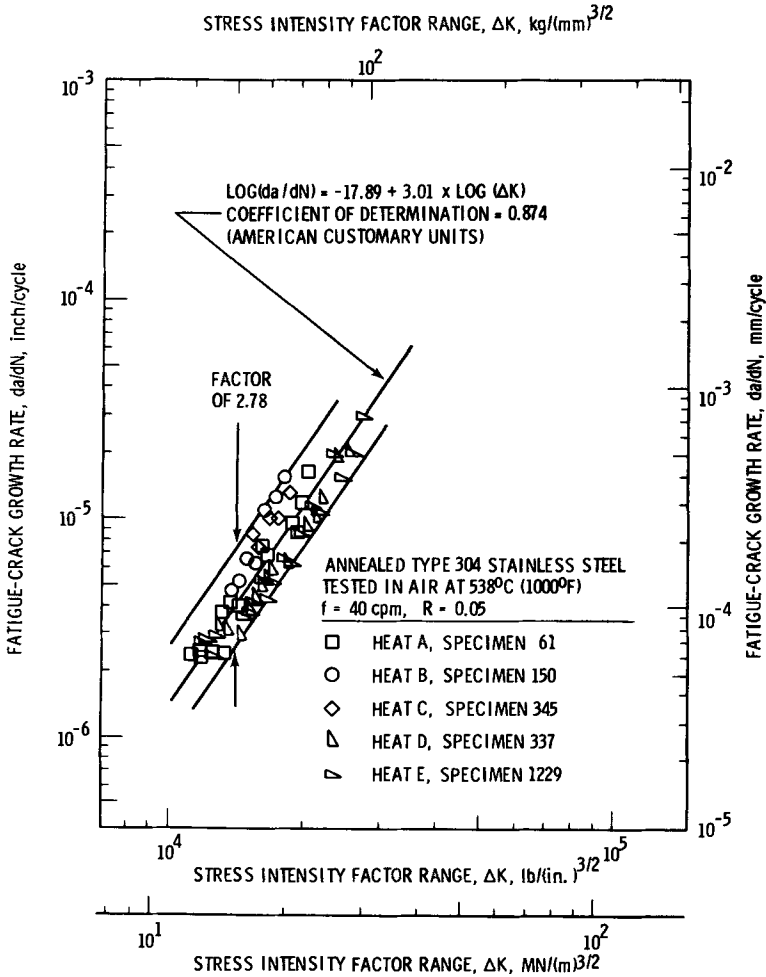


FIG. 2—Fatigue-crack growth behavior of five different heats of Type 304 tested under identical conditions at 538°C (1000°F).

In a similar fashion, the results for three heats of annealed Type 316 (Heats F–H) are shown plotted in Fig. 3. The total scatter band and coefficient of determination are similar to those observed in Fig. 2 for five heats of Type 304, and again there appears to be little or no heat-to-heat variation. Note also that three different melt practices are represented in the results of Fig. 3, and it appears that melt practice may also not be an important variable for this material.

Although they found no apparent heat-to-heat variation in the low-cycle fatigue behavior under continuous cycling conditions, Brinkman and Korth [9] did observe that one heat (Heat E in the present study) did exhibit

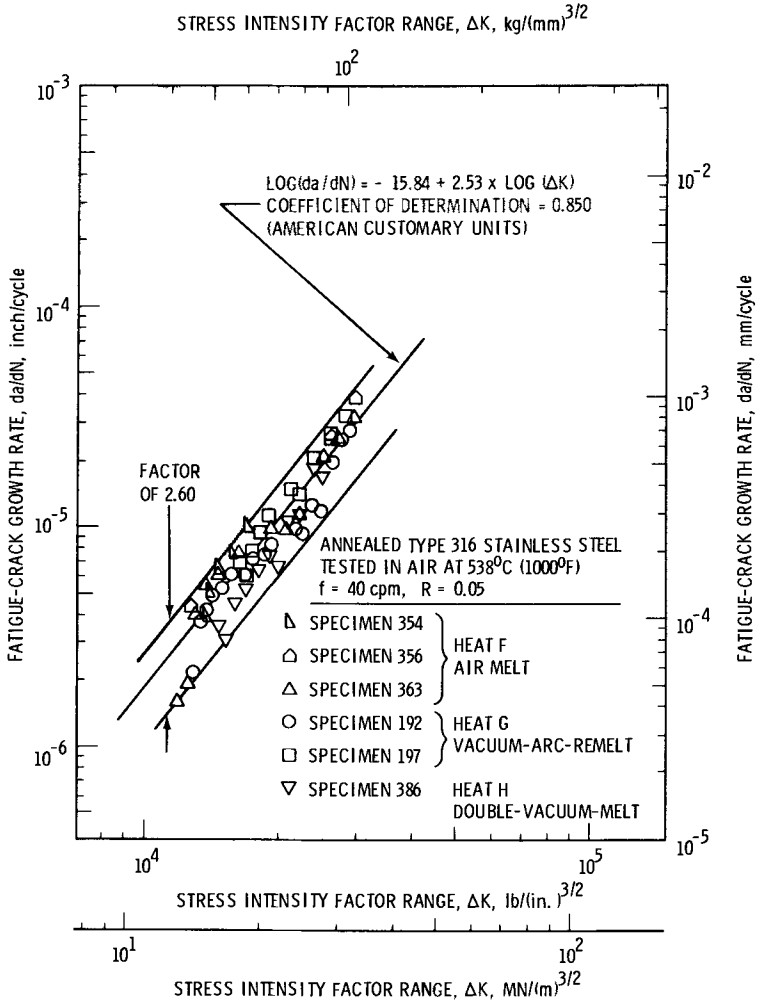


FIG. 3—Fatigue-crack growth behavior of three different heats of Type 316 (representing three different melt practices) tested under identical conditions at 538°F (1000°F).

improved LCF behavior under tensile hold-time conditions. Based on a comparison between unaged and aged specimens of Heat E, they suggested that the improved behavior of this heat was not due to thermomechanical processing history of heat treatment, but rather to subtle differences in chemistry, and results presented elsewhere in this publication now suggest that niobium content played an important role.

Because of the possibility of differences in behavior due to frequency/waveform variations, a second series of tests was conducted on Heats A and E using a “square” waveform at 0.083 cpm (0.00138 Hz) incorporating a 10.8-min hold-time. These results are shown in Fig. 4. Although there

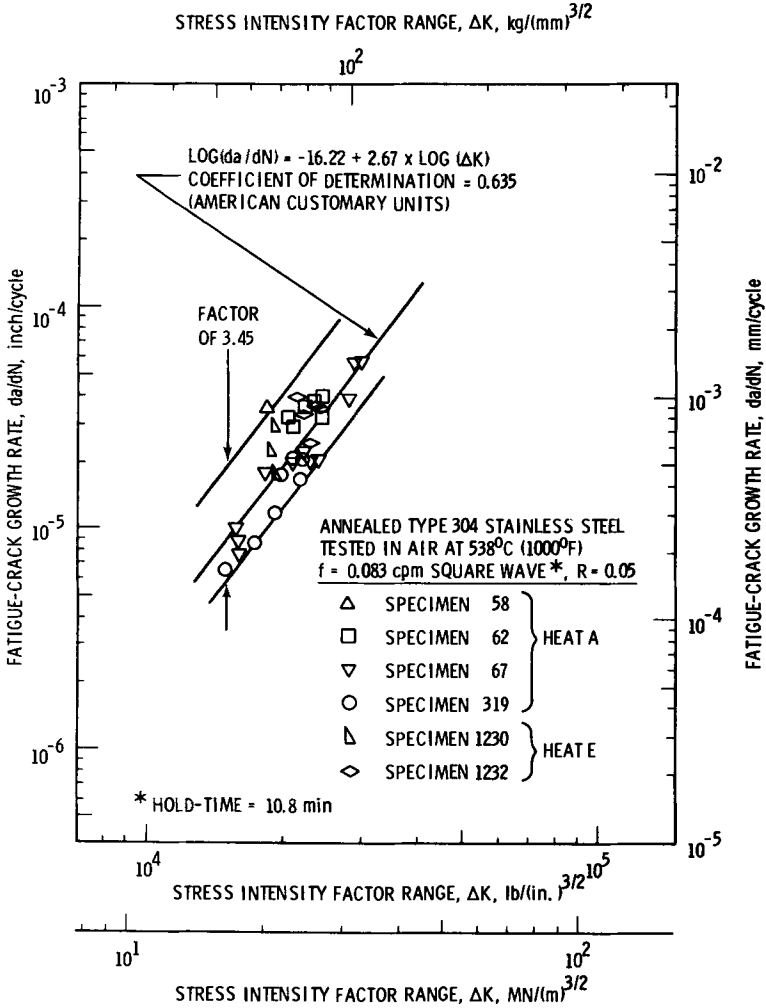


FIG. 4—Fatigue-crack growth behavior of two heats of Type 304 tested under conditions of tensile hold-time cycling at 538°C (1000°F).

is considerably more scatter in these data than in the continuous-cycling results of Figs. 1-3, there is apparently little or no difference in the behavior of the two heats. While the mode of crack extension under continuous-cycling conditions at 40 cpm (0.667 Hz) was predominately transgranular, the mode of cycling under hold-time conditions at 0.083 cpm (0.00138 Hz) was predominately intergranular (see Ref 4 for typical photo-micrographs of the crack-tip areas). The effect of cyclic frequency upon the fatigue-crack growth behavior of annealed Type 304 (Heat A in the present study) in an air environment at 538°C (1000°F) was studied in Ref 10 over the range

0.083 to 4000 cpm (0.00138 to 66.7 Hz), and in general crack growth rates increased with decreasing frequency. A sawtooth loading waveform was employed in all of the tests in Ref 10, and the mode of crack extension was predominately transgranular at all frequencies. The three lowest frequencies studied in Ref 10 [4, 0.4, and 0.083 cpm (0.0667, 0.00667, and 0.00138 Hz)] were repeated in Ref 4 (again on Heat A), but this time using a square wave with a tensile hold-time. As with the continuous-cycling tests of Ref 10, the hold-time tests of Ref 4 exhibited predominately transgranular crack extension except at 0.083 cpm (0.00138 Hz), where the mode was predominately intergranular. However, in spite of the change in crack extension mode, the crack-growth rates for the 0.083-cpm (0.00138 Hz) sawtooth waveform and the 0.083-cpm (0.00138 Hz) square wave with tensile hold were approximately the same; that is, waveform effects were minimal under these conditions. Similar conclusions regarding the two waveforms were made at the two higher frequencies, 4 and 0.4 cpm (0.0667 and 0.00667 Hz).

It will be noted that Figure 4 exhibits greater data scatter than Figs. 1-3. This is thought to be at least partially due to the following reasons: (1) the increased difficulty in experimentally determining the lengths of the intergranular cracks, (2) the inherent nature of intergranular cracking itself (for example, differing rates as the crack grows along grains of differing sizes), and (3) differing degrees of thermal aging between different specimens at the same ΔK levels leading perhaps to small differences in crack growth rates. (Because of the long test times involved at this low frequency, one specimen at a given level of ΔK may have had only a few dozen hours of exposure at the test temperature while another specimen at the same ΔK could have been exposed for thousands of hours. See Ref 11 for details.) Brinkman and Korth observed a scatter of approximately 2 in the LCF fatigue life of five heats tested under conditions of continuous cycling, and a similar factor for those hold-time conditions where sufficient data exist to evaluate scatter. On the other hand, the improvement in LCF fatigue lives between Heats A and E under hold-time conditions was approximately a factor of 3, suggesting that the improvement was real and not due to scatter. On the other hand, although the scatter in Fig. 4 is relatively large (for the aforementioned reasons), the results suggest little or no difference in the crack growth behavior of Heats A and E under the hold-time conditions tested, or at the very least any differences are within the normal data scatter.

The foregoing observation of little or no difference between Heats A and E under hold-time conditions is not necessarily contradictory to the findings of Brinkman and Korth. First of all, LCF crack-growth tests are characterized by a large stress gradient in the vicinity of the crack tip and generally elastic stress fields throughout the bulk of the specimen. Smooth-specimen LCF tests, on the other hand, are characterized by homo-

geneous, but generally plastic, stress fields. In addition, three different phases (crack initiation, crack propagation, and the final fracture) are included in the LCF results of Ref 9, while LEFM crack growth tests characterize only one phase—crack propagation. Hence, although different, the observations are not necessarily contradictory.

In an earlier study [11], the author investigated the effect of thermal aging upon crack growth behavior of Types 304 and 316 stainless steels. In general, long-time thermal aging produced a small improvement in the elevated temperature fatigue-crack growth behavior, and this was attributed to the precipitation of various carbides and intermetallics. However, specimens of thermally aged Type 304L (Heat B in the present study) exhibited slightly less improvement in the crack growth behavior than did specimens of Type 304 with approximately twice the carbon content (Heat A in the present study). The implication is that this is due to the lower carbon content (and hence fewer precipitated carbides). However, the differences were very slight and almost within the range of experimental scatter.

Finally, although there appears to be little or no heat-to-heat variation in the fatigue-crack growth behavior of these two austenitic stainless steels, such variations have been noted in the behavior of other alloy systems. For example, Logsdon [12] has noted considerable differences in behavior between several heats (representing several different melt practices) of precipitation heat-treated Inconel X-750, and smaller differences may also be present in the behavior of precipitation heat-treated Inconel 718 [13]. Also, minor differences in the crack growth behavior of a quenched-and-tempered ferritic steel have been attributed to different melt practices [14].

Summary and Conclusions

Five heats of annealed Type 304 (including one heat of Type 304L) and three heats of annealed Type 316 (including one heat of Type 316H) were tested in an air environment at 538°C (1000°F). Little or no effect of heat-to-heat variation upon fatigue-crack growth behavior was noted under either continuous cycling conditions at 40 cpm (0.667 Hz), or under tensile hold-time conditions at 0.083 cpm (0.00138 Hz). In addition, the three heats of Type 316 represented three different melt practices: air-melt, vacuum-arc remelt, and double-vacuum melt. Again, there was no apparent effect of melt practice upon the fatigue-crack growth behavior.

Although the observations in the present study for cycling under tensile hold-time conditions are different than previous observations on smooth-specimen LCF tests, they are not necessarily contradictory. This may be due to the inherent difference between LCF tests, which incorporate crack initiation, crack propagation, and the final fracture, and LEFM tests, which characterize only the crack propagation phase.

In any event, the results of the present study span relatively large variations in carbon, nitrogen, and residual element compositions, as well as several different melt practices, and, although a large number of heats were not studied, it appears that heat-to-heat variations in the crack growth behavior of these two steels is minimal.

Acknowledgments

This paper is based on work performed under U.S. Department of Energy's contract EY-76-C-14-2170 with the Westinghouse Hanford Co., a subsidiary of the Westinghouse Electric Corp.

References

- [1] James, L. A., *Journal of Pressure Vessel Technology, Transactions, American Society of Mechanical Engineers*, Vol. 96, No. 4, 1974, pp. 273-278.
- [2] Part I, Group 1, Section 2, Property Code 2431, *Nuclear Systems Materials Handbook*, Vol. 1, Report TID-26666, Westinghouse Hanford Co., Richland, Wash., 1976.
- [3] James, L. A., *Atomic Energy Review*, Vol. 14, No. 1, 1976, pp. 37-86.
- [4] James, L. A., *Nuclear Technology*, Vol. 16, No. 3, 1972, pp. 521-530.
- [5] Clark, W. G. and Hudak, S. J., *Journal of Testing and Evaluation*, Vol. 3, No. 6, pp. 454-476.
- [6] Srawley, J. E., *International Journal of Fracture*, Vol. 12, No. 3, 1976, pp. 475-476.
- [7] Claudson, T. T., "Fabrication History of Alloys Used in the Irradiation Effects on Reactor Structural Materials Program," Report BNWL-CC-236, Battelle-Northwest, Richland, Wash., 1965.
- [8] James, L. A., *Nuclear Technology*, Vol. 26, No. 1, 1975, pp. 46-53.
- [9] Brinkman, C. R. and Korth, G. E., *Journal of Nuclear Materials*, Vol. 48, No. 3, 1973, pp. 293-306.
- [10] James, L. A. in *Stress Analysis and Growth of Cracks, ASTM STP 513*, American Society for Testing and Materials, 1972, pp. 218-229.
- [11] James, L. A., *Metallurgical Transactions*, Vol. 5, No. 4, 1974, pp. 831-838.
- [12] Logsdon, W. A., "Cryogenic Fracture Mechanics Properties of Several Manufacturing Process/Heat Treatment Combinations of Inconel X750," presented at International Cryogenic Materials Conference, Queen's University, Kingston, Ont., Canada, July 1975 (available as Scientific Paper 75-1E7-CRYMT-P1, Westinghouse Research Laboratories, Pittsburgh, Pa.).
- [13] Logsdon, W. A., Kossowsky, R., and Wells, J. M., "The Influence of Processing and Heat Treatment on the Cryogenic Fracture Mechanics Properties of Inconel 718," presented at the International Cryogenic Materials Conference, University of Colorado, Boulder, Colo., Aug. 1977 (available as Scientific Paper 77-9E7-CRYMT-P2, Westinghouse Research Laboratories, Pittsburgh, Pa.).
- [14] Wilson, A. D., "Fatigue Crack Propagation in A533B Steels," ASME Paper 76-WA/PVP-6, American Society of Mechanical Engineers, 1976.

DISCUSSION

*Raymond Cockroft*¹ (*written discussion*)—It was mentioned that crack propagation rates were similar for transgranular and intergranular propagation. This infers a minimal effect of grain size. Were there any grain size differences in the materials examined?

Heat G (vacuum-arc remelted—Cameron Iron Works) could easily have had a niobium content of as high as 0.02 (quoted as not determined), as Cameron austenitic stainless heats frequently have niobium at 0.015 to 0.02.

L. A. James (*author's closure*)—Grain sizes were determined for most of the heats tested (see Table 3). This subject has been studied previously, and the results have been reviewed in Ref 3. In general, it was concluded that grain size had little or no influence upon crack growth behavior in austenitic stainless steels.

¹Cameron Iron Works.

J. J. Eckenrod¹ and C. W. Kovach¹

Effect of Nitrogen on the Sensitization, Corrosion, and Mechanical Properties of 18Cr-8Ni Stainless Steels

REFERENCE: Eckenrod, J. J. and Kovach, C. W., "Effect of Nitrogen on the Sensitization, Corrosion, and Mechanical Properties of 18Cr-8Ni Stainless Steels," *Properties of Austenitic Stainless Steels and Their Weld Metals (Influence of Slight Chemistry Variations)*, ASTM STP 679, C. R. Brinkman and H. W. Garvin, Eds., American Society for Testing and Materials, 1979, pp. 17-41.

ABSTRACT: Modern stainless steel melting and refining techniques now make it possible to consider nitrogen as an economic and controllable alloying addition to 18Cr-8Ni austenitic stainless steels. Studies show that nitrogen additions of up to about 0.16 percent to 18Cr-8Ni steels can result in some improved properties. Nitrogen is a strong strengthening element to 18Cr-8Ni steels and will increase yield strength by about 5.5 to 6.2 MPa (800 to 900 lb/in.²) for each 0.01 percent nitrogen. Isothermal time-temperature sensitization (TTS) diagrams developed for 18Cr-8Ni steels containing about 0.05 percent carbon and up to 0.25 percent nitrogen indicate that nitrogen at least up to 0.16 percent retards intergranular carbide precipitation. Corrosion tests on isothermally sensitized or welded specimens show reduced corrosion rates with nitrogen additions consistent with the TTS data. For low-carbon 18Cr-8Ni steels, nitrogen additions up to 0.15 percent have no apparent effect on the normally excellent sensitization resistance of these steels, at least as measured by corrosion tests on isothermally heated or welded specimens. Nitrogen additions were also found to improve pitting and crevice corrosion resistance as evaluated in anodic polarization or chloride pitting/crevice corrosion tests. Stress corrosion evaluations were conducted on solution-annealed material using constrained U-bend specimens in both severe and milder environments. The results indicated that nitrogen content up to 0.16 percent did not significantly affect stress corrosion cracking susceptibility, but 0.25 percent nitrogen appeared detrimental in some environments.

KEY WORDS: austenitic stainless steels, nitrogen, sensitizing, intergranular corrosion, electrochemical corrosion, pitting, stress corrosion, mechanical properties, welding

¹Supervisor and Technical director, Stainless Steels, respectively, Colt Industries, Crucible Research Center, P.O. Box 88, Pittsburgh, Penna. 15230.

Chromium-nickel (18-8) austenitic stainless steels are widely used in a variety of product forms for architectural, consumer, and industrial applications because of their excellent corrosion and oxidation resistance, ambient and elevated temperature strength, toughness, fabricability, and esthetic appearance. Improving one, several, or all of the aforementioned properties would likely further expand the usage of these steels provided the changes had no adverse effects on other properties. The strengths of austenitic stainless steels can be increased by alloying with nitrogen. The use of nitrogen as an alloying element in stainless steels is widely practiced as evidenced by AISI Types 201 and 202, which utilize nitrogen to substitute for a portion of the nickel. Other low or nickel-free nitrogen-bearing stainless steels have been developed; however, only recently has there been much interest in nitrogen-alloyed conventional 18Cr-8Ni stainless. As with the low or nickel-free steels, nitrogen can be added to the 18-8 types, which results in materials having some improved and useful engineering properties [1].² More importantly, modern stainless steel melting and refining techniques now make it possible to consider nitrogen as an economic and controllable alloy addition to 18-8 stainless steels. Therefore, a program was carried out to specifically explore the effects of nitrogen on the sensitization characteristics, corrosion resistance, weldability, and mechanical properties of the 18-8 stainless steels.

Materials

Table 1 lists the chemical compositions of the laboratory and commercial materials used for this study. The laboratory heats were processed to produce fully solution-annealed steel ranging from 0.8 to 6.4 mm thick and having an ASTM 5 to 6 grain size. Unless specified otherwise, the commercial materials used were in the mill-annealed condition.

Results and Discussion

Sensitization Characteristics

The literature and some studies conducted at our laboratory indicated that the chromium-nickel-manganese-nitrogen (Cr-Ni-Mn-N) stainless steels are more resistant to sensitization than are Cr-Ni steels having similar carbon contents [2,3]. Further studies suggested that the nitrogen additions were responsible for the improved sensitization resistance rather than the higher manganese or lower nickel in the Cr-Ni-Mn-N steels. These results suggest that similarly improved sensitization resistance might be attained by nitrogen additions to conventional 18Cr-8Ni steels.

²The italic numbers in brackets refer to the list of references appended to this paper.

TABLE 1—Chemical composition of laboratory and commercial 18Cr-8Ni stainless steels.

Heat No.	Melt Practice	Weight Percent										
		C	Mn	P	S	Si	Ni	Cr	Mo	Cu	N ₂	
3A37	laboratory AIM ^a	0.018	1.82	0.023	0.013	0.59	8.66	18.64	0.23	0.09	0.029	
1H32	laboratory AIM	0.028	1.71	0.028	0.013	0.36	8.50	18.26	0.36	0.21	0.036	
1E98	laboratory AIM	0.057	1.59	0.035	0.013	0.46	8.51	18.92	0.35	0.21	0.036	
3754	laboratory VIM ^b	0.053	1.77	0.031	0.008	0.41	8.49	19.27	0.36	0.16	0.040	
3751	laboratory VIM	0.044	1.77	0.034	0.007	0.46	8.59	18.87	0.36	0.16	0.110	
3A39	laboratory AIM	0.044	1.83	0.023	0.006	0.55	8.43	18.20	0.23	0.08	0.130	
3752	laboratory VIM	0.043	1.78	0.028	0.008	0.41	8.63	18.80	0.38	0.16	0.160	
3753A	laboratory VIM	0.046	1.37	0.030	0.008	0.40	8.89	18.90	0.38	0.17	0.250	
1E97	laboratory AIM	0.092	1.63	0.035	0.012	0.46	8.55	18.98	0.35	0.22	0.042	
3753	laboratory VIM	0.090	1.74	0.030	0.007	0.39	8.59	18.80	0.36	0.16	0.240	
632409	commercial AOD ^c	0.068	1.71	0.037	0.006	0.44	8.59	18.45	0.44	0.27	0.071	
650951	commercial AOD	0.068	1.67	0.032	0.005	0.18	8.53	18.97	0.36	0.24	0.130	
650874	commercial AOD	0.031	1.62	0.035	0.012	0.54	9.41	18.14	0.44	0.27	0.028	
632459	commercial AOD	0.023	1.69	0.033	0.008	0.48	9.62	18.35	0.47	0.29	0.016	
650946	commercial AOD	0.023	1.62	0.034	0.008	0.62	9.53	18.31	0.36	0.27	0.067	
650936	commercial AOD	0.018	1.66	0.038	0.009	0.50	9.65	18.51	0.42	0.26	0.092	
161154	commercial AOD	0.020	1.66	0.022	0.018	0.59	8.36	18.50	0.34	0.24	0.150	

^aAIM = air induction melt.^bVIM = vacuum induction melt.^cAOD = argon-oxygen decarburization.

To study the effect of nitrogen on sensitization resistance, solution-annealed 25.4-mm-square, 0.8-mm-thick specimens of laboratory-produced 18Cr-8Ni steel containing 0.028 to 0.092 percent carbon and 0.036 to 0.25 percent nitrogen were heated for up to 24 h in a molten lead bath maintained at temperatures within the normal sensitization range (480 to 870°C) for austenitic stainless steels. The lead bath provided maximum heating rates and the specimens were water quenched on removal from the bath. To eliminate any possible edge effects, each specimen was cut diagonally for metallographic mounting. Metallographic polishing and etching technique variations were minimized by mounting all the specimens of one alloy that had been heated for various times at the same temperature in the same mount and electrically connecting them. After the usual metallographic preparation, each mount was etched electrolytically for 1 min in 10 percent ammonium persulfate solution using a 6-V potential and rated for degree of sensitization using the chart shown in Fig. 1. Time-temperature sensitization (TTS) diagrams were constructed by plotting the sensitization ratings for each alloy as a function of time and temperature and enclosing areas having equivalent ratings.

TTS diagrams developed for 0.028, 0.053, and 0.092 percent carbon-residual nitrogen (0.04 percent) 18Cr-8Ni steels are compared in Fig. 2 and clearly illustrate the effect of carbon on sensitization characteristics.

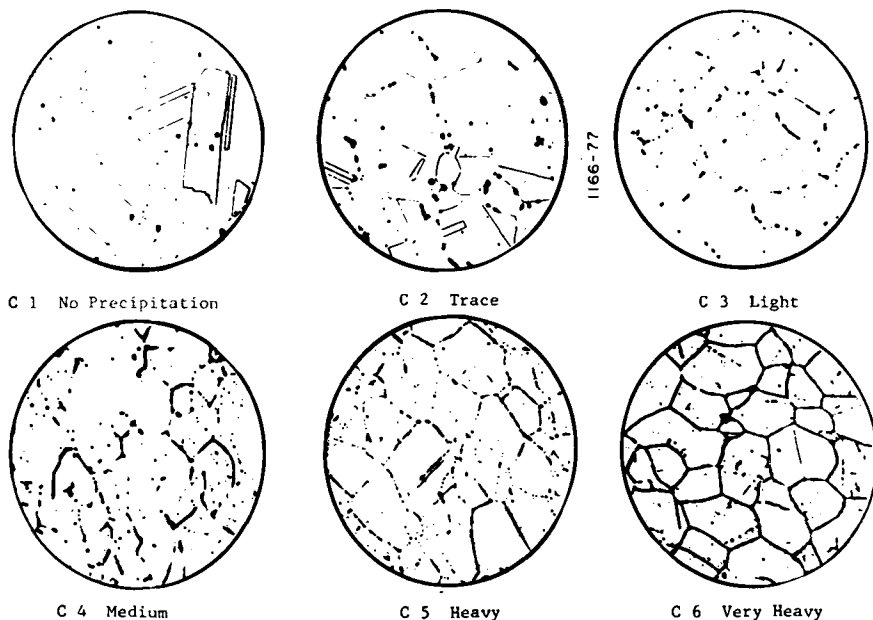


FIG. 1—Carbide precipitation chart for austenitic stainless steel. Ammonium persulfate electrolytic etch ($\times 500$).

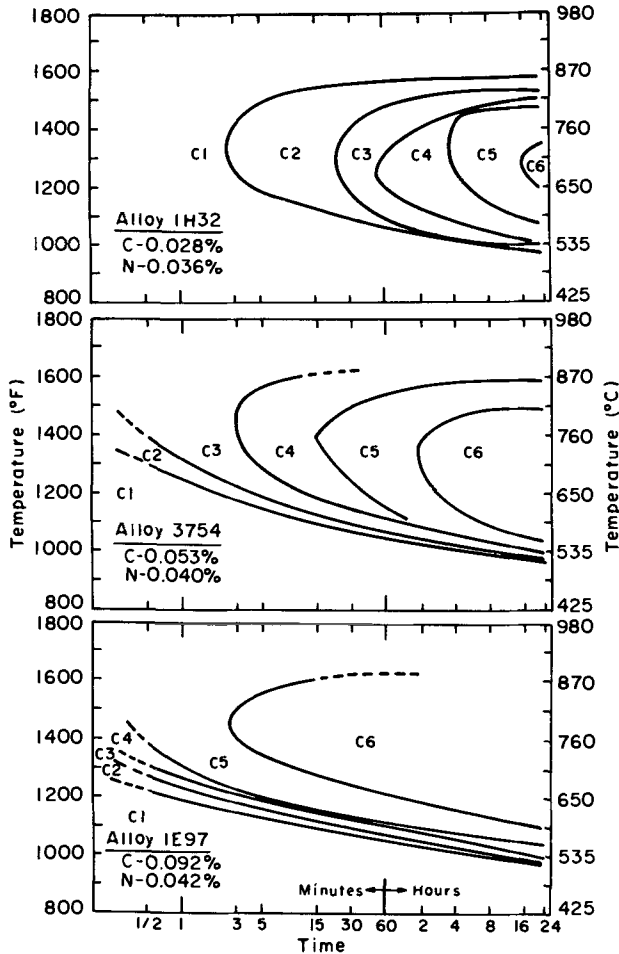


FIG. 2—TTS diagrams for 18Cr-8Ni stainless steel containing 0.028 and 0.092 percent carbon.

Carbide precipitation, that is, sensitization, occurs quite rapidly in 0.053 and 0.092 percent carbon steels; in fact, the materials appeared to sensitize somewhat during the rapid heating provided by the lead bath. Time to develop a given degree of sensitization becomes increasingly shorter with increasing carbon content. Increased carbon content also seemed to increase the temperature at which maximum sensitization occurs in these steels.

Fig. 3 compares the TTS diagrams developed for 18Cr-8Ni steels containing 0.04 to 0.25 percent nitrogen and shows that nitrogen additions retard carbide precipitation. For at least up to 0.16 percent nitrogen, the time required to reach a given carbide rating increases with increasing nitrogen.

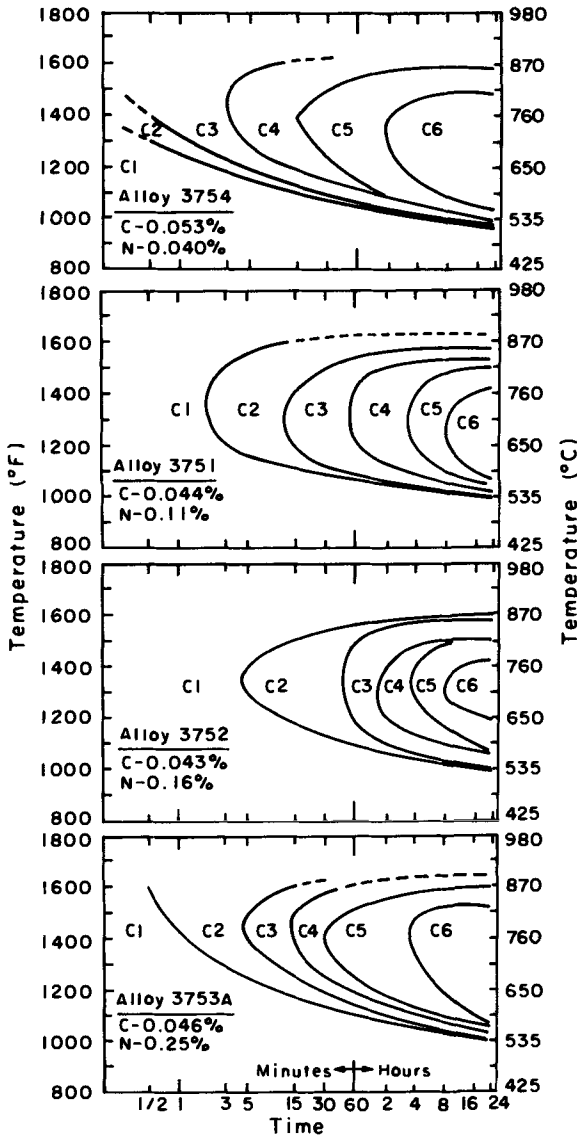


FIG. 3—TTS diagrams for 18Cr-8Ni stainless steel containing nitrogen.

The 0.25 percent nitrogen steel was somewhat less resistant to sensitization than the 0.16 percent steel but still more resistant than the residual nitrogen (0.04 percent) steel. Nitrogen appears to have a similar retardation effect in higher carbon steels as well (Fig. 4). This sensitization retardation effect is important because the amount of carbon that can be tolerated in a steel

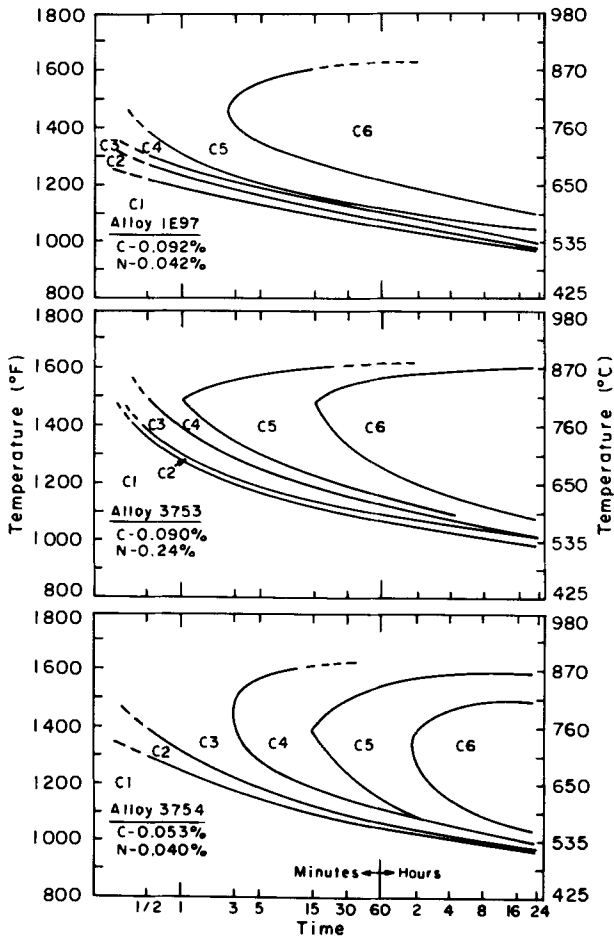


FIG. 4—TTS diagrams for 0.09 percent carbon 18Cr-8Ni steels containing 0.042 and 0.24 percent nitrogen.

without causing harmful sensitization is increased. For example, Fig. 5 shows that the TTS diagrams developed for the 0.11 and 0.16 percent nitrogen steels are similar to the one developed for a much lower carbon (0.028 percent) steel, indicating that a 0.04/0.05 percent carbon 18-8 steel with nitrogen additions should have sensitization resistance similar to that of much lower carbon steel. Fig. 6 allows determination of the optimum nitrogen content of a 0.05 percent carbon steel that will provide sensitization resistance similar to that of lower carbon grades. The times required to produce a given carbide rating in the low-carbon steel are represented by the dashed horizontal lines. The intersection of these lines with the solid maximum isocarbide lines gives the nitrogen content required to achieve a

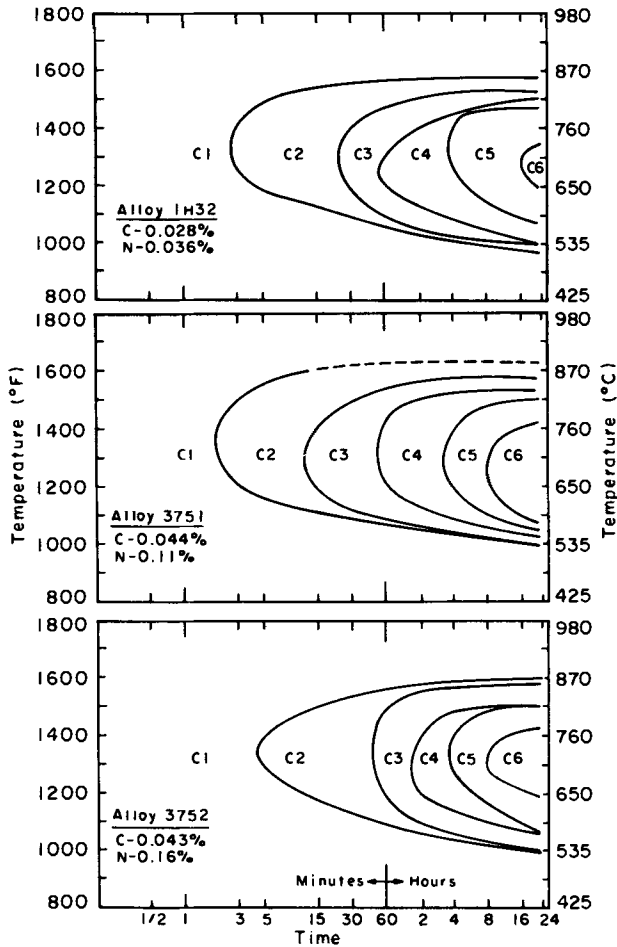


FIG. 5—TTS diagrams comparing nitrogen-bearing steels with a low-carbon 18-8 steel.

rating equivalent to the lower-carbon steel for the same exposure time and is about 0.11 to 0.13 percent nitrogen.

This retardation effect of nitrogen should also be evident in conventional tests used to evaluate stainless steels for sensitization. Huey tests were conducted on solution-annealed water-quenched specimens after sensitizing for 1 h at 675°C. The resulting carbide ratings were consistent with those predicted from the TTS curves. Fig. 7 shows that increasing nitrogen content results in lower corrosion rates, and the corrosion rate of the 0.16 percent nitrogen steel was similar to that of the lower-carbon one. The highest nitrogen (0.24 percent) heat displayed a slightly higher corrosion rate than did the lower-carbon one but was still considerably less than the

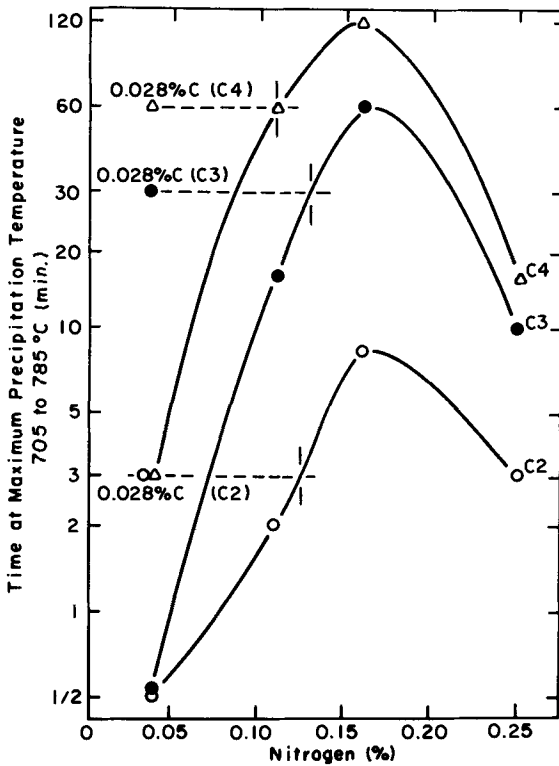


FIG. 6—Nitrogen content required in 0.05 percent carbon 18Cr-8Ni to achieve 0.028 percent carbon sensitization resistance.

0.05 percent carbon steel. Thus, the Huey test results confirm the TTS data and again show the beneficial retardation effect of nitrogen on intergranular carbide precipitation and resulting intergranular corrosion, at least for the sensitizing heat treatments normally used for 18Cr-8Ni steels.

The chief advantage of any reduced tendency toward carbide precipitation is in relation to weld heat-affected-zone (HAZ) sensitization. To evaluate the effect of nitrogen, solution-annealed 2.8- and 3.6-mm-thick specimens were gas-tungsten arc welded using welding conditions to achieve full penetration. After cooling to room temperature, a cross-weld was made using similar conditions to produce a double HAZ at the intersection of the welds. The welded specimens were evaluated using the 10 percent nitric-3 percent hydrofluoric acid weld decay test. Fig. 8 shows that for both thicknesses the low-carbon steel displayed a trace of attack in the weld HAZ whereas the residual nitrogen 0.05 percent carbon HAZ was severely attacked. The HAZ's of the steels containing 0.11 and 0.16 percent nitrogen were much more resistant to attack than was the residual nitrogen steel

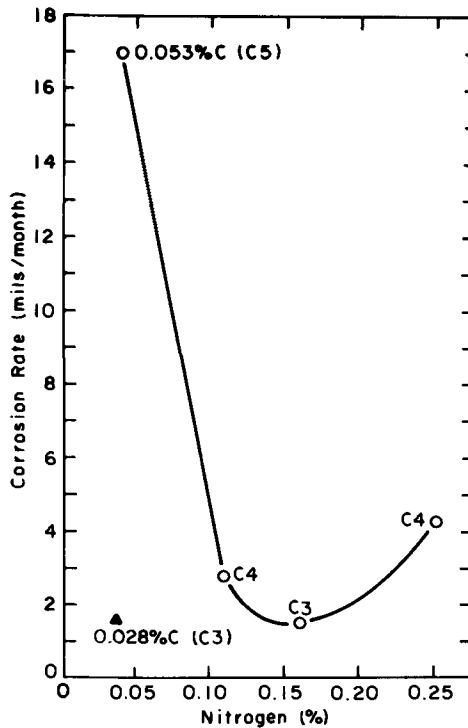


FIG. 7—Huey test results on sensitized (675°C —1 h) 18Cr-8Ni containing nitrogen. The sensitization ratings are given at the data points.

and performed at least as well as the low-carbon one. The HAZ of the 0.25 percent nitrogen steel was attacked to a greater degree than the 0.16 percent nitrogen and low-carbon steels but less so than the residual nitrogen steel. The results of these tests again confirm the isothermal data provided by the TTS diagrams and the Huey test results in that nitrogen does indeed retard intergranular carbide precipitation kinetics and the resulting intergranular corrosion, at least within the exposure times and temperatures required for evaluation tests and those encountered in the weld HAZ.

Material from several commercial heats of 18Cr-8Ni stainless steels containing nitrogen variations (0.016 to 0.15 percent) was also evaluated for sensitization characteristics to support the results obtained with the low-carbon laboratory heats. The carbide ratings and Huey and Streicher test results on both mill-annealed and sensitized (675°C for 1 h) specimens are listed in Table 2. As shown, none of the mill-annealed commercial materials displayed any evidence of sensitization, and corrosion rates in the Huey and Streicher tests were low. After sensitizing heat treatments, all of the steels displayed C2/C3 carbide ratings and again corrosion rates

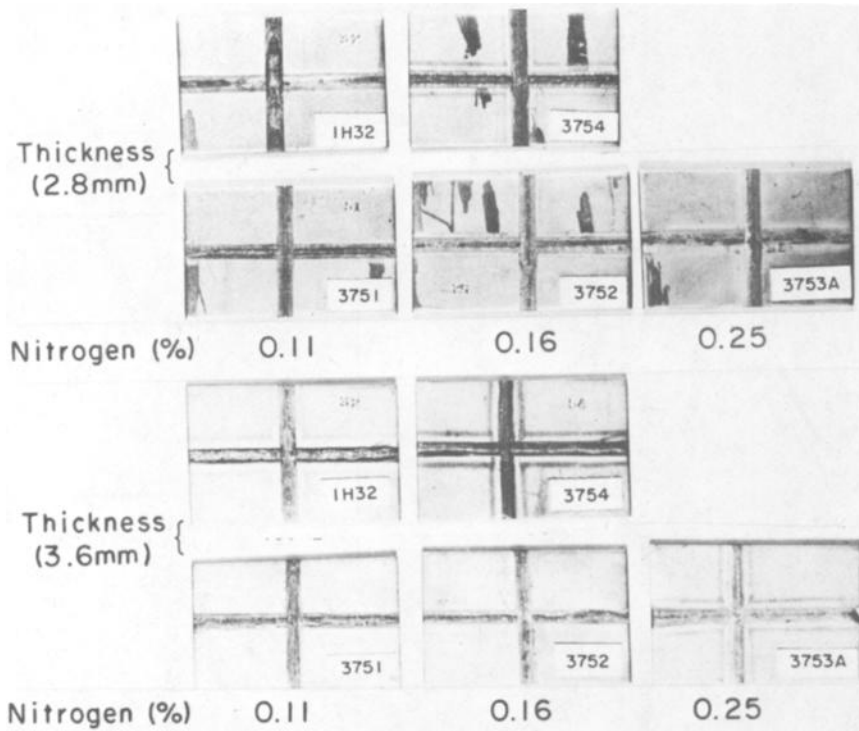


FIG. 8—Results of weld decay tests on 18Cr-8Ni stainless steels.

in Huey and Streicher tests were low. Thus, it appears that, at least up to 0.15 percent, nitrogen has little effect on the normally excellent sensitization resistance of the low-carbon 18Cr-8Ni stainless steels. Weld decay test results, Fig. 9, again indicated that nitrogen additions up to 0.15 percent do not adversely affect the HAZ sensitization resistance of these steels to the degree that it can be detected by this test.

Corrosion Resistance

General and Pitting Corrosion

The anodic polarization characteristics of solution-annealed nitrogen-containing 18Cr-8Ni steels were determined at room temperature in hydrogen-saturated 0.5 molar sodium chloride in a one normal sulfuric acid solution. The resulting anodic polarization curves are shown in Fig. 10 and indicate that increasing the nitrogen in these steels results in improved corrosion resistance as characterized by lower critical and passive currents, a wider passive region, and higher pitting potentials.

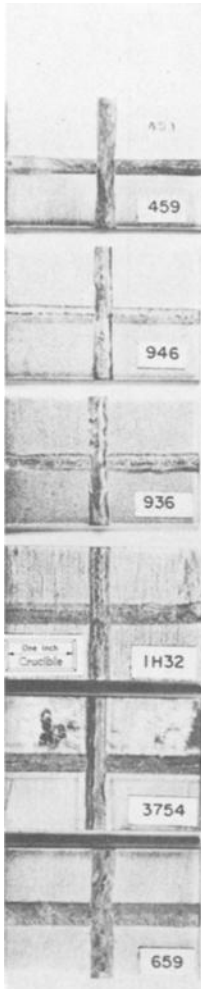
TABLE 2—Carbide ratings and Huey and Streicher test results on low-carbon 18Cr-8Ni stainless steels containing nitrogen.

Heat No.	%C	%N	Corrosion Rate, mils/month					
			Carbide Rating		Huey Test		Streicher Test	
			Annealed	Sensitized	Annealed	Sensitized	Annealed	Sensitized
632459	0.023	0.016	C1	C2-C3	0.61	0.66	1.62	1.42
650946	0.023	0.067	C1	C3	0.69 ^a	0.70 ^a	1.58	1.49
650936	0.018	0.092	C1	C3	0.63 ^a	0.75 ^a	1.64	1.42
161154	0.020	0.15	C1	C2	0.68	0.83

Annealed—1065°C, 15-min water quenched.

Sensitized—annealed + 675°C—1 h water quench.

^aTest malfunction during fourth test period; therefore rates given are only for three periods. Values are likely comparable to the other data because corrosion rates were decreasing.



Heat No.	Carbon (%)	Nitrogen (%)	Thickness (mm)
632459	0.023	0.016	3.9
650946	0.023	0.067	3.7
650936	0.018	0.092	3.7
1H32	0.028	0.036	6.4
3754	0.053	0.040	6.4
161154	0.020	0.15	6.0

FIG. 9—Weld decay test results on 18Cr-8Ni containing 0.016 to 0.15 percent nitrogen.

The anodic polarization data suggest that increased nitrogen should improve the pitting and crevice corrosion resistance of 18Cr-8Ni steels; therefore the laboratory-produced steels were evaluated in several chloride-type pitting and crevice corrosion tests. A ferric chloride immersion test revealed that the pitting frequency and weight loss decreases with increasing nitrogen, Fig. 11, again suggesting improved pitting resistance. Similar benefits for increased nitrogen were observed in a pitting test that utilizes increased sodium chloride concentrations, Fig. 12. Rubber band crevice corrosion tests in similar solutions also indicated improved resistance for the higher nitrogen steel, particularly at low chloride concentrations,

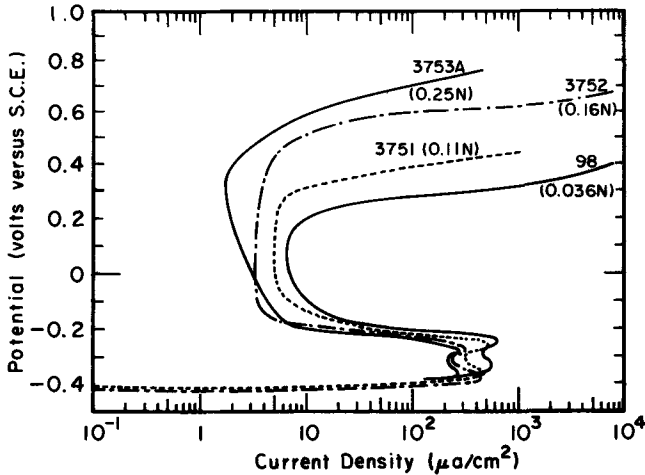


FIG. 10—Anodic polarization curves for 18Cr-8Ni stainless steels containing nitrogen. Hydrogen deaerated one normal H_2SO_4 plus 0.5 M NaCl at room temperature.

Fig. 13. In a more aggressive environment—the nitric-hydrofluoric acid solution normally used to evaluate weld decay—nitrogen had little or no effect on the corrosion rate, which ranged from 9.8 to 11.4 mg/cm²/h.

Stress Corrosion

The early literature on stress corrosion shows various effects for nitrogen which appear to depend on the structural stability of the base composition in regard to delta-ferrite, and initial purity in regard to carbon and nitrogen content. Base compositions of nominally 18Cr-8Ni steels that contain some delta-ferrite in the solution-annealed condition have reasonable stress corrosion resistance in magnesium chloride ($MgCl_2$), but susceptibility increases with nitrogen additions, which also eliminate delta-ferrite [4-6]. This behavior is consistent with many observations that delta-ferrite will improve resistance to stress corrosion. Studies on delta-ferrite-free alloys have generally used base compositions containing 12 or 20 percent nickel having high initial purity with regard to carbon and nitrogen. With nitrogen of about 0.016 percent, or less, good resistance to boiling $MgCl_2$ has been demonstrated [5, 7-11], but susceptibility increases rapidly as nitrogen reaches about 0.03 percent. Failure times continue to be very rapid for nitrogen exceeding 0.03 and up to at least 0.25 percent and so the data do not allow an interpretation as to whether the higher nitrogen produces a further detriment. A nitrogen level of about 0.03 percent is the typical residual level for electric furnace melted steels. This then is probably the reason that studies on commercial purity levels have often shown no effect for nitrogen [6, 12, 13].

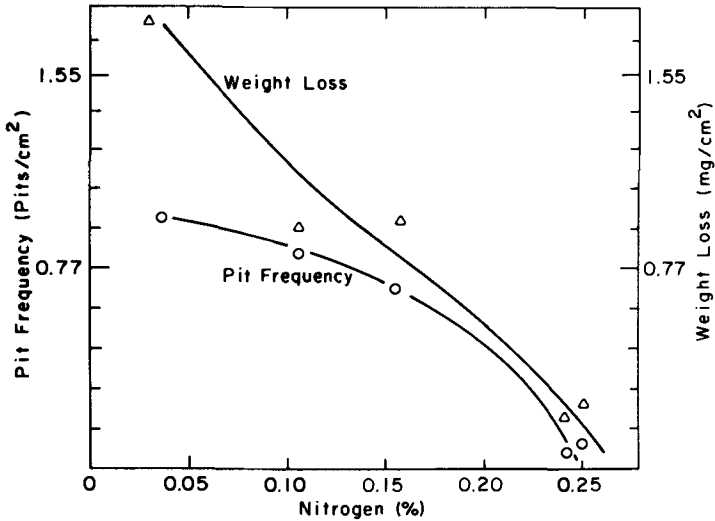


FIG. 11—Pitting resistance of 18Cr-8Ni in acidified 10 percent ferric chloride solution.

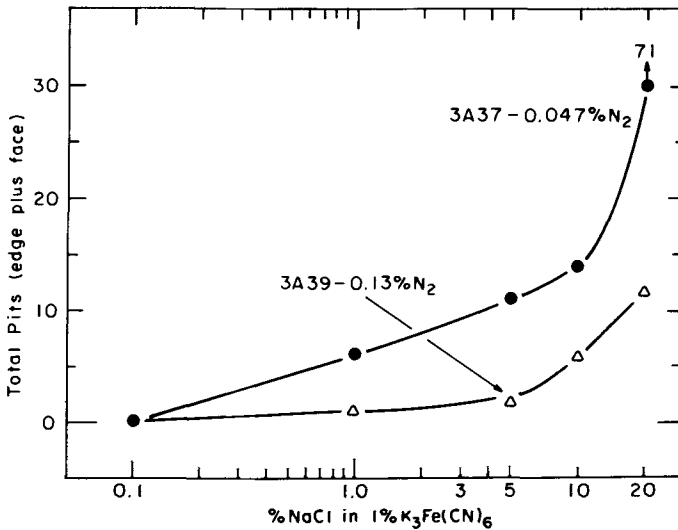


FIG. 12—Pitting test results on 18Cr-8Ni steels containing 0.047 and 0.13 percent nitrogen; 1 h exposure at room temperature.

Using U-bend specimens, it has been shown that nitrogen increasing over the range of 0.033 to 0.205 percent will increase stress corrosion susceptibility in boiling 42 percent MgCl₂ [14,15]. This susceptibility increase was produced by a rapidly increased time of crack initiation with nitrogen, but the rate of propagation decreased with higher nitrogen.

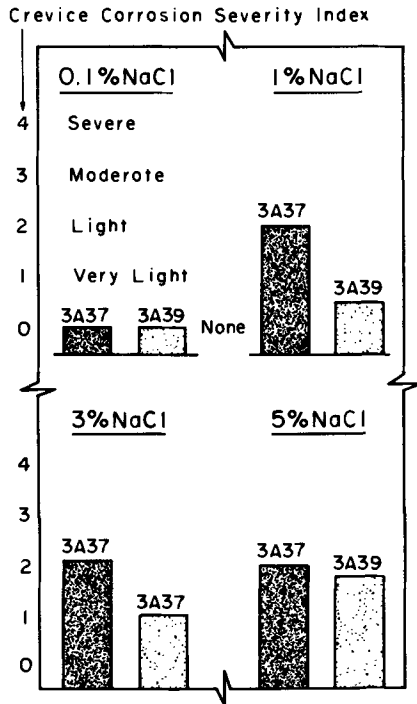


FIG. 13—Rubber band crevice corrosion test results on 0.047 (3A37) and 0.13 percent (3A39) nitrogen 18Cr-8Ni steels: 16 h at 39°C in the indicated sodium chloride concentration. Solutions also contained 1 percent potassium ferricyanide.

This suggests that the higher stresses produced by higher nitrogen in the U-bend specimens may have been the primary accelerating factor rather than nitrogen content per se. Also, aging treatments at 154 and 200°C prior to testing had a strong accelerating effect on crack initiation, indicating that the nitrogen effect may not occur in lower-temperature environments where the aging reaction might not take place.

Our experiments were designed to evaluate the effect of nitrogen in several halide environments in addition to (154°C) $MgCl_2$, some of which were intended to simulate the most commonly encountered industrial environment of sodium chloride containing cooling water. Temperatures were also maintained near 100°C, which is the maximum temperature encountered on the waterside of most water-cooled process equipment.

Experiments were conducted in boiling (154°C) $MgCl_2$ to compare the performance of U-bend, 90-deg bend, and bent-beam specimens. The specimens were prepared from 0.8-mm-thick solution-annealed material. In this test, all specimens developed cracks within 1 h of exposure regardless of nitrogen content. After 1 h exposure, cross sections were taken

from the edge, $\frac{1}{4}$ width, and mid-width of 90-deg bend specimens and evaluated for crack frequency and crack depth with the results shown in Fig. 14. Cracking frequency and maximum crack depth increased with nitrogen content but the average crack depth decreased. This trend became most pronounced as the nitrogen exceeded 0.16 percent. These results are in general agreement with the work of Eckel et al [14,15], showing increased initiation and lower crack propagation rates with nitrogen additions to 18Cr-8Ni stainless.

Two-point loaded bent-beam specimens were also evaluated in boiling (154°C) $MgCl_2$ at a calculated outer fiber stress level of 415 MPa (60000 lb/in.²), assuming elastic behavior. This stress was above the elastic limit of the solution-annealed specimens. This was intended to produce a more uniform stress level in the plastic region for various alloy nitrogen contents than would be achieved with U-bend specimens. With this test procedure and an exposure time of 237 h, no cracking occurred with nitrogen content over the range of 0.034 to 0.16 percent. Cracking occurred only at the 0.25 percent nitrogen level.

Stress corrosion evaluations using constrained 0.8-mm-thick U-bend specimens were conducted in six different aqueous chloride environments at temperatures of about 100°C. These environments were: 20 percent $MgCl_2$ boiling at 107°C, 20 percent $CaCl_2$ boiling at 107°C, 20 percent $NaCl$ boiling at 102°C, 10 percent $NaCl$ boiling at 100°C, synthetic sea-water boiling at 100°C, and 5 percent $NaCl$ -acetic acid (pH-3.0) cycling from wet to dry in 2 min over a temperature range of 60 to 110°C. The boiling environments were run continuously with condensers and no maintenance of the solution, whereas in the cyclic test the solution was replaced every 24 h to maintain a reasonably constant pH. The specimens

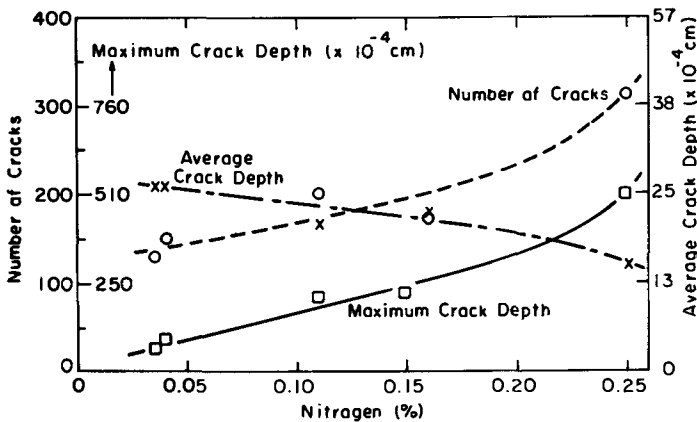


FIG. 14—Influence of nitrogen on the stress corrosion cracking of unrestrained 90-deg bends of 18Cr-8Ni steel in boiling (154°C) $MgCl_2$ solution.

were removed and examined periodically throughout the test period to make observations on the time of crack initiation, time of complete crack penetration, and on crack frequency and site of crack initiation. The alloys evaluated consisted of two 18Cr-8Ni heats containing normal residual nitrogen of 0.036 percent (Heats 1H32 and 3754) and three heats with nitrogen contents of 0.11, 0.16, and 0.25 percent (Heats 3751, 3752 and 3753).

The times for crack initiation or complete penetration did not display any consistent pattern within either the low- or high-nitrogen alloy groups and so the test data are summarized by group (A—residual nitrogen; B—0.11 to 0.25 percent nitrogen) in Fig. 15. In 20 percent $MgCl_2$, cracks initiated within 2 h in all alloys and the failure times were also essentially the same at between 30 and 36 h. In 20 percent $CaCl_2$, initiation times were also essentially the same but the failure times ranged to considerably longer times of 102 h for the high-nitrogen group compared with 62 h for the low-nitrogen group. Stress cracking did not occur in any of the boiling

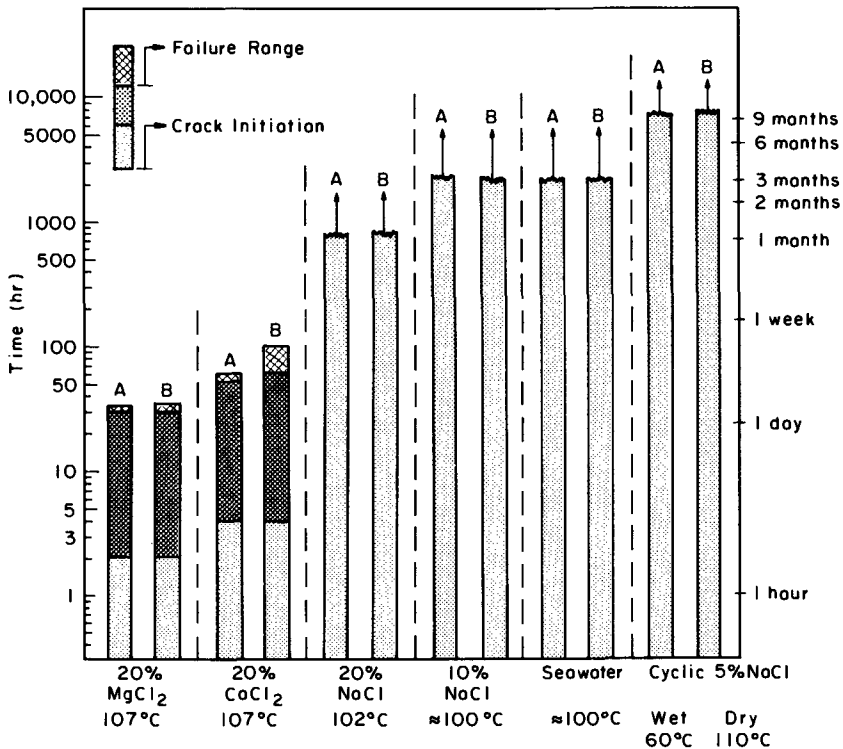


FIG. 15—Results of constrained U-bend stress-corrosion cracking tests on (a) residual nitrogen and (b) 0.11 to 0.25 percent nitrogen 18Cr-8Ni steels.

sodium chloride or seawater environments over test periods ranging from 1 to 3 months even though pitting had initiated. In the cyclic 5 percent sodium chloride environment, although pitting had initiated in 4½ months in the 0.25 percent nitrogen alloy and in all alloys after 6 months, cracking initiated after 9 months in all alloys regardless of nitrogen content and the initiation sites were prior corrosion pits. The stress corrosion cracks were the transgranular branching type, but the depth of penetration was considerably less at 0.11 and 0.16 percent nitrogen than at lower or higher nitrogen content as shown in Fig. 16.

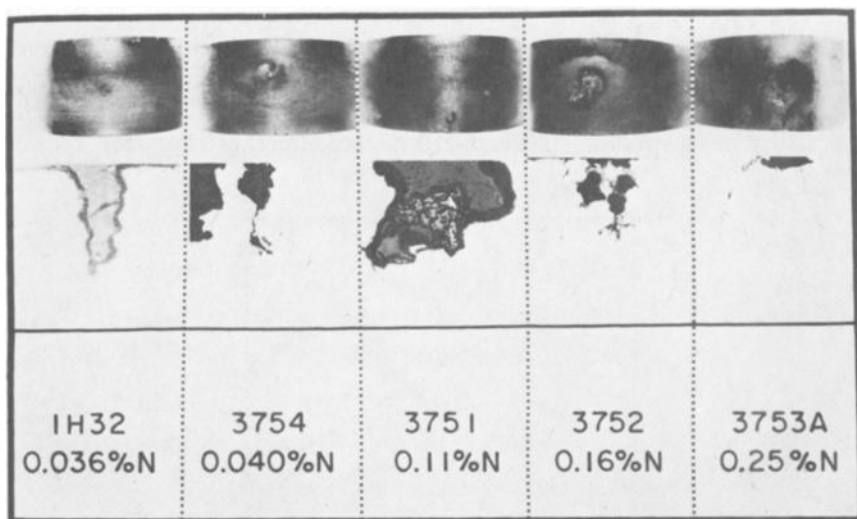


FIG. 16—Pitting and stress-corrosion crack penetration in U-bend specimens after nine months' exposure in an acidified sodium chloride wet-dry cyclic test (reduced 50 percent).

The overall results of these tests indicate that nitrogen over the range of 0.11 to 0.25 percent does not appear to accelerate the time of crack initiation. Nitrogen may also retard the rate of crack propagation over the 0.11 to 0.16 percent nitrogen range on the basis of longer failure times in 20 percent CaCl_2 and less crack penetration in cyclic 5 percent sodium chloride. These results are in conflict with some of the previously described studies showing a detrimental effect of high nitrogen in boiling (154°C) MgCl_2 using U-bend specimens. Since MgCl_2 and U-bend specimens were used in the present study, it appears that the lower temperatures employed may account for the results. It is possible that the aging reaction at 154 and 200°C demonstrated by Eckel et al, to accelerate cracking in high nitrogen alloys, is not operative or sufficiently retarded at 100°C so as to avoid a detriment from nitrogen of this temperature.

Mechanical Properties

Fig. 17 shows the effect of nitrogen on the strength and ductility of 18Cr-8Ni stainless steels. Although the data are plotted as a function of carbon plus nitrogen, the carbon range was relatively narrow in most cases so that the curves primarily reflect changes in nitrogen content. As is well known, nitrogen is demonstrated to be an effective austenite strengthener and, from the slopes of the curves, a 5.5 to 6.2-MPa (800 to 900 psi) increase in strength can be expected for each 0.01 percent nitrogen. The strengthening effects are similar for both yield and tensile strength, suggesting that nitrogen in relatively stable austenite has little or no effect on work-hardening rate. In fact, the measured work-hardening rates for both the laboratory and commercial steels were low and within a very narrow range, 0.27 to 0.31. Note that for a given carbon plus nitrogen content the commercial heats have slightly higher yield strengths than the laboratory heats, probably reflecting the more effective laboratory anneal.

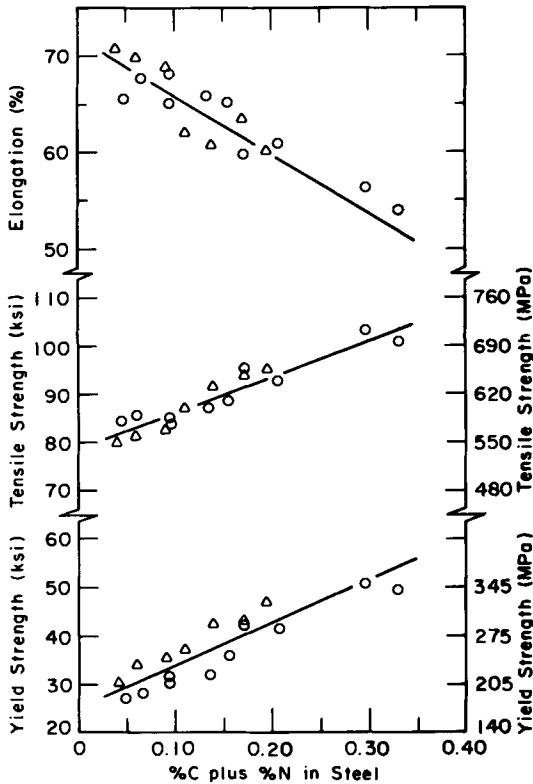


FIG. 17—Effect of nitrogen on the room-temperature mechanical properties of laboratory (circles) and commercial (triangles) 18Cr-8Ni steels.

In regard to ductility, the tensile elongation decreases with increased nitrogen; however, even the highest nitrogen alloy had 50 percent elongation, which is more than adequate for most applications. There was no apparent effect of nitrogen on Olsen cup ductility; cup heights ranged from 10.3 to 11.3 mm. The loads required to make the cup generally increased with increasing nitrogen, reflecting the higher strength.

To further study the effects of nitrogen on mechanical properties, tension test results on 210 commercial heats of 18-8 containing 0.016 to 0.29 percent nitrogen were reviewed and statistically analyzed. Included in the analysis were coils of varying thickness and processing and some published data on T-304 plate [1]. Only the yield strength was considered in the analysis, since yield strength is the criterion used for most design stresses. The average, ranges, and three standard deviations sorted to nitrogen ranges, for heats above and below 0.03 percent carbon, show general trends of increased yield strengths with increasing nitrogen below and above 0.03 percent carbon, Fig. 18. More importantly, note that the yield strength of the low-carbon steels containing 0.05 to 0.09 percent nitrogen is about the same as the higher carbon steel with less than 0.04 percent nitrogen.

The higher strength provided by nitrogen additions to 18Cr-8Ni steels persists to elevated temperatures (Fig. 19) and cryogenic temperatures [1] and results in improved creep properties [16]. Also, room-temperature strength and ductility of high-nitrogen (0.16 percent) Type 304L were affected less than 0.031 percent nitrogen Type 304L after long-time (3000 h) exposure during creep at temperatures of 595, 705, and 815°C [17].

Weldability

The effect of nitrogen on general weldability was evaluated by gas tungsten-arc welding 1.5-mm-thick sheets produced from the laboratory heats. There was no unusual behavior observed during welding and there was no difference in the general appearance of the welds. Microstructurally, the steels containing up to 0.16 percent nitrogen had typical as-cast dendritic structures with decreasing amounts of delta-ferrite with increasing nitrogen. The welds of the two highest nitrogen steels (0.24 and 0.25 percent) had wholly austenitic microstructures and tended to be coarser grained than the lower-nitrogen steels. In addition, the two highest-nitrogen welds displayed microporosity as well as visible pinholes.

Up to 0.16 percent nitrogen, the welds were ductile in that no cracks were evident in 180-deg bends made perpendicular and parallel to the welds. Although no cracks were observed on the 0.046 percent carbon-0.25 percent nitrogen steel, there was evidence of nonuniform deformation on the bend, which probably resulted from the large grain size. Some

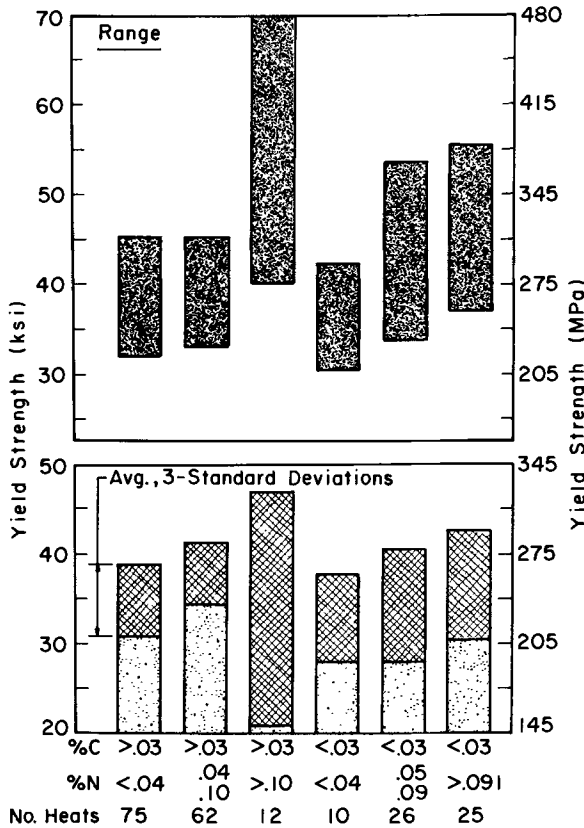


FIG. 18—Average, three standard deviations, and ranges of yield strength for mill-processed 18Cr-8Ni stainless strip and plate.

cracking was observed in the weld metal and HAZ of the high-carbon (0.090 percent)-nitrogen (0.24 percent) steel.

Fully austenitic, highly alloyed stainless steel welds and HAZ's are susceptible to hot-cracking; however, 18Cr-8Ni steel normally is not as susceptible as the higher-alloyed steels because of its relatively low total alloy content, and the chemical composition is such that welds usually contain some delta-ferrite, which minimizes cracking problems. Nitrogen-enriched 18-8 will contain less ferrite and, depending on chemical composition, can be wholly austenitic. However, there was no visible or microscopic evidence of weld or HAZ cracking in any of the laboratory welds. To further evaluate cracking susceptibility, circular weld tests were conducted on 3.5-mm-thick material from each of the laboratory steels and three commercial heats, 650874 (0.028 percent nitrogen), 650951 (0.13 percent nitrogen), and 161154 (0.15 percent nitrogen). Welding conditions were

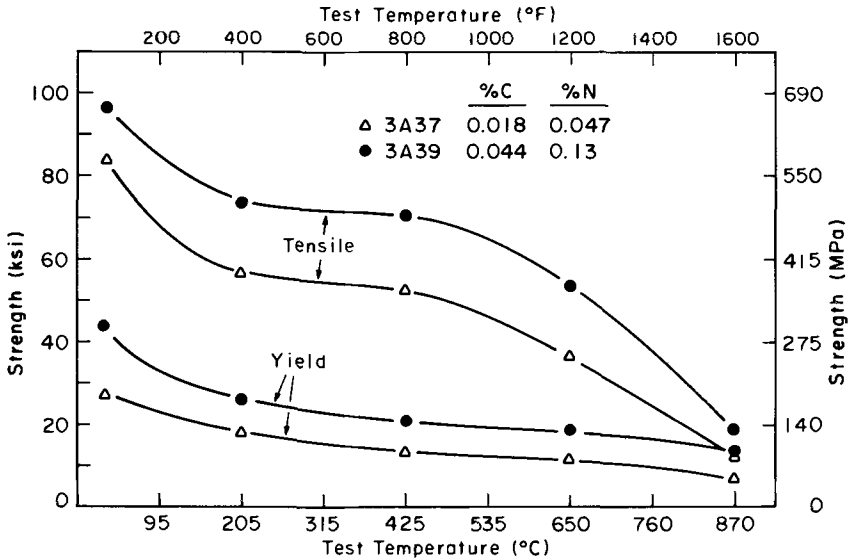


FIG. 19—Effect of nitrogen on the elevated-temperature mechanical properties of 18Cr-8Ni stainless steels.

selected that normally cause centerline weld cracks in wholly austenitic stainless steels. Under these conditions, no weld cracking was observed in any of the laboratory or commercial heats, except for the high-carbon (0.09 percent)-nitrogen (0.24 percent) steel, where one small transverse crack was found. Considerable gas tungsten-arc welded tubing and pipe has been produced from commercial AISI T-304 and T-304L containing up to 0.09 percent nitrogen, with no problems directly related to the nitrogen content.

Conclusions

In addition to its well-known effects as a potent austenitizing and strengthening element, nitrogen added to 18Cr-8Ni austenitic stainless steels provides other benefits as well. Nitrogen is a potent strengthening element when added to 18Cr-8Ni steels, and a 5.5 to 6.2-MPa (800 to 900 lb/in.²) increase in strength can be expected for each 0.01 percent nitrogen. This effect is particularly advantageous in the lower-carbon steels since it produces improved strength without degrading the normally excellent resistance to weld HAZ sensitization and intergranular corrosion after sensitizing heat treatments. The higher strength provided by the nitrogen persists to elevated temperatures and also results in improved creep properties.

Nitrogen additions of up to 0.16 percent retard sensitization and associated

intergranular corrosion of 0.04 to 0.09 percent carbon 18Cr-8Ni steels. In steels containing less than 0.03 percent carbon, nitrogen additions of up to 0.15 percent appear to have no detrimental effect on the normally excellent sensitization resistance of these steels.

Pitting and crevice corrosion resistance, as measured by anodic polarization and pitting and crevice corrosion tests in chloride-containing media, is improved by nitrogen additions. Stress corrosion cracking susceptibility evaluations in several chloride media showed no clear advantages or disadvantages for up to 0.16 percent nitrogen, but 0.25 percent appears to be detrimental in some environments.

Nitrogen additions of up to 0.16 percent had no apparent effect on weldability whereas higher nitrogen tended to produce microporosity and less than optimum weld ductility.

References

- [1] Gunia, R. B. and Woodrow, G. R., *Journal of Materials*, Vol. 5, No. 2, June 1970, pp. 413-430.
- [2] Binder, W. O., Thompson, J. and Bishop, C. R. in *Proceedings*, American Society for Testing and Materials, Vol. 56, 1956, pp. 903-920.
- [3] Renshaw, W. G. and Lula, R. A. in *Proceedings*, American Society for Testing and Materials, Vol. 56, 1956, p. 866.
- [4] Rocha, H. J., *Stahl und Eisen*, Vol. 62, 1942, p. 1091.
- [5] Uhlig, H. H. and White, R. A., *Transactions*, American Society for Metals, Vol. 52, 1959, pp. 830-847.
- [6] Kohl, H., *Radex Rundschau*, Vol. 4, 1965, pp. 606-619.
- [7] Uhlig, H. H. and Sova, J. P., *Corrosion Science*, Vol. 5, 1965, pp. 291-299.
- [8] Van Rooyen, D., "Some Aspects of Stress Corrosion Cracking in Austenitic Stainless Steel," U.S. Department of Commerce, OTS, AD Report 259-152, 1960, p. 18.
- [9] Van Rooyen, D. and Barnartt, S., "Stress Corrosion Cracking," U.S. Department of Commerce, OTS, AD 266-043, 1961, p. 11.
- [10] Lang, F. S., *Corrosion*, Vol. 18, 1962, pp. 378t-382t.
- [11] White, D. E. and Johnson, E. G., *Corrosion*, Vol. 16, 1960, pp. 321t-324t.
- [12] Denhard, E. E., *Corrosion*, Vol. 16, 1960, pp. 359-370.
- [13] Hines, J. G. and Jones, E. R., *Corrosion Science*, Vol. 1, 1961, pp. 88-107.
- [14] Eckel, J. F. and Cox, T. B., *Corrosion*, Vol. 24, 1968, pp. 218-222.
- [15] Eckel, J. F. and Clevinger, G. S., *Corrosion*, Vol. 26, 1970, pp. 251-255.
- [16] Brady, R. R., *Proceedings*, American Society for Testing and Materials, Vol. 59, 1959, pp. 774-785.
- [17] Dulis, E. J., Smith, G. V., and Houston, E. G., *Transactions*, American Society for Metals, Vol. 45, 1953, pp. 42-76.

DISCUSSION

*W. I. Weed*¹ (*written discussion*)—Very good paper. Confirms data we have developed. With regard to nitrogen levels, we have found that 0.25

¹J & L Steel Corp., Specialty Division, Pittsburgh, Pa.

to 0.30 percent nitrogen 18Cr-8Ni alloys can be welded with good ductility in the as-welded condition provided the welding conditions are adjusted, that is, weld speed reduced.

J. J. Eckenrod and C. W. Kovach (authors' closure)—Thank you for your comments on our paper and we are pleased to learn that 0.25 to 0.30 percent nitrogen 18Cr-8Ni alloys can be welded with good ductility in the as-welded condition. Our higher-carbon (0.090 percent)-0.24 percent nitrogen alloy was the only one that displayed somewhat poorer weld ductility. A lower-carbon (0.046 percent) alloy having about the same nitrogen content displayed good weld ductility. We have not performed any studies on adjusting welding conditions to improve the weld ductility of the higher-carbon alloy.

R. G. Thomas¹

Effect of Electrode Coating on the High-Temperature Mechanical Properties of AISI 316 Austenitic Weld Metals

REFERENCE: Thomas, R. G., "Effect of Electrode Coating on the High-Temperature Mechanical Properties of AISI 316 Austenitic Weld Metals," *Properties of Austenitic Stainless Steels and Their Weld Metals (Influence of Slight Chemistry Variations)*, ASTM STP 679, C. R. Brinkman and H. W. Garvin, Eds., American Society for Testing and Materials, 1979, pp. 42-55.

ABSTRACT: It is generally recognized that the long-term ductility of AISI 316 stainless steel weld metal is inferior to that of the parent metal but is influenced by weld metal composition. The present work is the initial part of a broadly based investigation of the high-temperature mechanical properties of AISI 316 weld metals. In particular, the correlation between manual metal-arc (MMA) electrode constitution and weld deposit tensile strength and ductility at temperatures between 500 and 700°C has been examined. It was found that these material properties depended upon the basicity of the electrode coating, and the observed variations have been explained in terms of differences in weld metal composition arising from changes in the slag/metal reactions which occur during welding.

Phosphorus and boron levels have also been investigated. Variations in the former have no effect on tensile properties, while 60-ppm boron increases deposit strength without significantly reducing ductility. This is probably a consequence of the effect of boron on the microstructural stability of the weld metal.

KEY WORDS: austenitic weld metals, electrode coating, high-temperature tensile properties, slag/metal reactions, residual elements, boron, phosphorus, microstructure

AISI 316 has been selected for widespread use in future power plant applications, and in many situations joints will be fabricated using the manual metal-arc (MMA) welding process. Electrodes commonly used for welding AISI 316 are basic coated (basicity index > 2 and typically 48 CaCO_3 -15 SiO_2). They deposit welds (of $\sim 17\text{Cr}$ -9 Ni -2 Mo composition containing between 3 and 8 percent delta-ferrite to overcome hot-cracking

¹Research officer, Central Electricity Generating Board, Marchwood Engineering Laboratories, Marchwood, South Hampshire, U.K.

problems) which have been shown to possess superior strength and ductility to weld metals of matching composition. However, some commercially available varieties of these electrodes can be difficult to handle and so the deposition of defect-free welds cannot be readily achieved. Rutile-coated electrodes (basicity index < 1 ; typically $6\text{CaCo}_3\text{-}13\text{SiO}_2\text{-}38\text{TiO}_2$) are available and have been considered for use [1]² since experience has shown that a high proportion of readily ionizable elements such as titanium stabilize the arc voltage at a relatively low level. Furthermore, the slag produced is more fluid and easily removed and, although this may possibly restrict positional welding, there should be a distinct advantage in terms of handleability. In addition, recent U.S. work has shown that it may be possible to improve the high-temperature mechanical properties of 308 weld deposits by controlling the levels of residual alloying elements present.

However, the role of electrode coating composition in determining 316 weld deposit mechanical properties has, as yet, received little attention. The present paper outlines results obtained from initial work aimed at correlating electrode coating composition, deoxidation practice, and weld deposit composition (notably boron and phosphorus levels) with the high-temperature mechanical properties of weld metals of essentially identical microstructure based on 17Cr-9Ni-2Mo.

Previous Work

Binkley, Goodwin, and Harman [2] first reported that the use of lime-titania or titania (rutile) electrodes for welding AISI 308 stainless steel markedly improved the creep rupture life of the weld metal when subsequently tested at 650°C . However, this enhanced creep life was accompanied not only by a reduction in creep ductility but also by a more rapid decrease in this property with increasing rupture time. No differences in deposit composition or microstructure were observed which could account for the measured variation in properties.

In order to improve this poor long-term ductility, Binkley, Berggren, and Goodwin [3] systematically varied the impurity levels of AISI 308 weld deposits and selected for study titanium, phosphorus, sulfur, and boron. They also varied the carbon and silicon levels in their program. Tests were again performed at 650°C (with up to ~ 700 h rupture life) and only phosphorus, boron, and titanium were found to benefit creep ductility without impairing creep life. Further work reported by Cole et al [4] claimed that combined optimum additions of these three elements at levels of approximately 0.007B-0.42P-0.06Ti benefited properties to an even greater extent. Less detailed tests carried out on AISI 316 illustrated a

²The italic numbers in brackets refer to the list of references appended to this paper.

similar general effect of enhanced creep properties due to a controlled residual element content.

The mechanisms by which these improvements in mechanical properties were achieved was considered to be related to the occurrence of sigma phase in the weld metal. The deposits contained ~8 percent delta-ferrite, which during testing at 650°C transformed to sigma. This phase was held responsible for the reduction in creep ductility with increasing creep life since creep cracks were found to form preferentially at sigma/austenite boundaries. They suggested that the presence of boron, phosphorus, and titanium was beneficial because they not only retarded the rate of sigma formation but also improved the interphase boundary properties in some unspecified way so that the overall creep deformation was controlled by the austenite matrix.

Experimental

Seven batches of experimental 4-mm MMA electrodes of varying basicity and deoxidant content were supplied by a commercial manufacturer. The electrodes, classified in Table 1, were all designed to deposit weld metals of similar composition (17Cr-9Ni-2Mo) and delta-ferrite content (~ 8 percent).

Butt welds were made in U-groove joints in 25-mm-thick buttered mild steel plate according to BS 2926 and subsequently examined radiographically. Longitudinal all-weld metal tension specimens were machined from each sound weld and tested in air at 50°C temperature intervals in the range 500 to 700°C at a crosshead speed of $8.33 \times 10^{-6} \text{ mm s}^{-1}$, selected to promote intergranular failure over the whole temperature range. During most of the test the crosshead speed corresponded to the specimen extension rate and failure occurred typically between 200 and 300 h in all tests.

Results

Chemical Analyses

Weld metal chemical analyses are given in Table 2 and are average values from specimens taken at two areas within each weld. Table 3 gives the analyses of most of the electrode slags.

Mechanical Properties

The results from the tension tests are shown in Figs. 1 and 2. Both ultimate tensile strength (UTS) and proof stress show a characteristic decrease with increasing test temperature until at 700°C they reach similar values. Despite some scatter, three distinct groups of data can be distin-

TABLE 1—Classification of electrodes.

R	rutile-coated 17Cr-9Ni-2Mo controlled delta-ferrite
B	basic-coated 17Cr-9Ni-2Mo controlled delta-ferrite
BED	as B but containing coating additions of titanium magnesium, and zirconium ferroalloys
RED1	as R but containing coating additions of titanium, magnesium, and zirconium ferroalloys
RED2	as RED1 but containing Fe ₂ O ₃ in coating
RLP	as R but with low phosphorus
RBO	as R but with boron coating additions

TABLE 2—Weld metal analyses.

	R	B	BED	RED1	RED2	RLP	RBO
Cr	17.30	17.80	18.70	17.80	17.60	17.20	17.50
Ni	9.00	8.83	9.00	8.74	8.62	8.30	9.40
Mo	2.30	2.20	2.10	2.10	2.30	2.10	2.00
C	0.08	0.09	0.09	0.08	0.09	0.09	0.08
Mn	1.61	1.53	1.53	1.64	1.72	1.61	1.60
Si	0.45	0.15	0.20	0.60	0.75	0.70	0.60
Ti	0.04	0.03	0.04	0.04	0.03	0.03	0.03
P	0.04	0.02	0.02	0.03	0.03	0.01	0.03
S	0.02	0.02	0.01	0.01	0.01	0.01	0.01
O	0.18	0.16	0.12	0.12	0.16	0.09	0.07
N	0.05	0.04	0.04	0.05	0.05	0.04	0.04
B	0.002	0.002	0.001	0.001	0.002	0.002	0.006

TABLE 3—Slag constitution.

	R	B	BED	RED1	RED2
K ₂ O	0.11	0.43	0.49	0.08	0.09
CaF ₂	5.60	32.00	32.00	5.60	6.60
CaO	9.00	25.00	25.00	9.80	7.00
MgO	<0.50	<0.50	<0.50	<0.50	<0.50
SiO ₂	14.70	20.50	19.50	14.40	13.40
Al ₂ O ₃	3.90	0.60	0.70	3.80	3.40
TiO ₂	38.70	7.80	8.20	37.60	35.00
Cr ₂ O ₃	12.30	5.40	5.30	11.30	9.50
FeO	4.00	2.80	3.70	3.60	3.80
MnO	9.80	4.10	3.90	8.60	8.20
P	0.11	0.06	0.04	0.11	0.09

guished corresponding to deposits from rutile-coated, basic-coated and boron-containing electrodes. The rutile electrodes—R, RED1, and RED2—deposit weld metal that exhibits improved strength properties compared with the deposits obtained from the basic electrodes B and BED. RBO, however, exhibits greater proof stresses than the other rutile electrodes over the whole temperature range and also significantly larger UTS values at temperatures between 600 and 700°C. It is also clear from Fig. 1 that there

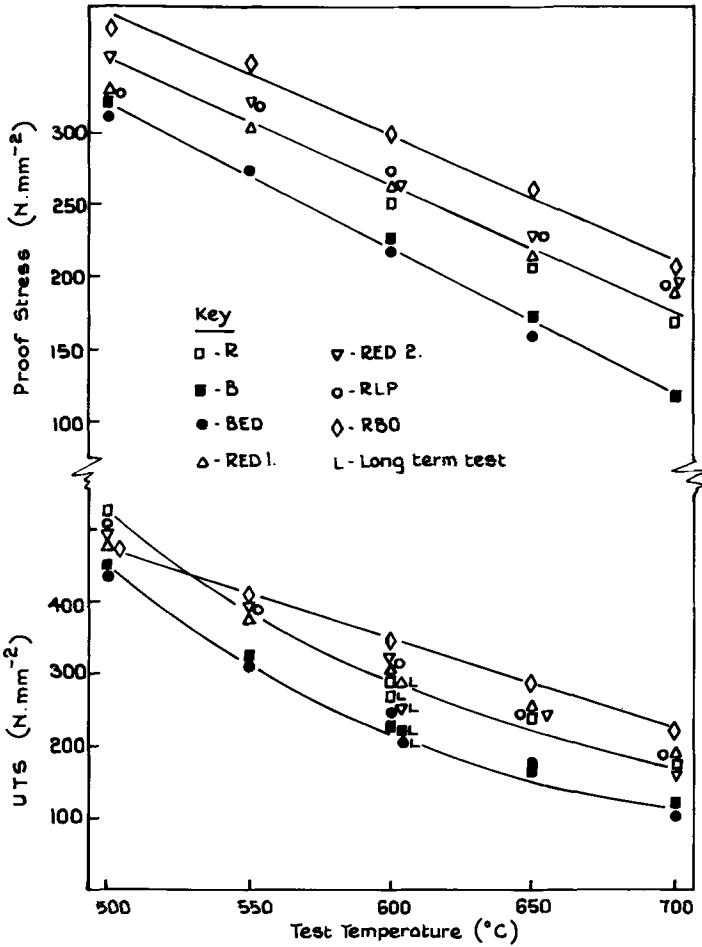


FIG. 1—High-temperature tensile strength.

is a small but consistent strengthening effect within the rutile electrode deposits and that the results for RLP fall within this group.

Specimen elongations at fracture separate into two groups (Fig. 2) with the deposits from rutile electrodes possessing poorer ductility, especially at higher temperatures. In this respect RLP and RBO are consistent with the other rutile electrodes. Reduction of area results reflects the fracture strains although the boundary between the two sets of data is not as well defined. The values shown are average measurements taken at the point of fracture.

In order to establish that the foregoing observations would be applicable to longer-term properties, additional tests were carried out at 600°C at a

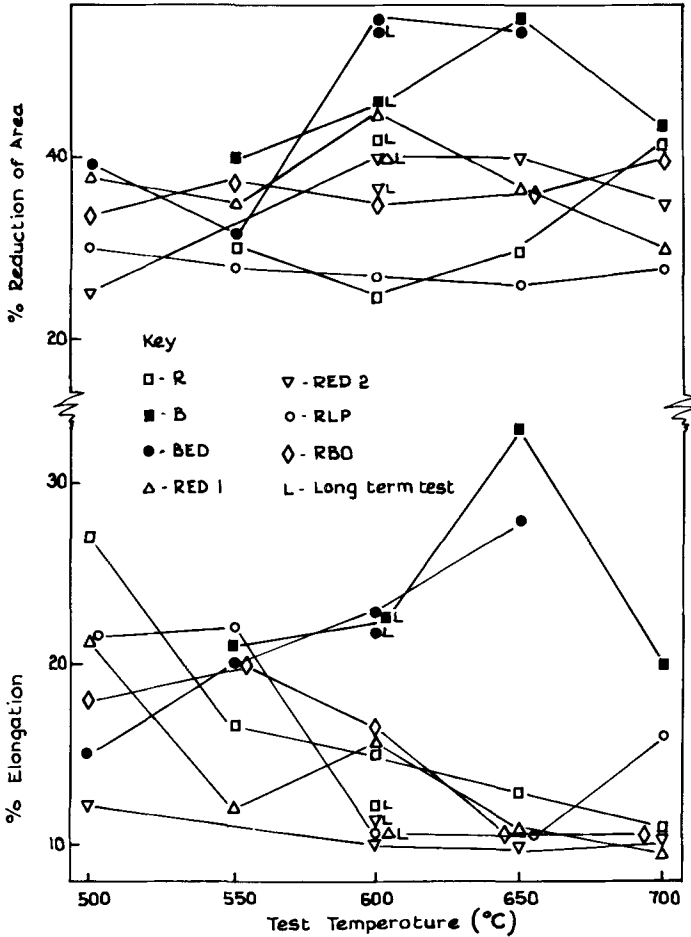


FIG. 2—High-temperature tensile ductility.

reduced extension rate of $3.33 \times 10^{-6} \text{ mm s}^{-1}$ which gave failure in ~ 1000 h. These results are also shown in Figs. 1 and 2 and, although the absolute values of UTS and strain at failure are strain rate dependent (decreased strain rate resulting in a lowering of UTS and ductility), the same influence of electrode coating prevails.

In addition to varying coating basicity, an attempt was made to vary the deoxidants in the weld metal by adding the additional deoxidizing titanium, magnesium, and zirconium elements to the coating. These variations in electrode coating composition were not discernible in the chemical analyses, but differences in oxygen contents between B and BED and R, RED1, and RED2 are evident in Table 2.

Microstructural Examination

Optical inspection of fractured tension specimens showed that final fracture occurred by linkage of cracks formed along delta-ferrite/austenite boundaries (Fig. 3). No significant microstructural differences were observed between any of the weld metals and Fig. 3 is representative of all seven. Metallographic examination also showed that there was essentially no variation in the inclusion contents of the weld metals.

The amount of delta-ferrite in each weld was determined magnetically using an Inspector gage, and was estimated from the weld metal composition via the Schaeffler diagram. Table 4 indicates virtually identical delta-ferrite contents in all deposits, and good agreement was obtained between the two methods.

It is well established that at high temperatures the delta-ferrite trans-

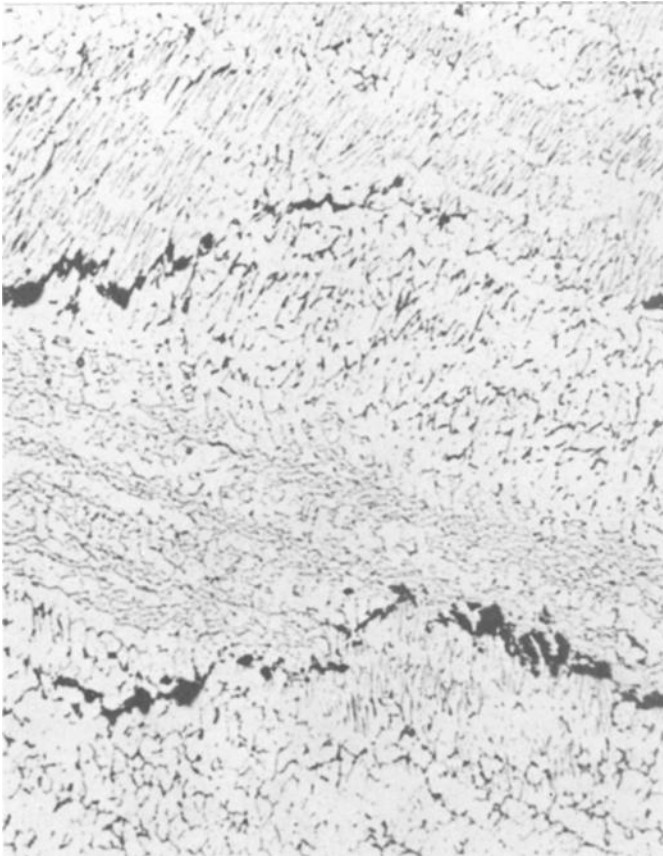


FIG. 3—Microstructure of failed tension specimen ($\times 250$).

TABLE 4—Delta-ferrite contents of as-welded deposits.

	R	B	BED	RED1	RED2	RLP	RBO
Schaeffler diagram	7%	7%	8%	8%	7%	8%	7%
Inspector gage	6.5%	6.5%	5.5%	7.5%	8%	7%	7%

forms to sigma phase, but although various etching techniques were attempted to highlight this phase no success was obtained.

Carbon replicas were also taken from a section of failed specimens and examined in the electron microscope. The precipitates were found to occupy predominantly the delta-ferrite and its boundaries with the austenite phase. Numerous selected area diffraction patterns of various precipitates were examined but only $M_{23}C_6$ was positively identified. This does not preclude the presence of sigma phase, however, since electron diffraction is critically influenced by particle size and orientation. Indeed, further magnetic measurements on fractured specimens indicated that a significant reduction in the ferrite content in some of the specimens had occurred during the tests, and the good agreement between Schaeffler diagram predictions and Inspector gage measurements obtained on specimens in the as-welded condition suggests that these results can also be viewed with confidence.

Treatment of Chemical Analysis Results

The weld deposit chemical analyses (Table 2) show that the largest changes have occurred in the magnesium, titanium, and silicon elements and consequently it is of interest to examine their distribution in terms of slag/weld metal chemistry. Wolstenholme [5] working on 2CrMo electrodes has shown that, assuming a reaction temperature of $\sim 1900^\circ\text{C}$, equilibrium is attained in the slag/metal reactions and it is possible to set up experimental reaction constants (K')

$$\frac{1}{2}(\text{Ti})_{\text{Fe}} + (\text{O})_{\text{Fe}} = \frac{1}{2}(\text{TiO}_2)_{\text{slag}}$$

$$K'_{\text{Ti}} = \frac{(\text{TiO}_2)_{\text{slag}}^{1/2}}{(\text{Ti})_{\text{Fe}}^{1/2} \times (\text{O})_{\text{Fe}}}$$

where $()_{\text{Fe}}$ and $()_{\text{slag}}$ refer to weight percent of constituents dissolved in weld metal and slag, respectively.

Using this approach, the way in which the slag affects the weld metal composition and hence properties may be further understood. Plotting

$$\frac{(\text{TiO}_2)_{\text{slag}}^{1/2}}{(\text{Ti})_{\text{Fe}}^{1/2}} \text{ versus } (\text{O})_{\text{Fe}}$$

illustrates the partitioning of the deoxidant between weld metal and slag. This is shown in Fig. 4 for magnesium, silicon, and titanium for the R, RED1, RED2, B, and BED electrodes. In each case it is apparent that the oxide/metal ratios are indeed related to weld oxygen content. Although the paucity of data and inevitable scatter inherent in the analysis of complex weldings slags mean that only tentative conclusions may be drawn, it is possible nevertheless, to discern separate trends for each element.

In order to explain these trends, it is necessary to define the true equilibrium reaction constant (K); for example

$$K_{\text{Ti}} = \frac{(a_{\text{TiO}_2})^{1/2}}{(h_{\text{Ti}})^{1/2}h_o} = K'_{\text{Ti}} \frac{(\gamma_{\text{TiO}_2})^{1/2}}{(f_{\text{Ti}})^{1/2}} \times \frac{1}{fo} \quad (1)$$

where

- a_{TiO_2} = Raoultian activity of the oxide in molten slag,
- h_{Ti}, h_o = Henrian activities of titanium and oxygen, respectively,
- γ_{TiO_2} = Raoultian activity coefficient of the oxide, and
- f_{Ti}, fo = Henrian activity coefficients of titanium and oxygen.

K_{Ti} is constant for any particular reaction occurring in the weld pool; K_{Si} and K_{Mn} can be similarly defined. However, the ratio $K_{\text{Ti}}/K'_{\text{Ti}}$ will depend upon the activity coefficients of the species involved, which will in turn depend upon the slag composition. This argument explains the clear separation of R, RED1, and RED2 from B and BED in Fig. 4, since the activity coefficients of the oxides in the rutile slag are significantly different from those in the basic slag. A similar observation was made by Wolstenholme [5], who found that the presence of ~25 percent CaF_2 in a basic MMA slag raised the apparent activity coefficients of both iron and manganese oxide.

The separation of oxide/metal ratios according to the basicity of the electrode coating (Fig. 4) occurs in a sense that would be anticipated from a general consideration of the nature of the reactions involved. Slags of high basicity show a greater capacity for the removal of silicon, which forms the acid oxide silica, while the reverse is true for the manganese, which forms a basic oxide. Titanium, being amphoteric, cannot be categorized in the same empirical manner.

Figure 5 shows the interdependence of the oxide/metal ratios of silicon and manganese which arises out of their mutual relationship with the weld metal oxygen content. Thus

$$\frac{(\text{SiO}_2)_{\text{slag}}^{1/2}}{(\text{Si})_{\text{Fe}}^{1/2}} = K_{\text{Si}} \frac{(f_{\text{Si}})^{1/2}}{(\gamma_{\text{SiO}_2})^{1/2}} \times fo(\text{O})_{\text{Fe}}$$

and

$$\frac{(\text{MnO})_{\text{slag}}}{(\text{Mn})_{\text{Fe}}} = K_{\text{Mn}} \frac{f_{\text{Mn}}}{\gamma_{\text{MnO}}} \times fo(\text{O})_{\text{Fe}}$$

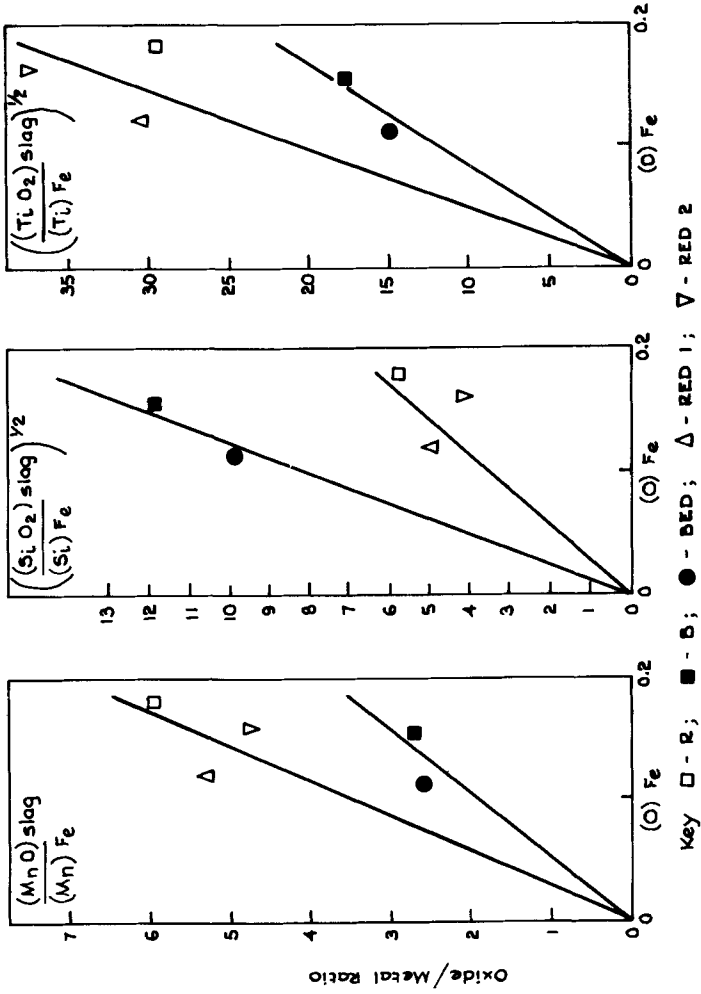


FIG. 4—Relationship between oxide/metal ratios and weld metal oxygen content.

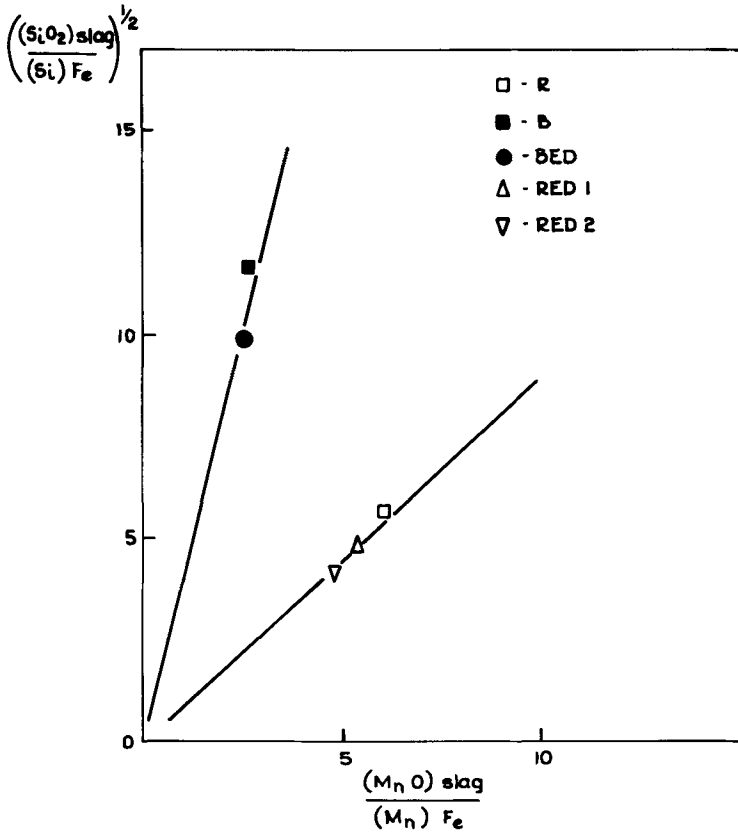


FIG. 5—Relationship between oxide/metal ratios of manganese and silicon.

Combining

$$\frac{(\text{SiO}_2)_{\text{slag}}^{1/2}}{(\text{Si})_{\text{Fe}}^{1/2}} = \frac{(\text{MnO})_{\text{slag}}}{(\text{Mn})_{\text{Fe}}} \frac{K_{\text{Si}}}{K_{\text{Mn}}} \left[\frac{f_{\text{Si}}^{1/2} \times \gamma_{\text{MnO}}}{f_{\text{Mn}} \times (\gamma_{\text{SiO}_2})^{1/2}} \right] \quad (2)$$

Again the term in [] in Eq 2 varies with slag constitution and is responsible for the separation of the data in Fig. 5 into two distinct groups. However, there is a distinct lack of thermodynamic data on welding slags and hence it is not possible at present to give a detailed quantitative analysis.

Discussion

Mechanical Properties

The results of the present work indicate that the type of electrode chosen for MMA welding will influence the mechanical properties of the weld

deposit. For as-welded deposits of identical microstructure, this effect must be caused by certain inherent coating characteristics which induce slight compositional variations in the weld metals. The chemical analyses of the deposits tested here are given in Table 2.

As far as the effect of coating basicity (that is, R, RED1, and RED2 compared with B, and BED) on mechanical properties is concerned, it is apparent from Table 2 that the observed differences in properties are compatible with variations in one or all of the following elements: phosphorus, nitrogen, manganese, and silicon.

The higher phosphorus content of deposits from rutile electrodes is primarily a consequence of the higher phosphorus in the original electrode coating, in which materials with intrinsically greater phosphorus impurity levels are used. The poorer recovery of the element by the rutile slag, which is low in calcium oxide, is unlikely to be of importance in determining the weld metal phosphorus level because of the unfavorably low percentage of iron oxide (~ 4 percent) present [8]. However, in view of the good agreement between the results for RLP (which has a phosphorus content similar to B and BED) and the remaining rutile electrode deposits, it is clear that the difference in tensile properties as a function of coating basicity cannot be ascribed simply to variations in phosphorus content.

The increased nitrogen content of weld metals from rutile electrodes is due to the poorer gas shielding properties of the coating, which has an intrinsically low CaCO_3 content. The reported effects of this element upon mechanical properties are conflicting; Davis and Cullen [6] state that up to 0.29 percent nitrogen (N_2) has little effect on AISI 308 weld metal while Stone [7] claims a beneficial influence. From concurrent work in progress at Marchwood Engineering Laboratories (MEL) it is felt that variations in nitrogen content will only be important at levels which significantly affect the delta-ferrite content of the weld. In the present work the differences in N_2 content between the two types of coating are in any case small.

From Fig. 4 it is clear the $(K_{\text{Mn}'})_{\text{basic}} < (K_{\text{Mn}'})_{\text{rutile}}$ and $(K_{\text{Si}'})_{\text{basic}} > (K_{\text{Si}'})_{\text{rutile}}$ and that the ratio of $(K_{\text{Mn}'})_{\text{rutile}}$ to $(K_{\text{Mn}'})_{\text{basic}}$ is less than the ratio of $(K_{\text{Si}'})_{\text{basic}}$ to $(K_{\text{Si}'})_{\text{rutile}}$. This explains the lower variation in manganese content between rutile and basic deposits, which in fact is unlikely to cause a noticeable change in properties. The equilibrium reaction constants also determine the absolute levels of particular elements in the deposited weld metal, and from Fig. 4 it is apparent that deposits from rutile electrodes will invariably contain higher silicon contents than those from basic electrodes. Silicon is well known as a solid solution hardener and, in fact, Binkley, Berggren, and Goodwin [3] noted a marked difference in creep properties between AISI 308 weld metals containing 0.29 and 0.47 percent silicon, which are levels similar to the present work. Within each electrode class there is an ostensible effect of deoxidant procedure upon mechanical properties (Figs. 1 and 2) which appears to be related to silicon content.

Microstructure

In general the enhanced tensile strength of deposits from rutile electrodes is gained at the expense of ductility. The drop in ductility is about 10 percent elongation but the weld metal still retains overall ~12 percent elongation and ~30 percent reduction of area.

The temperature range over which the current work was carried out (500 to 700°C) spans a large part of the region where the ferrite → sigma transformation occurs. The kinetic data of Weiss and Stickler [9] on solution-treated 316, Willingham and Gooch [10] on 316 weld metal, and magnetic measurements indicate qualitatively that a certain amount of sigma formation may have occurred at the higher end of the temperature range (600 to 700°C), where failure times were typically ~300 h. However, these same sources suggest that at 500 and 550°C the extent of sigma-phase transformation will have been very limited. Despite this, the experimental results Figs. 1 and 2 display the trends previously discussed over the entire temperature range. Consequently, in the present work, the occurrence of sigma phase must play only a minor part in determining the observed mechanical properties, and differences between deposits from rutile and basic electrodes are probably unrelated to changes in the kinetics of formation of sigma phase caused by the presence of certain alloying elements.

By contrast, the boron-containing deposit shows a strength (UTS) improvement only at higher temperatures and so it may be inferred that this element influences the kinetics of sigma phase formation from delta-ferrite. This is supported by work carried out on wrought 316 by Williams et al [11], who showed that boron forms borocarbides $M_{23}(C, B)_6$ and stabilizes them at the expense of sigma-phase formation.

Conclusions

The use of rutile coated electrodes appears to offer distinct advantages in terms of handleability and strength, especially if improvements in long-term ductility can be achieved by further compositional controls. In this respect the rate of formation of sigma phase from delta-ferrite and its retardation by certain residual elements may play a significant role. Based on relatively short-term high-temperature work, the following conclusions may be drawn.

1. In the manual metal-arc welding of AISI 316 stainless steel the basicity of the electrode coating significantly influences the high-temperature tensile properties of the deposit. Rutile-coated electrodes deposit welds of superior strength but slightly inferior ductility compared with welds from basic-coated electrodes.

2. The observed variation in properties probably stems from the higher silicon content of rutile deposits which is consistent with the slag chemistry of rutile electrodes.

3. Silicon achieves the effect just mentioned by solid solution hardening and not by influencing the rate of sigma formation.

4. The addition of boron to the weld metal increases both proof stress and UTS but leaves ductility largely unaffected.

5. Boron probably achieves the aforementioned effect by delaying the formation of sigma phase.

6. Additions of phosphorus up to ~0.04 weight percent have no effect on high-temperature tensile properties.

Acknowledgments

The author wishes to thank Mr. F. T. Fabling, who carried out the mechanical testing.

This paper is published by permission of the Central Electricity Generating Board.

References

- [1] Thomas, R. G. and Jones, W. K. C., Central Electricity Generating Board Welding Research Memorandum No. 46/7 Marchwood, South Hampshire, U. K., 1975.
- [2] Binkley, N. C., Goodwin, G. M., and Harman, D. G., *Welding Journal Research Supplement*, Vol. 52, No. 7, 1973, pp. 306s-311s.
- [3] Binkley, N. C., Berggren, R. G., and Goodwin, G. M., *Welding Journal Research Supplement*, Vol. 53, No. 2, 1974, pp. 91s-95s.
- [4] Cole, N. S., Berggren, R. G., Goodwin, G. M., King, R. T., and Slaughter, G. M. in *Proceedings*, 55th Annual Meeting, American Welding Society, Houston, Tex., May 1974.
- [5] Wolstenholme, D. A., Central Electricity Generating Board Report No. R/M/R187, Marchwood, South Hampshire, U.K., 1973.
- [6] Davis, M. W. and Cullen, T. M. in *Proceedings*, 49th National Meeting, American Welding Society, Chicago, Ill., 1968, pp. 54-65.
- [7] Stone, P. G., BISRA/ISI Conference, Eastbourne, U. K., Paper No. 41, 1966.
- [8] Ward, R. G., *An Introduction to the Physical Chemistry of Iron and Steel Making*, Arnold, London, U.K., 1962.
- [9] Weiss, B. and Stickler, R., *Metallurgical Transactions*, Vol. 3, 1972, p. 85.
- [10] Willingham, D. C. and Gooch, T. G., *Welding Institute Research Bulletin*. Vol. 12, Aug. 1971, pp. 215-218.
- [11] Williams, T. M., Harries, D., and Furnival, J., *Journal of the Iron and Steel Institute*, Vol. 210, No. 5, 1972, p. 357.

D. P. Edmonds,¹ R. T. King,¹ and G. M. Goodwin¹

Residual Elements Have Significant Effects on the Elevated-Temperature Properties of Austenitic Stainless Steel Welds*

REFERENCE: Edmonds, D. P., King, R. T., and Goodwin, G. M., "**Residual Elements Have Significant Effects on the Elevated-Temperature Properties of Austenitic Stainless Steel Welds,**" *Properties of Austenitic Stainless Steels and Their Weld Metals (Influence of Slight Chemistry Variations)*, ASTM STP 679, C. R. Brinkman and H. W. Garvin, Eds., American Society for Testing and Materials, 1979, pp. 56-68.

ABSTRACT: The influence of various residual elements on the elevated-temperature properties of austenitic stainless steel welds has been investigated at the Oak Ridge National Laboratory (ORNL). Included in this investigation are the effects of boron, phosphorus, titanium, carbon, sulfur, and silicon. This work is aimed at developing austenitic stainless steel weld materials with enhanced elevated-temperature properties.

The materials investigated include types 308, 316, and 16-8-2 stainless steel weld metals. Processes investigated include shielded metal-arc (SMA), gas tungsten-arc (GTA), and submerged-arc (SA) welding. Early work was done with Types 308 and 316 SMA weld metals, where the greatest enhancement of properties resulted from controlled additions of boron, phosphorus, and titanium to the deposits. Significant improvements in the properties of GTA and SA welds also result from the addition of these residual elements. The optimum residual element compositions were determined to be nominally 0.05Ti-0.04P-0.006B for SMA welds and 0.5Ti-0.04P-0.006B for GTA welds. Submerged-arc welds with 0.2Ti have exhibited improved creep strengths for all three materials.

KEY WORDS: austenitic stainless steels, weld metal properties, welding, creep-rupture properties

A significant problem in the production of fully austenitic stainless steel welds is their tendency for hot-cracking and microfissuring. To minimize this tendency, the compositions of welding materials are generally modified

*Work performed under ERDA/RDD 189a OHO24, Joining Technology Development.

¹Development engineer, Welding and Brazing Laboratory group leader, and Division of Fossil Energy program manager, respectively, Oak Ridge National Laboratory, Oak Ridge, Tenn. 37830.

to produce small amounts of delta ferrite (usually 3 to 7 volume percent) in the as-welded structure [1].² However, when these materials are exposed to elevated temperatures (500 to 900°C) for extended periods of time, the ferrite can transform to a hard, brittle phase known as sigma phase [2]. This transformation can lead to low-ductility ruptures (and low strength in some cases) when sufficiently high stresses are applied at elevated temperatures. When this occurs, ruptures generally occur along intersubstructural boundaries between the austenite and sigma phases [3]. Therefore, the transformation of ferrite to sigma phase is recognized to cause low-ductility/low-strength ruptures in many cases. In an attempt to produce austenitic stainless steel materials which do not exhibit this type of rupture after extended times at these temperatures, we are investigating factors that affect the properties of gas tungsten-arc (GTA), shielded metal-arc (SMA), and submerged-arc (SA) welds.

Development Work

Early work [4] on this program revealed that welds made with Type 308 SMA electrodes with titania and lime-titania coatings had higher creep strengths than welds made with lime-coated electrodes (Fig. 1). This indicated that titanium from the electrode coating had a major effect on the creep properties of the weld. Electrodes were then made by a commercial manufacturer using standard lime-titania coatings formulated to yield deposits with high and low levels of carbon, silicon, sulfur, phosphorus, and boron. The following results were obtained from this study.

1. Higher carbon contents (up to 0.074 percent) markedly increase rupture lives but decrease creep ductilities (Fig. 2).
2. Reducing silicon content (to 0.29 percent) increases ductility, with negligible effects on rupture life (Fig. 3).
3. Higher levels of phosphorus (up to 0.04 percent) increase rupture life and ductility (Fig. 4).
4. Variations in sulfur content (0.006 to 0.027 percent) have negligible effects on creep (Fig. 5).
5. Higher levels of boron (up to 0.06 percent) increase rupture life and ductility (Fig. 6).

Similar work was done for Type 316 stainless steel SMA weld metals. Results of this study led to the development of SMA Types 308 and 316 stainless steel weld metals with enhanced creep strengths and ductilities (Type 308 data are shown in Fig. 7). These materials are called Controlled Residual Elements (CRE) electrodes and produce nominally 0.05Ti-0.04P-0.006B in the deposit.

We have also investigated Types 308, 316, and 16-8-2 GTA welds.

²The italic numbers in brackets refer to the list of references appended to this paper.

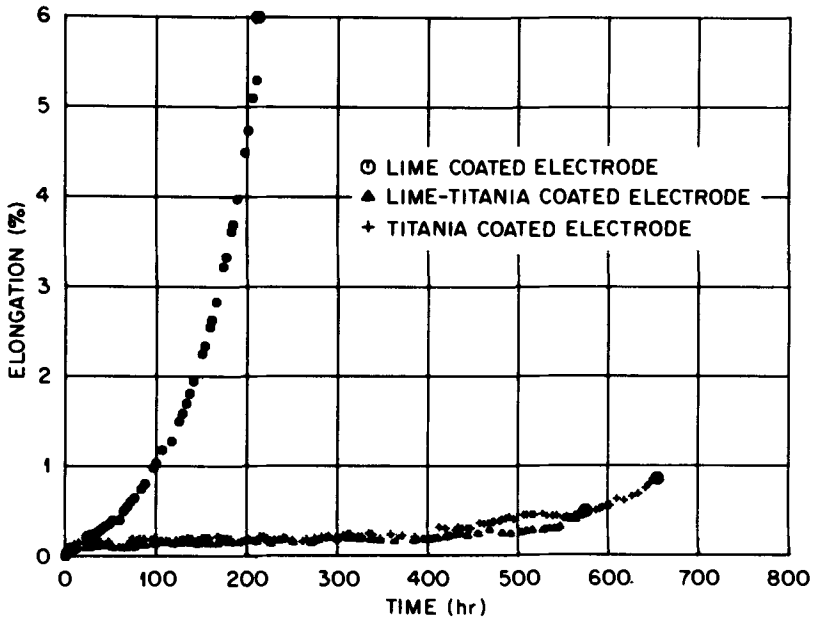


FIG. 1—Comparison of creep-rupture curves for Type 308 stainless steel SMA welds tested at 649°C (1200°F) and 125 MPa [18 000 (lb/in.²)]

Several small heats of GTA welding wire with varying amounts of boron, phosphorus and titanium were made at Oak Ridge National Laboratory (ORNL). Results from creep testing of welds made from these heats showed that titanium is the most potent strengthener and produces the greatest increases in ductility. In addition to improving properties, the extra titanium increased the amount of ferrite in the welds without the low-ductility ruptures commonly associated with the instability of this phase. It was determined (Figs. 8 and 9) that the best combination of residual elements in the Type 308 stainless steel GTA welds is nominally 0.5Ti-0.04P-0.006B, with the levels of all other residuals as low as possible. Similar results were obtained for Type 316 stainless steel GTA weld metals. These residual element additions did not significantly improve the properties of Type 16-8-2 stainless steel GTA weld metals.

In an attempt to demonstrate commercial capabilities for producing CRE wires, we have procured several large (225 kg) stainless steel ingots from four steelmakers. Wires have been drawn from these ingots for GTA and SA welding. Preliminary results from creep testing of GTA welds made from these wires indicate that several of the large heats have properties comparable with the smaller CRE heats described in the foregoing (Type 308 weld metal data are shown in Figs. 10 and 11). Similar results were obtained for Type 316 GTA weld metals. Also, SA test welds have

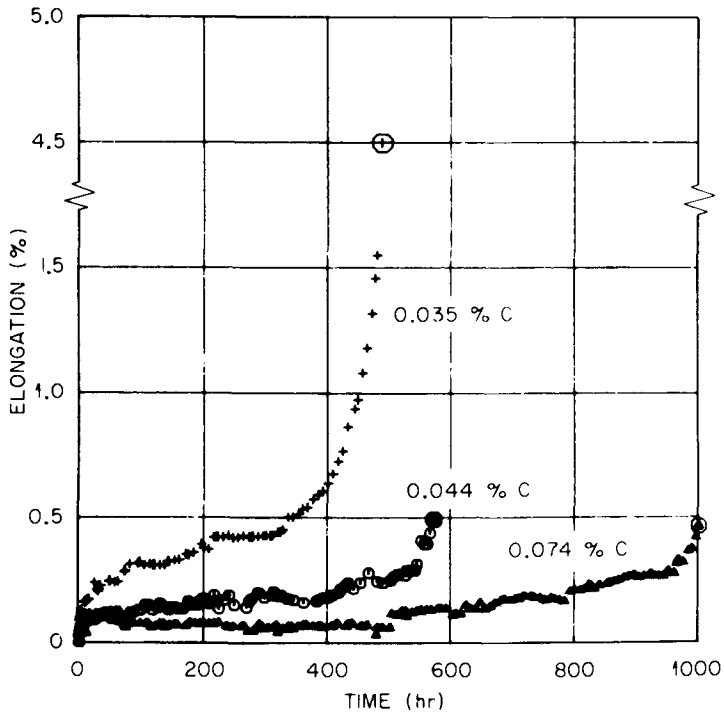


FIG. 2—Effect of carbon content on the creep of Type 308 stainless steel SMA weld metal at 649°C (1200°F) and 125 MPa [18 000 (lb/in.²)]

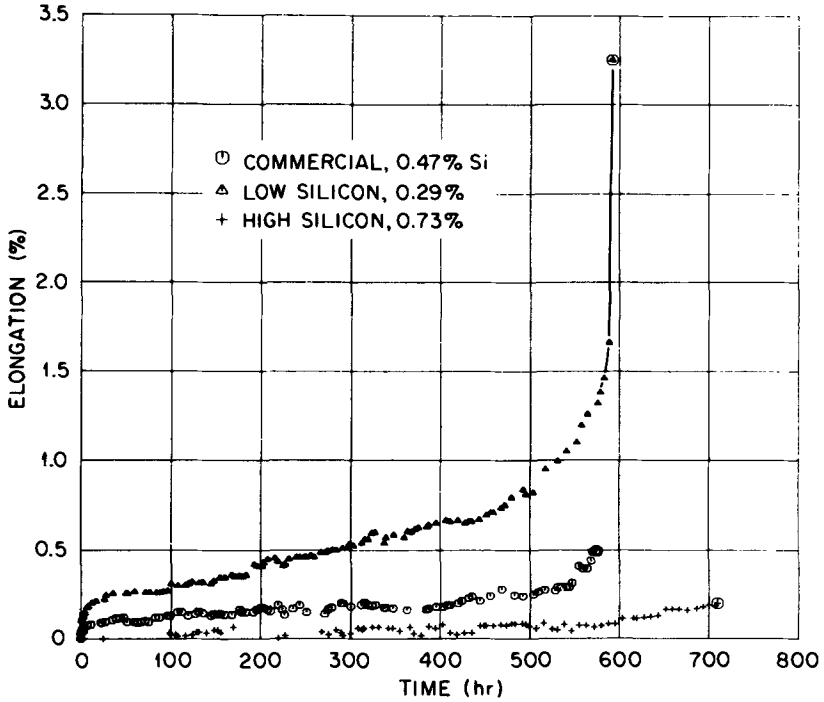


FIG. 3—Effect of silicon content on the creep of Type 308 SMA stainless steel weld metal at 649°C (1200°F) and 125 MPa [18 000 (lb/in.²)]

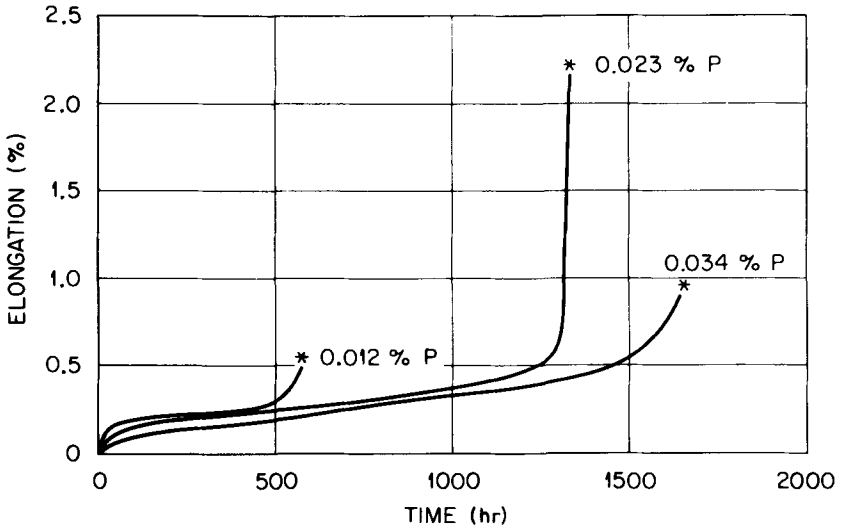


FIG. 4—Effect of phosphorus content on the creep of Type 308 stainless steel SMA weld metal at 649°C (1200°F) and 125 MPa [18 000 (lb/in.²)]

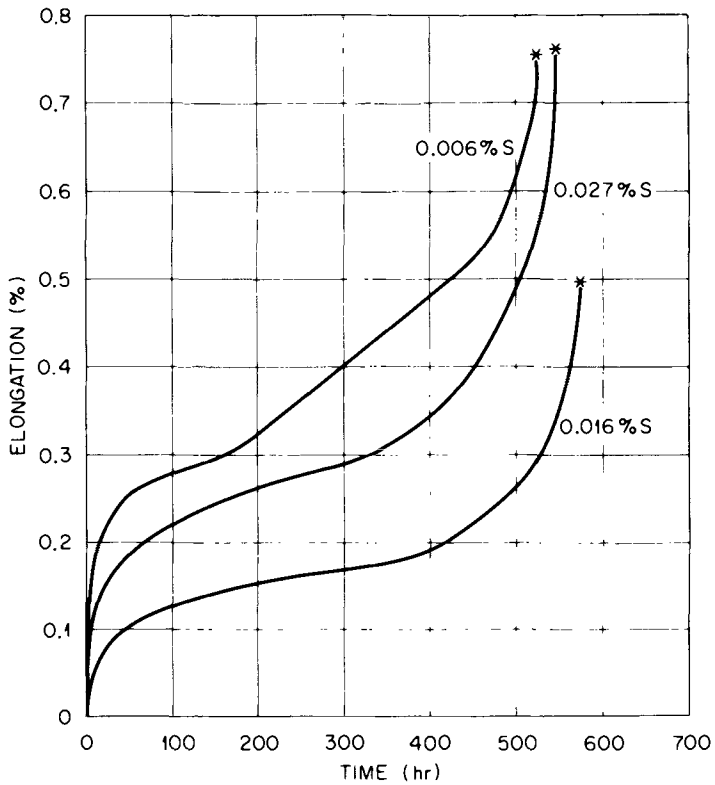


FIG. 5—Effect of sulfur content on the creep of Type 308 stainless steel SMA weld metal at 649°C (1200°F) and 125 MPa [18 000 (lb/in.²)]

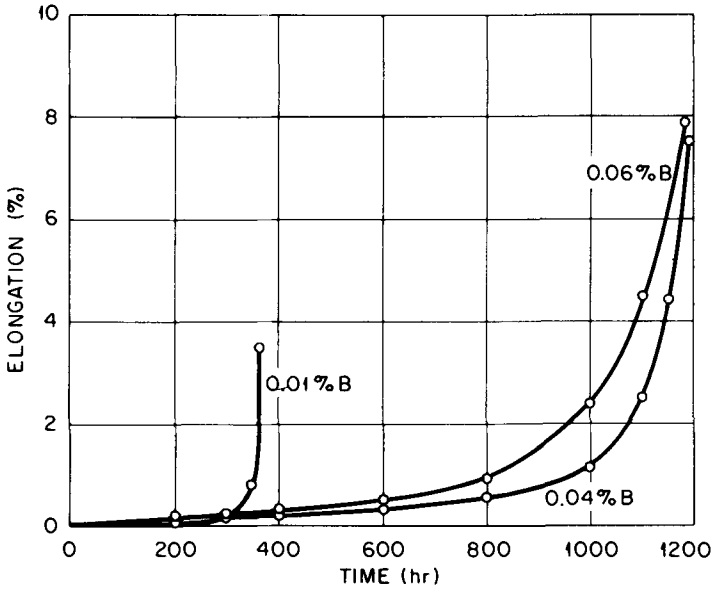


FIG. 6—Effect of boron content on the creep of Type 308 stainless steel SMA weld metal at 649°C (1200°F) and 139 MPa [20 000 (lb/in.²)]

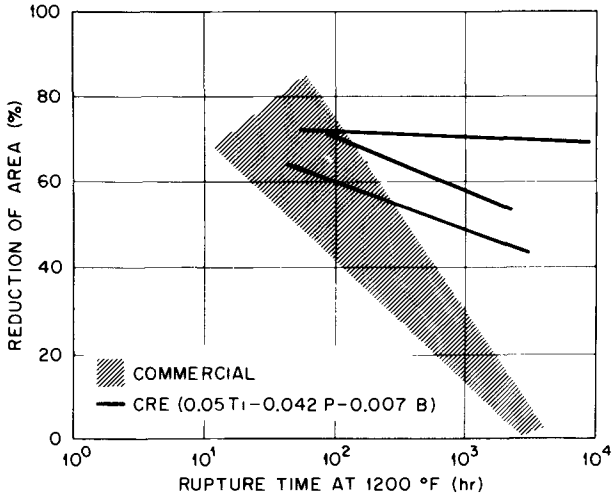


FIG. 7—Creep-rupture properties of Type 308 stainless steel SMA welds.

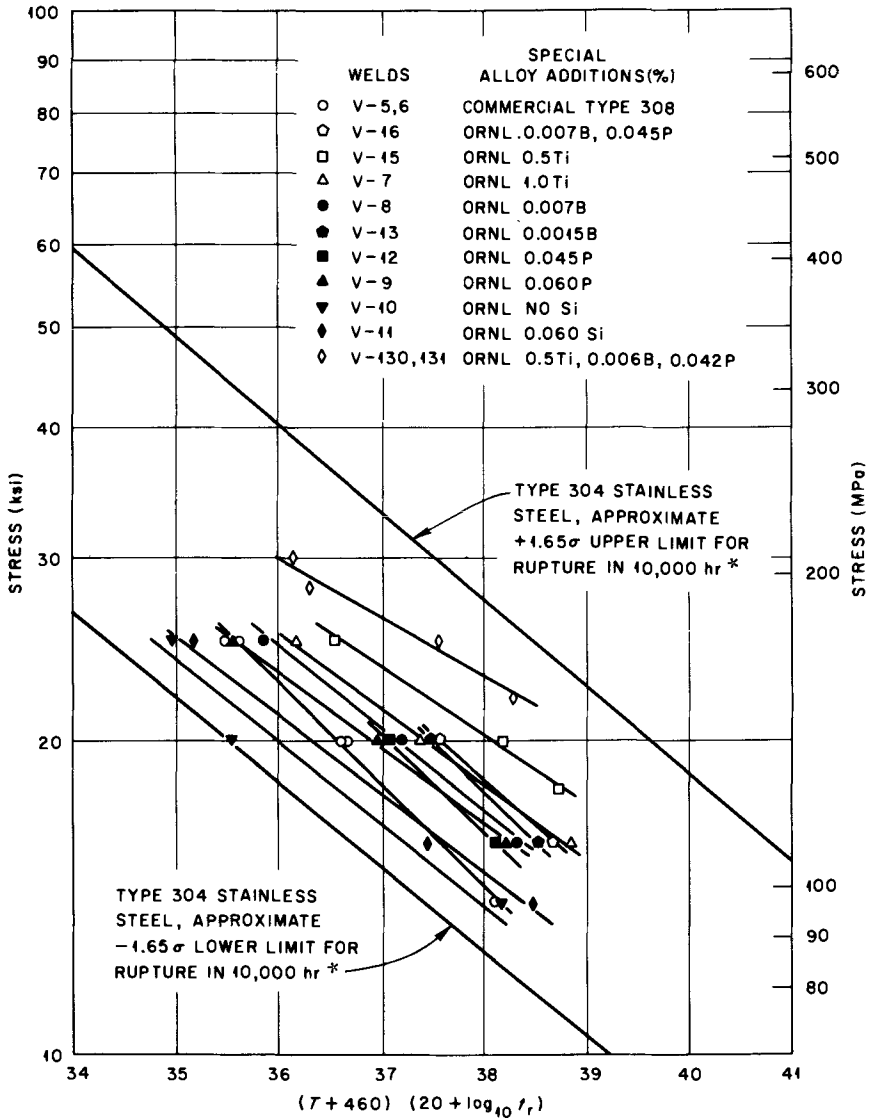


FIG. 8—Creep-rupture properties of Type 308 stainless steel GTA weldments at 649°C (1200°F). (Asterisks denote limits derived from Ref 5.)

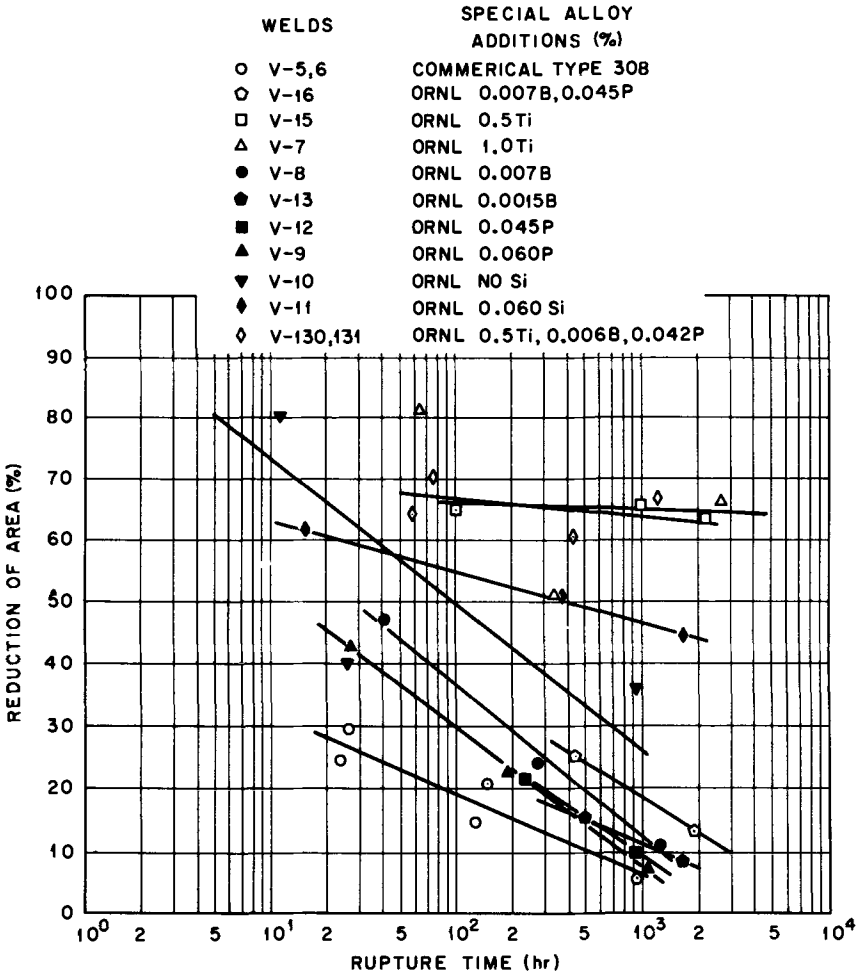


FIG. 9—Creep-rupture properties of Type 308 stainless steel manual GTA weldments at 649°C (1200°F).

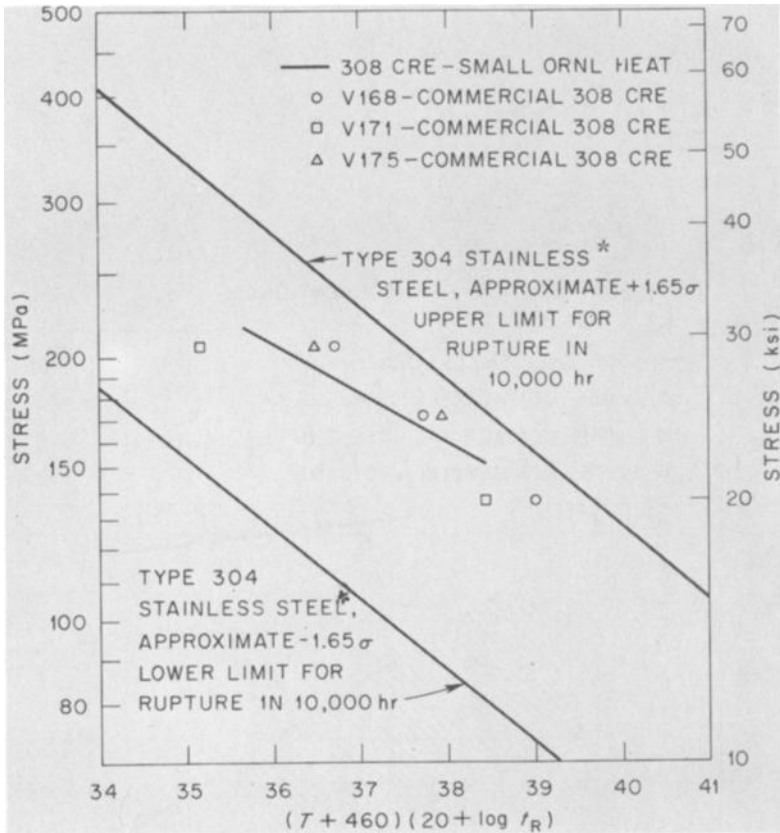


FIG. 10—Creep-rupture strength of Type 308 stainless steel GTA weldments at 649°C (1200°F). (Asterisks denote limits derived from Ref 5.)

been made with these wires using various commercial fluxes. Creep-rupture testing (Type 308 weld metal data are given in Fig. 12) has shown that higher than normal titanium concentrations (approximately 0.2 percent) in these SA welds greatly enhance the creep strength. Similar results were obtained with Types 316 and 16-8-2 weld metals.

In summary, we have found that additions of boron, phosphorus, and titanium to Types 308, 316, and 16-8-2 stainless steel welds can produce enhanced elevated-temperature properties. The optimum residual element compositions for Types 308 and 316 were determined to be nominally 0.05Ti-0.04P-0.006B for SMA welds and 0.5Ti-0.04P-0.006B for GTA welds. Submerged-arc welds with approximately 0.2Ti have exhibited improved creep strengths for all three materials.

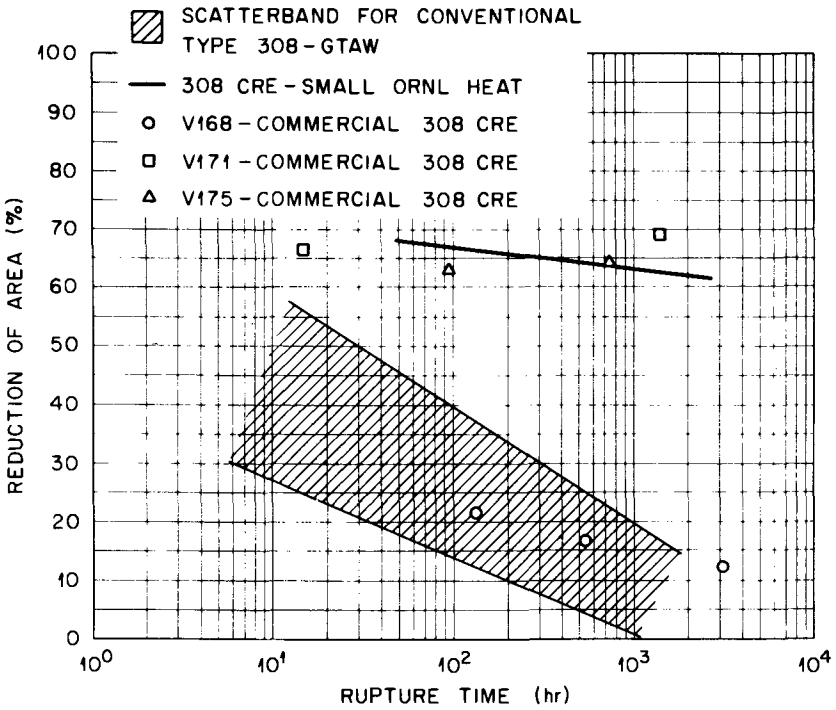


FIG. 11—Creep-rupture ductility of Type 308 stainless steel gas tungsten-arc weldments (GTAW) at 649°C (1200°F).

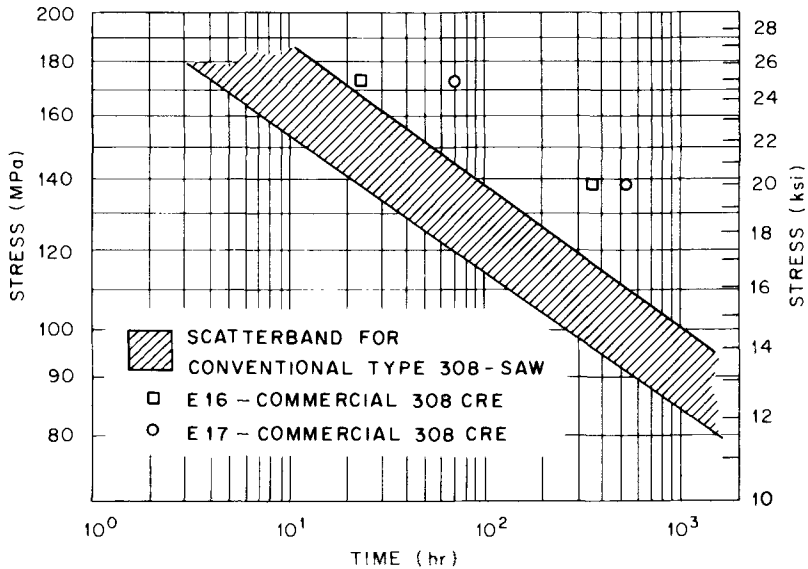


FIG. 12—Creep-rupture strength of Type 308 stainless steel submerged-arc weldments (SAW) at 649°C (1200°F).

Acknowledgments

The authors gratefully acknowledge the contributions of those who have aided in these efforts. These contributions include: preparation of welds by V. T. Houchin and J. D. Hudson, mechanical testing by E. Bolling, review of manuscript by J. F. King and T. K. Roche, editing by Debbie Stevens, and preparation of manuscript by Kathryn Witherspoon of the Metals and Ceramics Reports Office.

References

- [1] Borland, J. C. and Younger, R. N., "Some Aspects of Cracking in Welded Chromium-Nickel Austenitic Steels," British Welding Research Association Report B5/1/59, Aug. 1959.
- [2] Malone, M. O., *Welding Journal* (New York), Vol. 46 No. 6, June 1967, pp. 241s-253s.
- [3] Binkley, N. C., Goodwin, G. M., and Harman, D. G., *Welding Journal* (Miami), Vol. 52, No. 7, July 1973, pp. 306s-311s.
- [4] Binkley, N. C., Berggren, R. G., and Goodwin, G. M., *Welding Journal* (Miami), Vol. 53, No. 2, Feb. 1974, pp. 91s-95s.
- [5] Blackburn, L. D. in *The Generation of Isochronous Stress-Strain Curves*, A. O. Schaefer, Ed., American Society of Mechanical Engineers, New York, 1972, pp. 15-48.

DISCUSSION

*Raymond Cockroft*¹ (*written discussion*)—Are the authors totally convinced that high-temperature fissuring in sigma-containing welds starts/initiates at the sigma-austenite phase boundary?

D. P. Edmonds, R. T. King, and G. M. Goodman (*authors' closure*)—In most cases where we have done extensive optical and electron microscopy of ruptured creep specimens, we have found the creep fractures to propagate along austenite-sigma phase boundaries. This leads us to believe that when sigma phase is present in austenitic stainless steel welds, creep voids initiate at austenite-sigma boundaries.

¹Cameron Iron Works, Houston, Texas.

V. K. Sikka,¹ A. J. Moorhead,¹ and C. R. Brinkman¹

Influence of Small Amounts of Niobium on Mechanical and Corrosion Properties of Type 304 Stainless Steel*

REFERENCE: Sikka, V. K., Moorhead, A. J., and Brinkman, C. R., "Influence of Small Amounts of Niobium on Mechanical and Corrosion Properties of Type 304 Stainless Steel," *Properties of Austenitic Stainless Steels and Their Weld Metals (Influence of Slight Chemistry Variations)*, ASTM STP 679, C. R. Brinkman and H. W. Garvin, Eds., American Society for Testing and Materials, 1979, pp. 69-102.

ABSTRACT: Creep and creep-rupture properties of several experimental heats of Type 304 stainless steel containing 20, 50, 100, 200, 500, 700, and 1000 ppm (by weight) of niobium were investigated in the temperature range of 482 to 649°C. Resistance to intergranular corrosion of these heats was also studied. Results of tests on the experimental heats were compared with the creep properties of 20 commercial heats of Type 304 stainless steel and data from the literature on several heats of Type 347 (4000 to 3000 ppm niobium) stainless steel.

Results on experimental heats were used to check that heat-to-heat variations in creep properties of 20 commercial heats of Type 304 stainless steel are caused by variations in carbon, nitrogen, grain size, and for the most part by residual niobium (10 to 200 ppm). The time to rupture increased and minimum creep rate decreased with increasing niobium content until a saturation level was attained at about 500 to 1000 ppm.

Type 304 stainless steel containing 500-ppm niobium offers superior creep and creep-rupture properties with improved creep ductility and a factor of approximately 5 better intergranular corrosion resistance [in boiling copper sulfate (CuSO₄) solution] than Type 304 stainless steel (20-ppm niobium). In their welding work on the same heats, Moorhead et al have observed that Type 304 containing 500 to 1000 ppm niobium exhibits a weldability similar to that of Type 304 stainless steel.

KEY WORDS: niobium, austenitic stainless steel, tensile properties, creep properties, yield, ultimate tensile strength, corrosion resistance, heat-to-heat variations, mechanical properties

*Research sponsored by the Division of Reactor Research and Technology, U. S. Department of Energy, under Contract W-7045-eng-26 with the Union Carbide Corp.

¹Metallurgist, Mechanical Properties Group, metallurgist, Welding and Brazing Group, and group leader, Mechanical Properties Group, respectively, Metals and Ceramics Division, Oak Ridge National Laboratory, Oak Ridge, Tenn. 37830.

Austenitic stainless steels of Types 304 and 316 are the currently accepted structural material for breeder reactors. These steels are purchased to ASTM specifications. The range of allowable chemistry and thermo-mechanical processing history permitted by applicable material procurement specifications results in considerable variation in certain resultant mechanical properties [1-6].² It is the purpose of this paper to show the following:

1. Commercial heats exhibit variations in time to rupture (t_r) and minimum creep rate ($\dot{\epsilon}_m$).

2. Whereas carbon and nitrogen variations are known to be responsible for significant variations in mechanical behavior, niobium content is also a major factor as determined from studies conducted on 20 commercial heats of Type 304 stainless steel.

3. Time to rupture (t_r) as measured from uniaxial creep tests increases with increasing niobium up to 500 to 700 ppm and saturates beyond this range.

4. Type 304 stainless steel containing 500 ppm niobium offers creep-rupture properties comparable to Types 316 and 347 stainless steels, but with improved ductility.

5. Type 304 containing 500 ppm niobium is an optimum composition for improved creep and creep-rupture properties and intergranular attack in copper sulfate (CuSO_4) solution. The work of Moorhead et al [7] on the same heats has shown little effect on the weldability of Type 304 containing 500-ppm niobium as compared with Type 304.

Materials and Testing Procedures

Materials

Twenty commercial heats were used to study heat-to-heat variations, all of which were air-melted. These heats included 17 procured as plate, three as bar, and one as a 710 by 9.5-mm seamless pipe. The details of heat numbers, vendor, product form, and grain size of 20 heats are presented in Table 1 and their chemical compositions are summarized in Table 2.

One group of experimental heats (used to explain heat-to-heat variations in commercial heats) contained niobium in the range of 20 to 200 ppm (by weight). Experimental heats with niobium contents of 500, 700, and 1000 ppm were made to determine an optimum composition yielding improved creep properties as compared with Type 304 stainless steel and the niobium-stabilized Type 347 stainless steel ($\text{Nb} \geq 10 \times \text{C}$).

The experimental heats were made by remelting one of the commercial

²The italic numbers in brackets refer to the list of references appended to this paper.

TABLE 1—Summary of vendor, product form, and grain size of 20 heats of Type 304 stainless steel.

Heat	Heat Symbol	Vendor	Dimension		As Received		Reannealed	
			mm	in.	Grain Size ^a		Grain Size ^a	
					ASTM	μm	ASTM	μm
9T2796	796	USS ^b	50.8	2.00	0.26	280	0.26	280
X22807	807	USS	63.5	2.50	4.7	61	4.6	64
9T2797	797	USS	25.4	1.00	3.2	103	2.2	150
R23283	283	USS	19.0	0.75	5.2	52	4.8	60
R22926	926	USS	50.8	2.00	3.6	90	3.5	94
337187	187	Allegheny Ludlum	38.1	1.50	2.1	150	2.3	140
55697	697	Allegheny Ludlum	15.9	0.63	2.9	115	1.0	220
345866	866	Allegheny Ludlum	76.2	3.00	4.2	73	3.2	103
346544	544	Allegheny Ludlum	50.8	2.00	4.0	78	5.4	48
337330	330	Allegheny Ludlum	28.6	1.13	5.6	45	5.0	55
346845	845	Allegheny Ludlum	69.9	2.75	3.8	84	4.0	78
346779	779	Allegheny Ludlum	63.5	2.50	4.1	76	4.4	68
310390	390	Carlson	50.8	2.00	3.4	97	3.4	97
600414	414	Carlson	60.3	2.38	3.7	97	2.7	140
60551	551	Carlson	127 × 178	5 × 7	4.0	78	3.7	87
616737	737	Carlson	66.7	2.63	4.0	78	3.2	104
300380	380	Carlson	60.3	2.38	4.0	78	4.6	64
544086	086	Carlson	25.4	1.00	5.8	42	4.6	64
8043813	813	Republic	25.4	1.00	3.8	84	4.0	78
3121	121	Cameron	710 × 9.5	28 OD × 3/8 wall	1.1	215	1.7	175

^aMethod of Hillard, J. E., *Metallurgical Progress*, Vol. 85, No. 5, May 1964, pp. 98-102.

^bUnited States Steel.

TABLE 2—Summary of chemical analysis of 20 heats of Type 304 stainless steel.

Heat Symbol	Content, %						
	C	N	P	B	O	H	Ni
796	0.047	0.031	0.029	...	0.0110	0.0006	9.58
807	0.029	0.021	0.024	0.0005	0.010	0.0012	9.67
797	0.059	0.055	0.028	0.0020	0.0075	0.0007	9.78
283	0.043	0.025	0.018	0.0003	0.0140	0.0009	9.12
926	0.053	0.041	0.020	...	0.0084	0.0007	9.79
187	0.068	0.031	0.018	...	0.0042	0.0005	9.43
697	0.057	0.034	0.016	...	0.0150	0.0005	9.38
866	0.044	0.022	0.023	0.0002	0.0096	0.0010	8.98
544	0.063	0.019	0.023	0.0002	0.0081	0.0006	9.12
330	0.068	0.031	0.018	...	0.0042	0.0005	9.43
845	0.057	0.024	0.023	0.0002	0.0092	0.0013	9.28
779	0.065	0.023	0.024	0.0002	0.0056	0.0009	9.46
390	0.066	0.086	0.018	0.0020	0.0052	<0.0001	8.75
414	0.073	0.058	0.016	...	0.0190	0.0004	9.52
551	0.043	0.027	0.022	0.0010	0.0220	0.0013	9.40
737	0.064	0.075	0.026	0.00005	0.0072	<0.0001	9.01
380	0.063	0.068	0.018	...	0.0260	0.0009	8.30
086	0.050	0.043	0.025	...	0.0091	0.0005	9.46
813	0.062	0.033	0.044	0.0003	8.95
121	0.065	0.140	0.019	0.00005	0.0026	0.0011	9.19

Heat Symbol	Content, %						
	Mn	Cr	Si	Mo	S	Nb	V
796	1.22	18.5	0.47	0.10	0.012	0.008	0.037
807	1.26	18.8	0.50	0.20	0.023	0.0015	0.012
797	1.49	18.3	0.60	0.30	0.011	0.0050	0.020
283	1.32	18.2	0.45	0.30	0.020	0.0030	0.030
926	1.16	19.0	0.68	0.10	0.025	0.0180	0.050
187	0.83	18.2	0.59	0.07	0.008	0.0020	0.060
697	0.91	18.5	0.50	0.05	0.037	0.0030	0.030
866	1.51	18.5	0.47	0.2	0.007	0.0010	0.018
544	0.99	18.4	0.47	0.2	0.006	0.0050	0.025
330	0.83	18.2	0.59	0.07	0.008	0.0100	0.025
845	0.92	18.4	0.53	0.10	0.006	0.0100	0.050
779	0.94	18.1	0.47	0.20	0.005	0.0035	0.029
390	1.57	18.6	0.60	0.30	0.006	0.0160	0.020
414	0.94	18.7	0.69	0.10	0.015	0.0100	0.025
551	1.20	18.5	0.59	0.30	0.018	0.0140	0.050
737	1.71	18.3	0.50	0.30	0.012	0.0140	0.031
380	0.97	18.4	0.55	0.07	0.010	0.0100	0.028
086	1.23	18.4	0.53	0.20	0.016	0.0030	0.019
813	1.87	17.8	0.48	0.32	0.004	0.0200	0.022
121	1.92	18.1	0.30	0.14	0.010	0.0010	0.035

TABLE 2—Continued

Heat Symbol	Content, %						
	Ti	Ta	W	Cu	Co	Pb	Sn
796	0.003	<0.0005	0.022	0.10	0.05	0.01	0.02
807	0.002	<0.0005	0.020	0.11	0.03	0.01	0.01
797	0.005	0.0005	0.050	0.30	0.07	0.002	0.005
283	0.0010	<0.0005	0.021	0.14	0.05	0.01	0.01
926	0.0100	0.0010	0.030	0.070	0.05	0.010	0.02
187	0.003	<0.0005	0.015	0.15	0.05	0.01	0.02
697	0.002	<0.0005	0.011	0.10	0.05	0.01	0.02
866	0.0005	0.0005	0.007	0.13	0.04	0.01	0.01
544	0.017	0.0006	0.026	0.12	0.05	0.01	0.01
330	0.002	<0.0005	0.0060	0.15	0.05	0.01	0.02
845	0.008	<0.0005	0.007	0.11	0.07	0.01	0.01
779	0.010	0.0020	0.043	0.16	0.02	0.01	0.01
390	0.001	0.0006	0.043	0.20	0.07	0.0007	0.002
414	0.002	<0.0005	0.027	0.10	0.05	0.01	0.02
551	0.025	<0.0005	0.049	0.25	0.08	0.01	0.01
737	0.001	<0.0005	0.016	0.50	0.07	<0.0003	0.0050
380	0.004	<0.0005	0.016	0.10	0.05	0.01	0.02
086	0.006	<0.0005	0.021	0.10	0.05	0.01	0.02
813	0.002	<0.0005	0.02
121	0.016	<0.0005	0.015	0.07	0.07	<0.0003	0.002

heats (Heat 187 containing 20 ppm niobium, Tables 1 and 2) and adding niobium to reach final levels of 50, 100, 200, 500, 700, and 1000 ppm. These heats were made by melting the commercial heat in a water-cooled copper mold and remelting six times with a nonconsumable tungsten electrode in an evacuated chamber backfilled with partial pressure of argon. The final melt was drop-cast into a 19-mm-diameter water-cooled copper mold. The drop-casts were preheated at 1000°C and hot-swaged into 10-mm-diameter rods, which were used in machining tension and creep specimens. The chemical analyses of experimental heats are summarized in Table 3.

Test Specimens

The test specimens for commercial and the experimental heats were threaded-end bars having a gage diameter of 6.35 mm and a reduced section of 31.8 mm. In a few instances a larger specimen having a 57.2-mm reduced section was used for the commercial heats. All specimens were lathe machined. The machined specimens were inspected, cleaned, and those to receive additional heat treatment were reannealed at 1065°C for 0.5 h in argon. The commercial heats were tested in both the as-received (mill-annealed) and reannealed (laboratory annealed) conditions, whereas experimental heats were tested only in the reannealed condition. All ex-

TABLE 3—Summary of chemical analysis and grain size of Type 304 stainless steel containing small niobium, additions. Table also contains chemical analysis of a Type 347 plate used for corrosion studies.

Heat No.	187 ^{a,b}	187-1 ^{c,b}	187-1-A ^{d,e}	187-2 ^{c,b}	187-3 ^{c,b}
Grain size (intercept) ASTM (μm)	2.3 (140)	6 (38)	7.7 (22)	6 (38)	6 (38)
Chemical composition					
carbon	0.068	0.0488	0.052	0.0484	0.0485
nitrogen	0.031	0.028	0.029	0.0270	0.0270
phosphorus	0.018	0.023	0.029	0.0220	0.0190
boron		0.0002	0.0010	0.0002	0.0002
oxygen	0.0042	0.0020		0.0028	0.0051
hydrogen	0.0005	0.0004		0.0002	0.0008
nickel	9.43	9.68	9.48	9.32	9.62
manganese	0.83	0.99	0.96	0.96	0.98
chromium	18.20	18.30	18.22	17.6	18.40
silicon	0.59	0.46	0.44	0.50	0.60
molybdenum	0.07	0.15	0.14	0.21	0.25
sulfur	0.008	0.0055	0.009	0.0055	0.0050
niobium	0.0020	0.0020	<0.01	0.0050	0.010
vanadium	0.060		0.06
titanium	0.003	0.01	<0.01	0.01	0.01
tantalum	<0.0005	0.001	...	0.001	0.001
tungsten	0.015	0.05	...	0.05	0.05
copper	0.15	0.10	0.12	0.1	0.1
cobalt	0.05	0.10	0.10	0.1	0.1
lead	0.01	<0.001	...	<0.001	<0.001
tin	0.02	0.005	...	0.005	0.005
aluminum	...	0.005	0.01	0.005	0.005

^aCommercial Type 304.

^bAnalysis performed at Oak Ridge National Laboratory (ORNL).

^cFirst melt.

^dSecond melt.

^eAnalysis performed at Combustion Engineering.

perimental heats were tested after annealing for 0.5 h at 1065°C. However, some heats were also tested after reannealing for 0.5 h at 1093, 1150, and 1250°C. The grain sizes for both the commercial and experimental heats were measured and are summarized in Tables 1 and 3, respectively.

Testing Procedures

The creep tests were performed according to the ASTM Recommended Practice for Conducting Creep, Creep-Rupture, and Stress-Rupture Tests of Metallic Materials (E 139-70) [8]. The stress-rupture tests were conducted in standard lever-arm creep machines calibrated to a load accuracy of ± 0.5 percent. The temperature was measured by three Chromel-versus-Alumel thermocouples (of wire accuracy $\pm 3/8$ percent) wired to the specimen. The temperature variation along the specimen gage length was

TABLE 3—Continued.

Heat No.	187-4 ^{c,b}	187-5 ^{c,b}	187-5-A ^{d,e}	187-6-A ^{d,e}	187-7-A ^{d,e}	Type 347 ^e
Grain size (intercept) ASTM (μm)	6.2 (36)	6.6 (33)	7.9 (21)	7.8 (21)	7.9 (20)	<9 (~10)
Chemical composition						
carbon	0.0575	0.0480	0.049	0.050	0.051	0.070
nitrogen	0.0290	0.0290	0.030	0.028	0.029	0.039
phosphorus	0.020	0.0230	0.028	0.029	0.029	0.040
boron	0.0002	0.0002	0.001	0.001	0.001	0.001
oxygen	0.0035	0.0029
hydrogen	0.0004	0.0006
nickel	9.92	9.75	9.53	9.57	9.51	11.50
manganese	0.91	0.96	0.94	0.96	0.95	1.53
chromium	18.40	18.20	18.13	18.18	18.10	17.05
silicon	0.57	0.56	0.43	0.44	0.43	0.68
molybdenum	0.24	0.24	0.14	0.15	0.14	0.41
sulfur	0.0050	0.0055	0.009	0.009	0.009	0.006
niobium	0.020	0.05	0.05	0.07	0.10	0.78
vanadium	0.06	0.06	0.06	0.03
titanium	0.01	0.01	<0.01	<0.01	<0.01	<0.01
tantalum	<0.001	<0.001
tungsten	0.05	0.05
copper	0.1	0.1	0.12	0.12	0.12	0.20
cobalt	0.1	0.1	0.10	0.10	0.10	0.12
lead	<0.001	<0.001
tin	0.005	0.005
aluminum	0.01	0.005	<0.01	<0.01	<0.01	<0.01

approximately $\pm 1^\circ\text{C}$, and the highest temperature was taken as the nominal test temperature.

Length changes were measured by extensometers attached by setscrews to small grooves in the specimen shoulders. The extensometer movement was read by both dial gages and averaging transducers. The dial gages and transducers had an accuracy of $\pm 2.5 \mu\text{m}$. The specimen shoulder effects were negligible as compared with overall creep elongation.

Results and Discussion

Time to Rupture (t_r) and Minimum Creep Rate ($\dot{\epsilon}_m$)

Heat-to-Heat Variations—Time to rupture data at 593°C on 20 heats of Type 304 stainless steel are plotted as a function of stress in Fig. 1. These data are on materials in both mill-annealed and laboratory annealed conditions. Minimum creep rate data on the same heats are plotted in Fig. 2. Figure 1 shows that time to rupture can vary by factors of 30 to 40 for 20 heats in both the mill-annealed and laboratory-annealed conditions. Heat-to-heat variations observed for short-term data are also becoming obvious

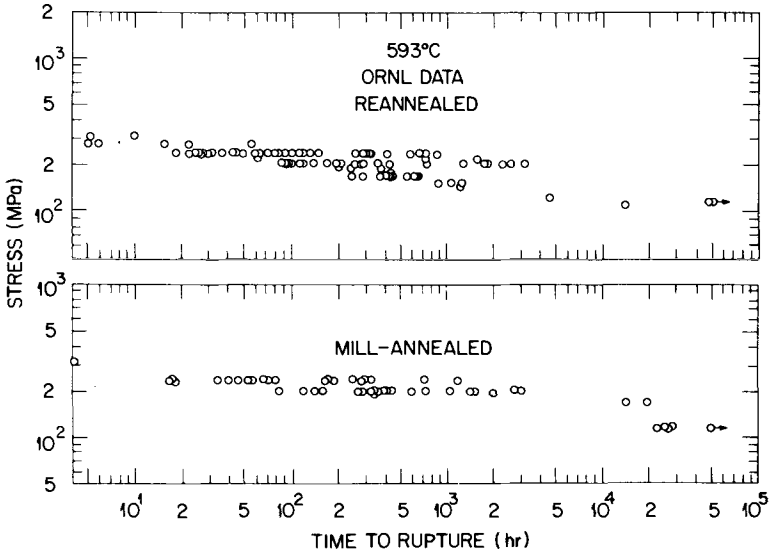


FIG. 1—Heat-to-heat variations in time to rupture at 593°C for 20 commercial heats of Type 304 stainless steel.

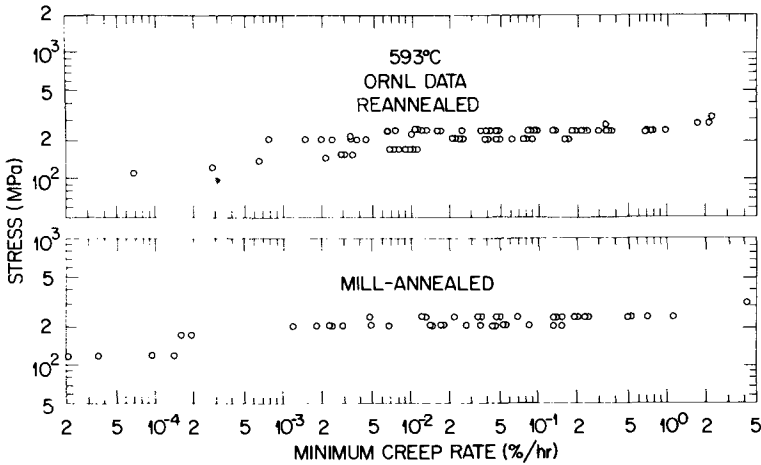


FIG. 2—Heat-to-heat variations in minimum creep rate at 593°C for 20 commercial heats of Type 304 stainless steel.

in long-term data extending to test times beyond 50000 h. Figure 2 shows that minimum creep rate can vary by factors of 100 for the same heats. This is apparent for both the short-term and long-term creep data.

The stress exponent, n_r , ($t_r = A\sigma^{-n_r}$) for rupture data on various heats varied from 8.2 to 14.5 for weak to strong heats, respectively. The stress

exponent, n_m , for $\dot{\epsilon}_m$ ($\dot{\epsilon}_m = B\sigma^{n_m}$) ranged from 9.6 to 16.5 for the same heats. In general, the stress exponents n_r and n_m were low for the weak heats and high for the strong heats.

Correlations Between Heat-to-Heat Variations and Chemical Composition—A summary [9] of several studies has shown that t_r increases and $\dot{\epsilon}_m$ decreases with increasing amounts of carbon and nitrogen (C+N). Thus, t_r and $\dot{\epsilon}_m$ data on 20 heats at 593°C and 207 MPa were plotted as a function of (C+N) in Figs. 3a and 4a. These figures show that the heats containing the highest (C+N) have a higher time to rupture and a lower minimum creep rate compared with heats of lower (C+N) levels. However, data scatter is too great to observe any definite trends. The same data,

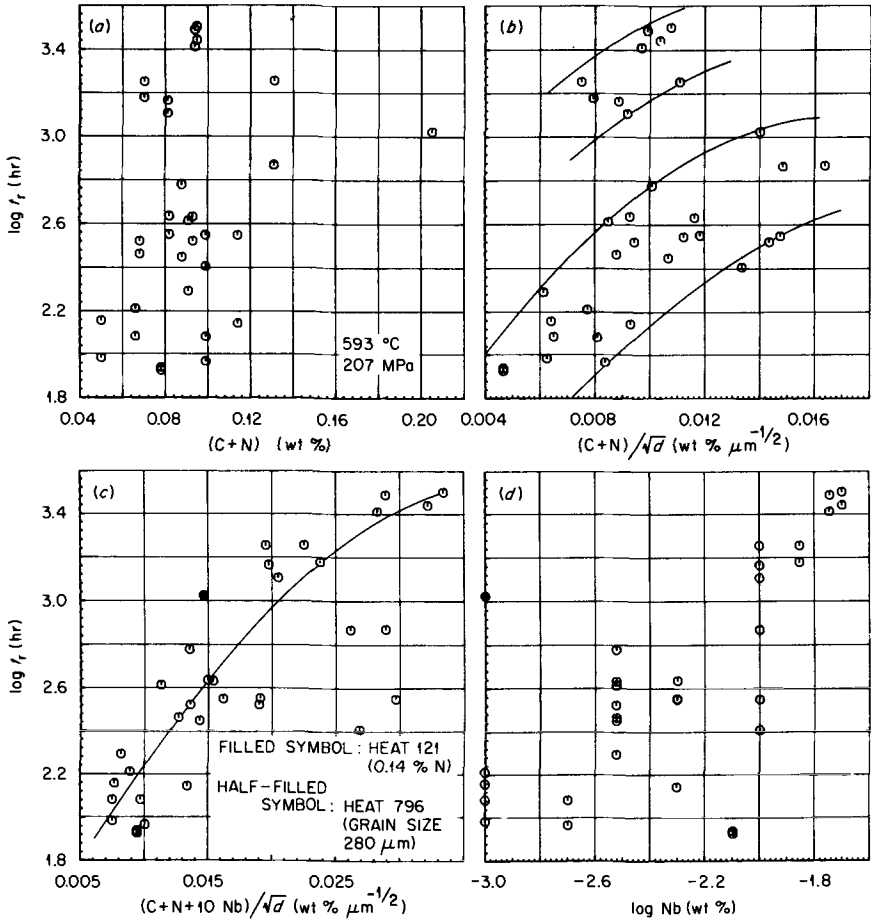


FIG. 3—Plots of time to rupture (t_r) at 593°C and 207 MPa versus various chemical composition and grain size factors for 20 commercial heats of Type 304 stainless steel. (a) t_r versus C+N; (b) t_r versus $(C+N)/\sqrt{d}$; (c) t_r versus $(C+N+10\text{Nb})/\sqrt{d}$; and (d) t_r versus Nb content. Bands in (b) and curve in (c) are visual and were drawn to show the trends.

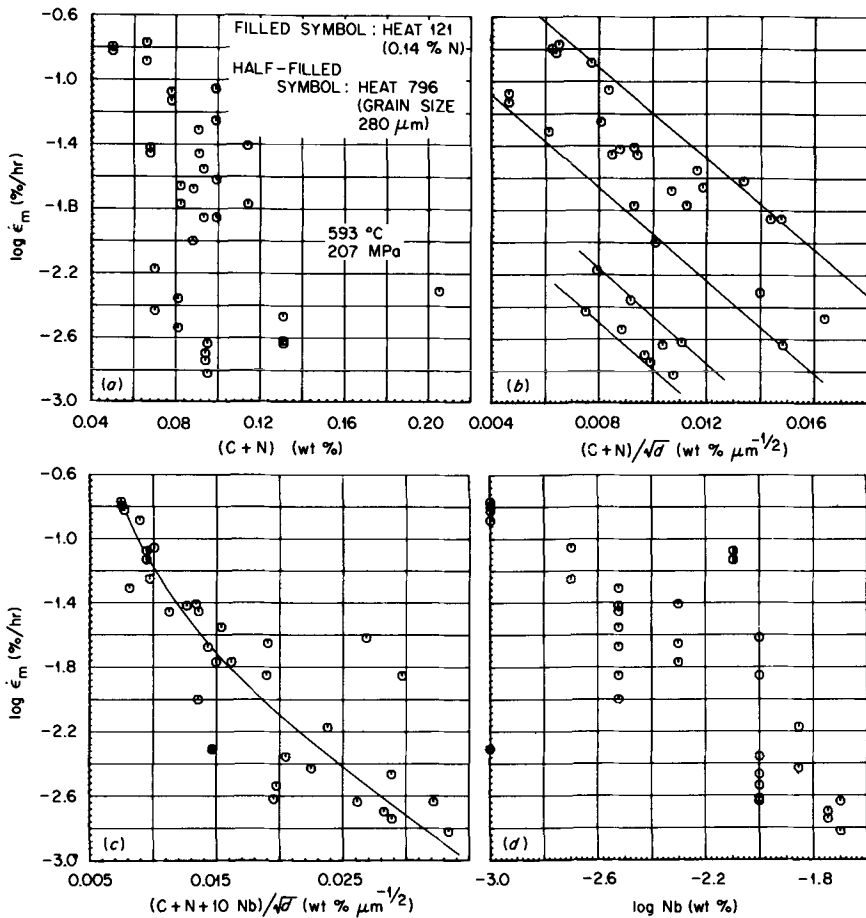


FIG. 4—Plots of minimum creep rate ($\dot{\epsilon}_m$) at 593°C and 207 MPa versus various chemical composition and grain size factors for 20 commercial heats of Type 304 stainless steel. (a) $\dot{\epsilon}_m$ versus $(C+N)$; (b) $\dot{\epsilon}_m$ versus $(C+N)/\sqrt{d}$; (c) $\dot{\epsilon}_m$ versus $(C+N+10 \text{ Nb})/\sqrt{d}$; and (d) $\dot{\epsilon}_m$ versus Nb content. Bands in (b) and curve in (c) are visual and were drawn to show the trends.

when plotted as a function of $(C+N)/\sqrt{d}$ (Figs. 3b and 4b) show that grain size, d , plays an important role in heat-to-heat variations. These figures still show the separation of data into two bands, showing the general trend of increasing t_r and decreasing $\dot{\epsilon}_m$ with an increase in $(C+N)/\sqrt{d}$. Figures 3c and 4c show that the data in two bands can be combined by plotting them against $(C+N+10 \text{ Nb})/\sqrt{d}$.

The correlation coefficient R^2 for t_r improved from 31.31 to 65.9 percent in going from $(C+N)/\sqrt{d}$ to $(C+N+10 \text{ Nb})/\sqrt{d}$. Similar improvement in $\dot{\epsilon}_m$ correlations was from 35.50 to 78.03 percent. A correlation coefficient of 100 percent describes the data perfectly. A multiplication factor of 10

required to account for niobium effects indicated that niobium is probably a more potent strengthener than carbon, nitrogen, and the small grain size. In order to check this hypothesis, we have plotted t_r and $\dot{\epsilon}_m$ as a function of niobium content in Figs. 3d and 4d. The correlation coefficients for a least-squares analysis of these plots were 57.53 and 61.0 percent, respectively. The filled and half-filled symbols are for commercial heats with rather high nitrogen content (0.14 percent), Heat 121, and large grain size (280 m), Heat 796, respectively, and therefore they are described better by a $(C+N + 10 Nb)/\sqrt{d}$ relationship (Figs. 3c and 4c). A comparison of correlation coefficients for various chemical composition and grain size parameters indicated that, although a complex relationship like $(C+N + 10 Nb)/\sqrt{d}$ best describes the data, a single term like niobium content can describe most of the heat-to-heat variations in creep data on 20 heats of Type 304 stainless steel.

Experimental Versus Commercial Heats—In order to confirm the importance of niobium in heat-to-heat variations, we remelted Heat 187, which originally contained 20 ppm niobium, and made several experimental heats containing 20 (remelted condition), 50, 100, 200, 500, 700, and 1000 ppm niobium. Heats containing 20, 50, 100, 200, and 500-ppm niobium were made during the first melt. A second melt was used to make 20, 500, 700, and 1000-ppm heats. Since the first and second melts were slightly different in properties, their data have been identified separately.

Creep tests on the experimental heats were performed at 482, 538, 593, and 649°C and the results are summarized in Table 4. Results obtained from experimental and commercial heats are compared in Figs. 5 and 6. These data show a good correlation between creep behavior and niobium content for both experimental and commercial heats and confirm the findings given earlier that variation in niobium content is an important factor in explaining heat-to-heat variations.

Comparisons Between Experimental Heats of Type 304 Stainless Steel and Commercial Heats of Type 347 Stainless Steel—Figures 5 and 6 also include data [10] on commercially available niobium-stabilized Type 347 stainless steel. This steel contains $(Nb \geq 10 C)$ by weight percent, which is 1000 times greater than that in the weakest heat of Type 304 and a factor of 10 greater than in the highest niobium-containing experimental heats. These figures show that t_r does not increase monotonically with increasing niobium, but has a saturation effect beyond 500 to 1000-ppm niobium. Thus, increasing niobium to levels used in Type 347 stainless steel produces no additional improvement in creep properties. However, Type 347 stainless steels with the high niobium content were originally developed for improved resistance to intergranular corrosion attack.

Heat Treatment Effects on Creep Properties of Experimental Heats—Both commercial and experimental heats were annealed for 0.5 h at 1065°C prior to creep testing in the reannealed condition. However, experimental

TABLE 4—Summary of creep data on Type 304 stainless

Test No.	Specimen No.	Condition ^a	Temperature, °C	Stress, MPa	Strain,			
					Loading, e_l	Transient, e_{pc}	Primary, e_1	Secondary, e_2
								20-ppm Nb
9680	187 15	A240	538	317	16.61	0.05	0.10	5.40
9443	187 4	A240	593	117	0.47	1.00	1.25	2.55
9375	187 3	A240	593	207	4.34	1.25	2.80	6.05
9471	187 6	1065	593	207	6.71	2.00	4.63	9.63
9475	187 5	1065	593	241	7.05	0.40	1.00	5.50
9369	187 2	A240	593	241	6.01	0.50	1.30	4.70
14500	187 21	1065	593	241	9.96	1.70	3.78	9.15
9669	187 14	A240	649	172	4.00	1.00	2.45	10.25
								20-ppm
18118	1871 C2	1065	482 ^b	207	2.98
17316	1871 3	1065	583	276	10.09	0.75	2.25	7.25
17347	1871 6	1065	593	172	2.82	1.15	2.10	15.00
16683	1871 1	1065	593	207	5.68	1.50	3.50	13.50
17177	1871 5	1093	649	110	0.69	2.75	8.50	17.50
16880	1871 2	1065	649	110	0.74	2.25
17339	1871 4	1065	649	172	3.31	2.00	3.50	14.00
17913	1871 C1	1065	649	172	2.34	1.50	3.50	16.00
18535	1871 C6	1150	649	172	2.61	2.25	6.00	16.75
								50-ppm
17392	1872 5	1065	538	276	9.46	0.13	1.25	5.00
17502	1872 4	1065	593	172	2.79	3.00	8.75	24.00
16700	1872 1	1065	593	207	5.23	1.50	4.00	9.00
16873	1872 2	1065	649	110	0.80	4.00	6.50	10.00
17337	1872 3	1065	649	172	3.03	2.00	3.50	28.50
								100-ppm
16694	1873 1	1065	593	207	4.37	1.50	2.75	6.00
16874	1873 2	1064	649	110	0.90	3.88	5.00	8.75
17340	1874 3	1065	649	172	2.58	2.50	5.00	15.00
								200-ppm
16697	1874 1	1065	593	207	5.49	1.75	3.00	6.25
17129	1874 2	1065	649	110	0.55	2.00	2.25	4.25
17344	1874 3	1065	649	172	2.78	3.00	5.00	11.50
								500-ppm
18123	1875 C2	1065	482 ^b	207	2.63
17697	1875 5	1065	538	276	7.86	0.625	0.875	2.25
16701	1875 1	1065	593	207	4.00	1.50	1.75	5.00
17527	1875 2	1065	649	110	0.64	1.00	1.25	2.50
17911	1875 C1	1065	649	172	1.78	1.50	2.00	3.00
18567	1875 C6	1150	649	172	2.31	0.75	0.88	1.25
17346	1875 3	1065	649	172	2.92	1.45	2.05	3.10
								700-ppm
18246	1876 B3	1065	482	207	2.41
17912	1876 B1	1065	593 ^c	207	2.55	0.54
17941	1876 B2	1065	649	172	1.80	0.88	1.00	2.00
								1000-ppm
17956	1877 B1	1065	593 ^c	207	2.69	1.08
17958	1877 B2	1065	649	172	1.90	1.25	1.75	2.75
18710	1877 B6	1150	649	172	2.03	0.375	0.425	0.75

^aA240 = as-received; 1065, 1093, and 1150°C indicate annealing temperatures for 0.5 h durations.

^bTests discontinued prior to rupture.

^cTests in progress.

steel containing small niobium additions.

%		Time, h				Minimum Creep Rate, ϵ_m (9%/h)	Reduction of area, %
0.2% Offset, e_s	Fracture, e_f	Primary, t_1	Secondary, t_2	0.2% Offset, t_s	Rupture, t_r		
Commercial							
5.90	30.21	8.5	47.0	49.5	60.7	0.113	27.53
2.93	9.97	3000.0	15500.0	17500.0	22622.2	9625E-5	8.80
6.90	13.44	28.0	85.0	98.0	120.5	0.0525	6.33
10.31	27.71	29.5	87.0	91.0	92.7	0.088	21.35
6.30	22.85	2.0	17.3	19.3	25.8	0.290	22.65
5.70	23.71	2.3	12.5	14.8	18.3	0.335	20.45
10.48	27.28	11.5	40.8	46.7	59.2	0.183	25.22
15.25	35.60	2.8	20.5	25.0	36.8	0.560	31.20
Experimental							
...	2008.4	...	2.86
8.25	39.71	125.0	450.0	515.0	863.0	0.0147	48.86
15.50	65.20	52.0	745.0	770.0	1859.0	0.0184	70.65
15.50	63.36	17.5	97.5	111.3	215.5	0.128	63.13
18.75	69.71	360.0	925.0	1000.0	1871.71	0.0156	64.09
...	1061.3	0.0199	18.78
15.00	80.67	2.5	16.5	18.0	47.1	0.7100	78.10
19.50	56.47	8.0	57.0	69.0	116.5	0.2520	54.50
18.75	47.27	26.0	101.0	113.0	176.9	0.1425	44.47
Experimental							
6.50	52.39	130.0	570.0	700.0	1531.0	0.0087	58.20
26.00	72.10	500.0	1775.0	1900.0	2835.5	0.0126	73.75
10.25	64.09	50.0	142.5	162.5	409.9	0.0530	70.48
11.25	63.88	675.0	1750.0	2075.0	4692.6	0.0033	61.99
29.50	79.50	3.5	52.0	53.6	79.0	0.5100	79.27
Experimental							
7.25	54.70	45.0	150.0	190.0	654.2	0.0290	72.63
9.75	42.97	800.0	3200.0	3700.0	6646.9	0.0017	61.25
16.50	82.48	8.0	47.5	53.0	121.9	0.2600	81.58
Experimental							
7.50	47.26	120.0	450.0	550.0	1249.6	0.0099	62.86
5.00	51.16	475.0	3500.0	3900.0	8295.1	6.5E-4	57.35
13.00	56.40	18.0	80.0	92.0	199.0	0.1075	71.74
Experimental							
...	2183.6	...	2.62
3.250	30.05	900.0	5500.0	7800.0	14585.0	2.9E-4	41.49
6.00	30.62	150.0	2350.0	2750.0	6121.9	1.5E-3	47.61
3.00	45.10	500.0	3600.0	4300.0	11404.2	3.75E-4	62.41
3.50	38.27	90.0	290.0	350.0	1097.3	0.0048	35.04
1.75	37.19	40.0	300.0	430.0	1186.7	0.0019	46.91
4.05	55.21	50.0	135.0	195.0	545.0	0.0121	72.41
Experimental							
...	2033.0	...	2.91
...	14373.0	2.2E-4	...
2.75	29.08	50.0	400.0	550.0	1592.1	0.0029	43.45
Experimental							
...	13627.0	4.3E-4	...
3.50	43.29	120.0	330.0	440.0	1433.9	0.0048	56.76
1.125	41.46	12.5	525.0	800.0	2695.4	0.00065	53.86

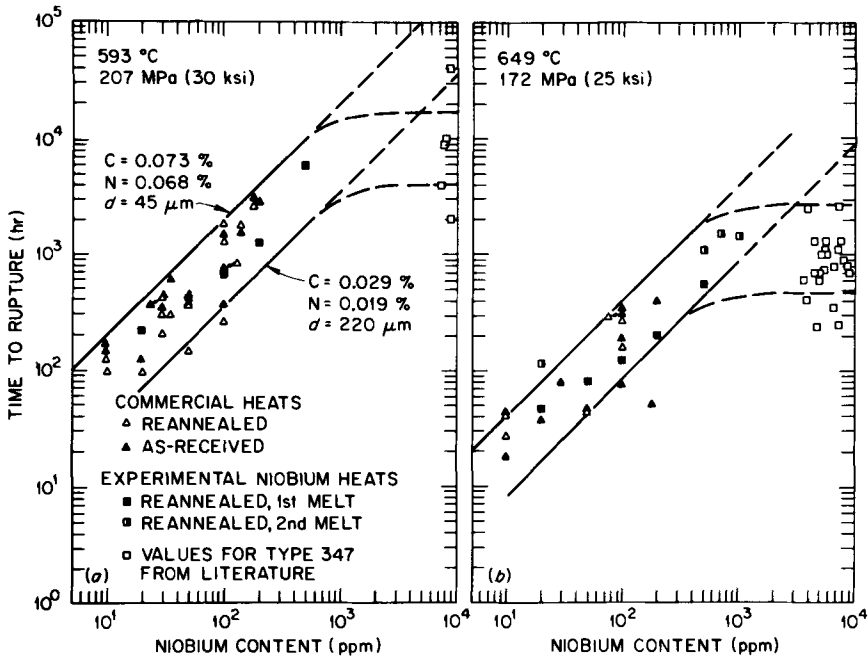


FIG. 5—Time to rupture as a function of niobium content for the commercial and experimental heats of Type 304 stainless steel and commercial heats of Type 347. (a) At 593°C and 207 MPa, and (b) at 649°C and 172 MPa. Bands in these plots are visual and were drawn to show the trends.

heats containing 20, 500, and 1000-ppm niobium were also annealed for 0.5 h at 1150°C to check their response to heat treatment temperature. Results of these tests, included in Table 4, show that the higher annealing treatment produces slightly lower creep rates with improved rupture life. Thus, experimental heats containing varying amounts of niobium appear stable to high heat treatment temperatures.

Comparison of Experimental Heat Behavior with that of Commercial Heats of Type 304 and 316 Stainless Steel—Figure 7a shows a comparison of rupture data obtained from the experimental niobium-containing heats with upper and lower statistically defined data bounds observed for Type 304 stainless steel. These bounds were developed by Sikka and Booker [11] on the creep data collected from various sources in the United States. The upper and lower bounds represent expected ± 2 standard error of estimates (SEE) in $\log t_r$. Figure 7b shows a similar comparison with the upper and lower bound observed for Type 316 stainless steel. For the sake of clarity, this figure includes only data on 20, 500, 700, and 1000-ppm niobium heats. From Fig. 7a we can see that while the 20-ppm heat falls close to the

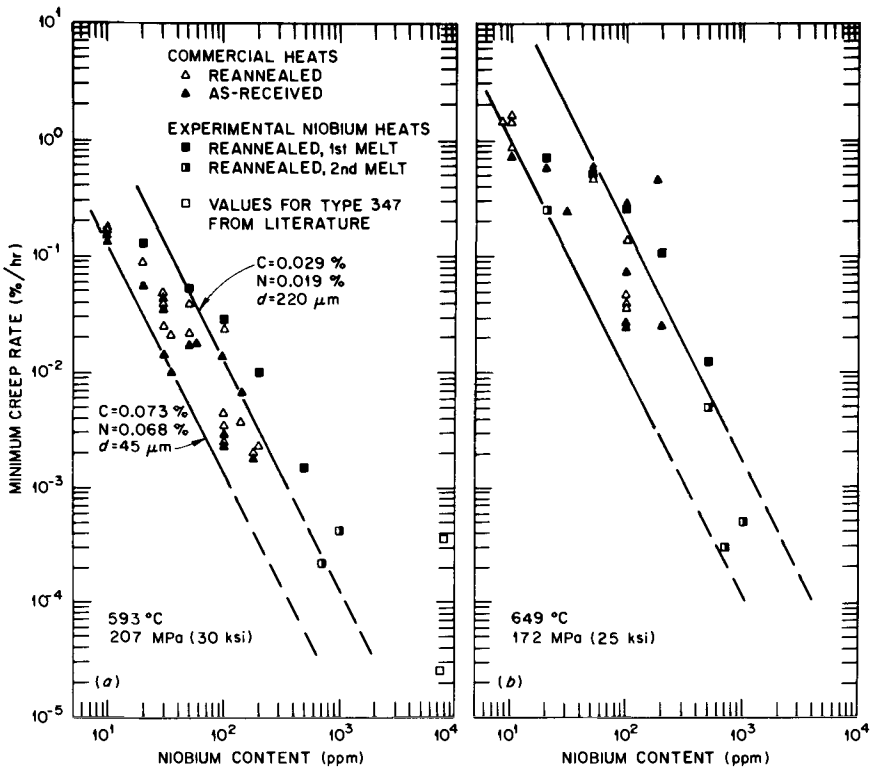


FIG. 6—Minimum creep rate as a function of niobium content for the commercial and experimental heats of Type 304 stainless steel and commercial heats of Type 347. (a) At 593°C and 207 MPa, and (b) at 649°C and 172 MPa. Bands in these plots are visual and were drawn to show the trends.

lower bound, heats containing 500 ppm and higher niobium fall close to the upper bound for Type 304 stainless steel. Figure 7b shows that the 500 ppm and higher niobium heats also fall above average or closer to the upper bound for Type 316 stainless steel. Figures 5a and 6a have already shown that experimental heats containing 500 to 1000-ppm niobium heats have creep and creep-rupture properties similar to those of Type 347, which contains ($Nb = 10 C$). Thus, we have observed from the experimental heats that variations in niobium content at small concentration levels can result in substantial heat-to-heat variations in creep response, but increasing the niobium content improved results in creep and creep-rupture properties of Type 304 stainless steel.

Creep Properties at Low Temperatures—Creep and creep-rupture properties have thus far been described only at high temperatures of 593 and 649°C. However, these steels may have to operate in many instances be-

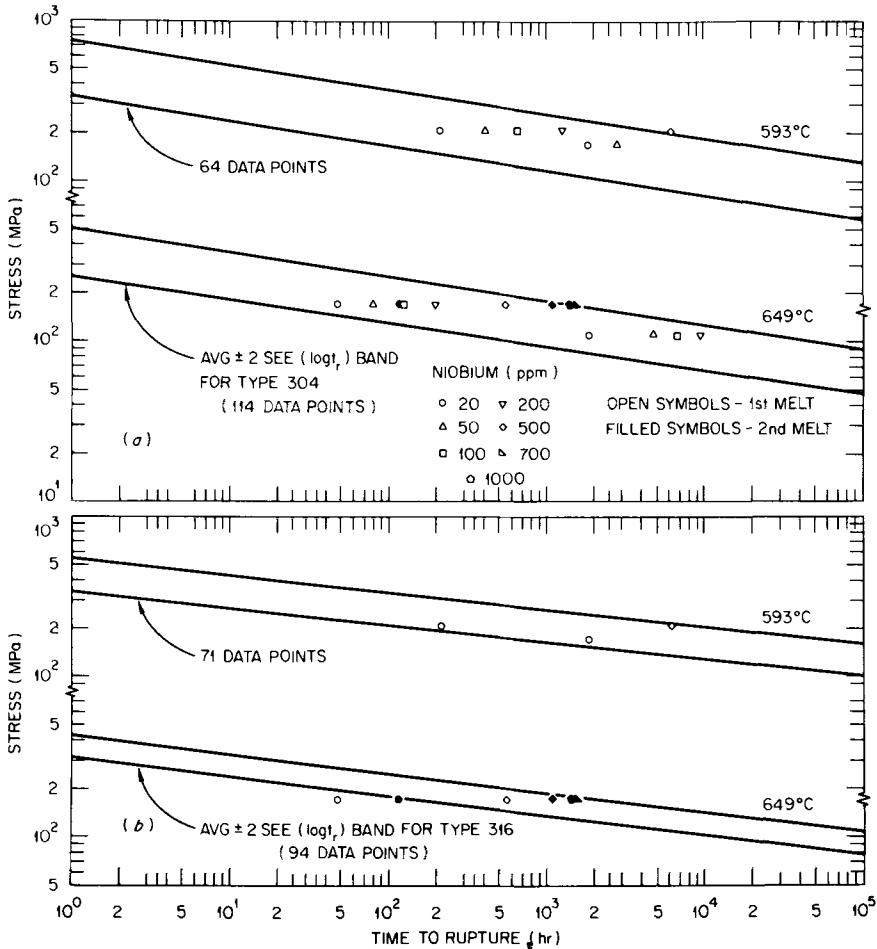


FIG. 7—Comparison of time-to-rupture data on niobium-containing heats with upper and lower data scatter bounds for Types 304 and 316 stainless steels at 593 and 649°C. (a) Type 304; (b) Type 316.

tween 427 and 538°C if used in breeder reactor applications. Thus, a few creep tests were performed at 482 and 538°C and their results are shown in Fig. 8a and b. The creep curves in this figure clearly show a significant improvement in creep resistance of steels containing 500 ppm and higher niobium content even at low test temperatures. Thus, small additions of niobium not only improve creep and creep-rupture properties at high temperatures but at low temperatures as well.

Creep Time (t_s) and Strain (ε_s) to Onset of Tertiary Creep—These properties are plotted as a function of niobium content in Figs. 9 and 10. These figures show that t_s increases with increasing niobium, while ε_s de-

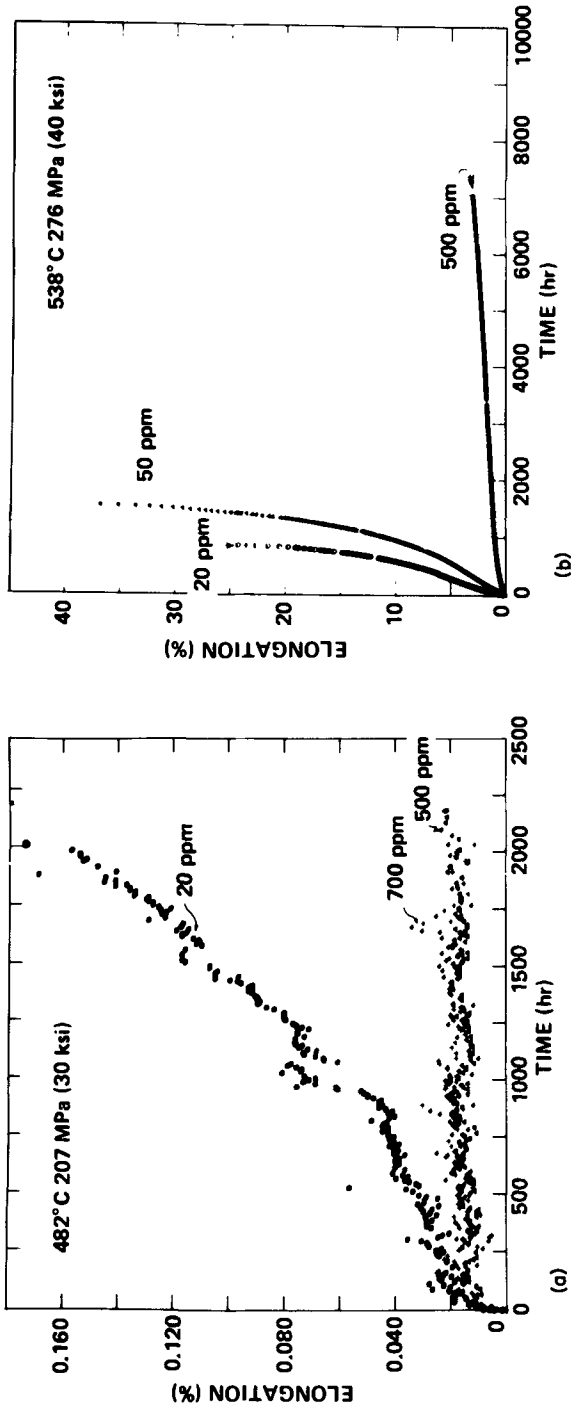


FIG. 8—Creep curves for experimental heats of Type 304 stainless steel containing various amounts of niobium. (a) At 482 and 207 MPa; (b) at 538 and 276 MPa. Note the significant improvement in creep resistance for heats containing 500-ppm niobium.

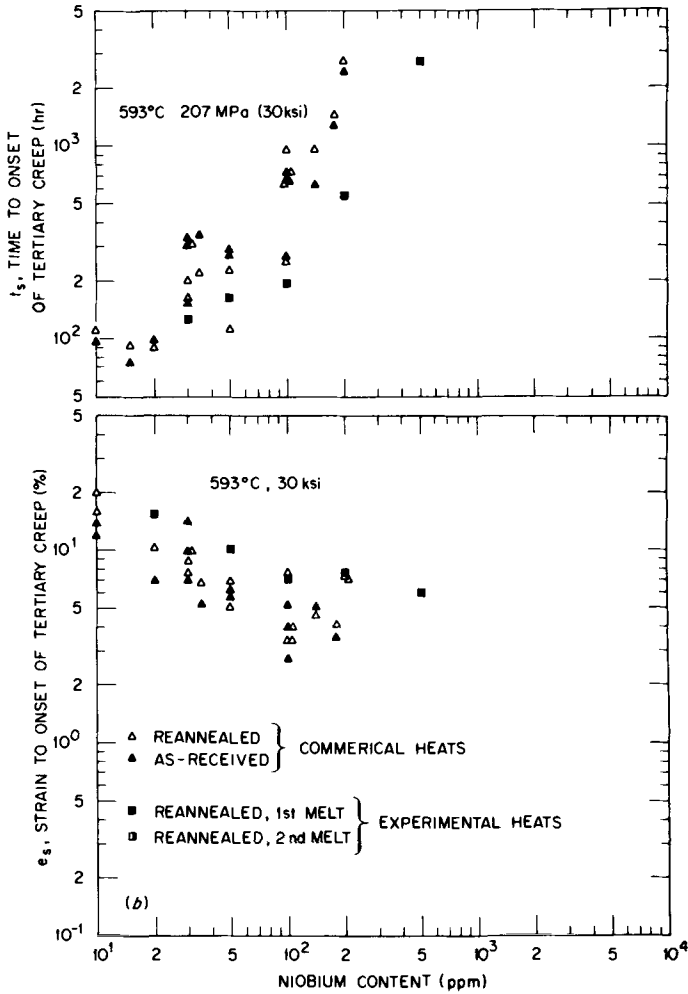


FIG. 9—Tertiary creep data as a function of niobium content for commercial and experimental heats of Type 304 stainless steel at 593°C and 207 MPa. (a) Time to onset of tertiary creep; (b) strain to onset of tertiary creep.

creases, and also that there is excellent agreement between the commercial and experimental heats with respect to behavior based on niobium content. The increase in t_s with increasing niobium content suggests that the improved properties of niobium-containing steels are derived not only from delaying the rupture process, but also from the overall creep deformation process.

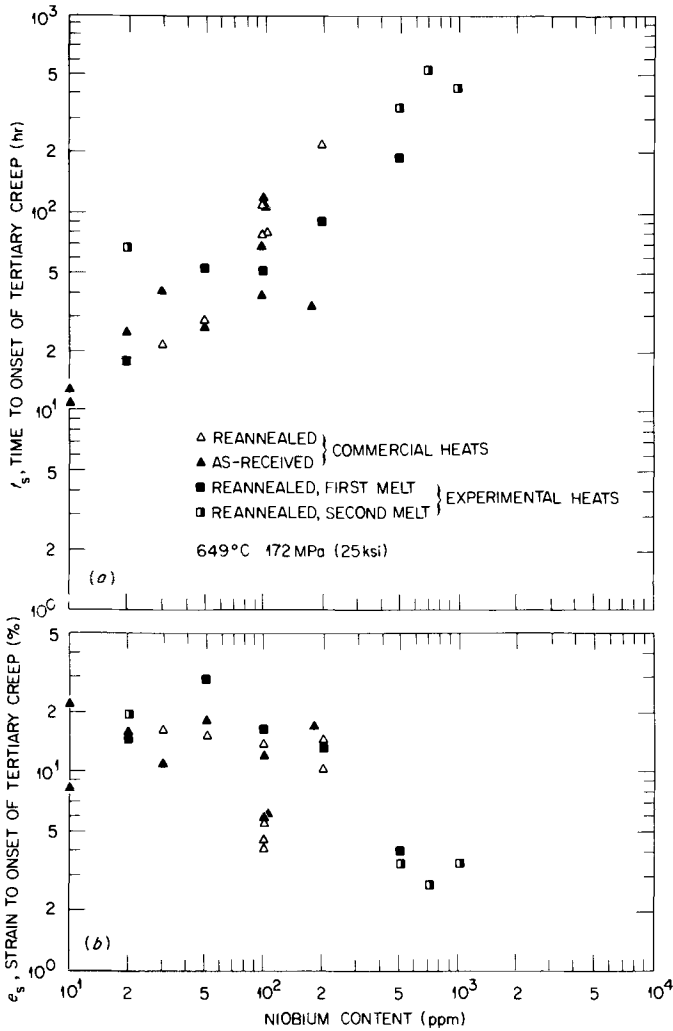


FIG. 10—Tertiary creep data as a function of niobium content for commercial and experimental heats of Type 304 stainless steel at 649°C and 172 MPa. (a) Time to onset of tertiary creep; (b) strain to onset of tertiary creep.

In a previous paper Booker and Sikka [12] have shown that t_s is related to t_r by

$$t_s = 0.752t_r^{0.977} \tag{1}$$

Equation 1 is valid over a temperature range of 482 to 816°C. Figure 11 shows a comparison of data on experimental heats with the average and

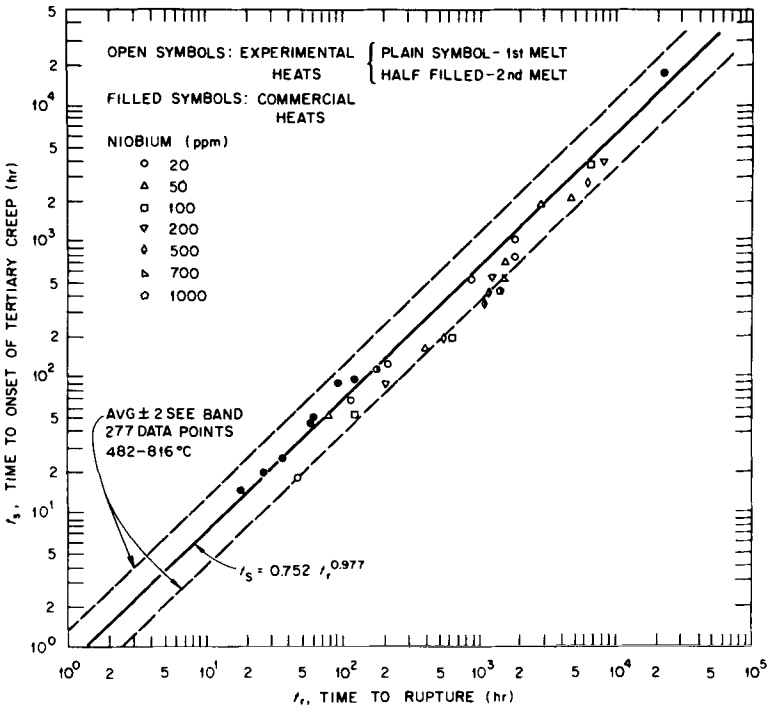


FIG. 11—Comparisons of time to onset of tertiary (t_s) creep data on experimental niobium heats with the average and upper and lower bounds of t_s versus t_r for Type 304 stainless steel.

upper and lower bounds derived from Eq 1. This figure shows that the data on experimental heats are still within the upper and lower bounds, but on the lower side for the higher niobium heats, which suggests that t_s may be a lower fraction of t_r for these heats compared with Type 304 stainless steel. However, the results in Figs. 9a and 10a have shown that, besides being a lower fraction of t_r , t_s still increases with increasing niobium content. Thus, it can be concluded that increasing niobium content of Type 304 stainless steel does not cause any premature occurrence of the onset of tertiary creep.

Creep-Rupture Ductility—Figure 12a and b shows total creep elongation for the experimental niobium-containing heats and for Type 347 stainless steel compared with the upper and lower bound [11] for Type 304 stainless steel. These figures show that total elongation values of Type 347 heats fall below the lower bound for Type 304 and even reach values as low as 1 percent. However, total elongation values for the experimental niobium-containing heats fall close to the upper bound.

Correlation Between Tensile and Creep Properties—Tension tests were performed on the experimental heats (Table 5) at the creep test tempera-

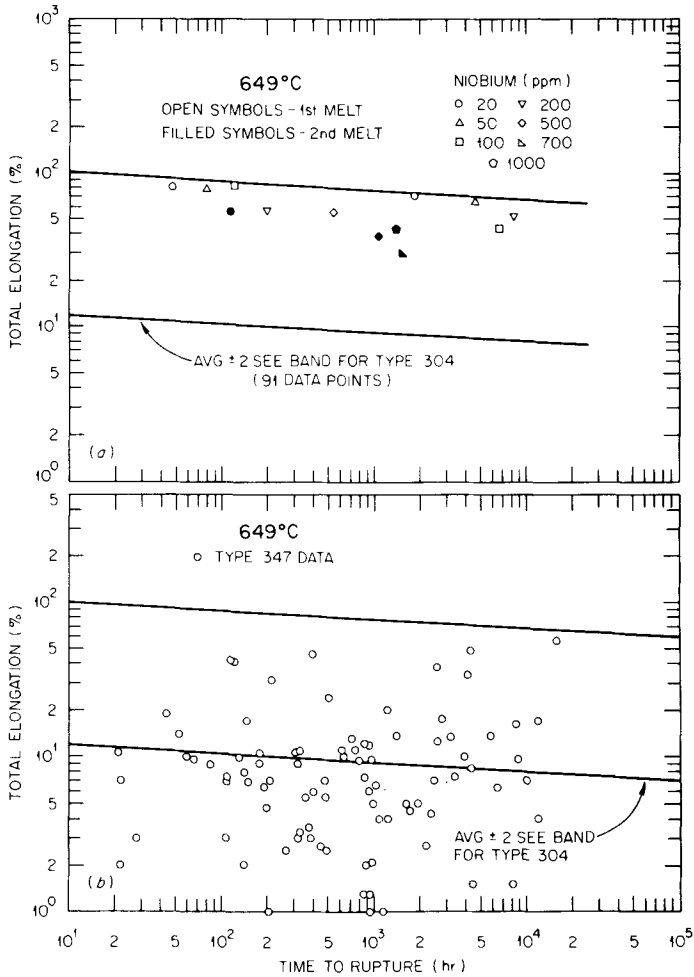


FIG. 12—Comparison of creep total elongation data on experimental niobium heats and commercial heats of Type 347 stainless steel with upper and lower bounds for Type 304 stainless steel. (a) Experimental niobium heats; (b) Type 347.

ture to check the validity of previously developed [13] models of t_r and $\dot{\epsilon}_m$ containing elevated-temperature ultimate tensile strength (U) terms, which are given by

$$\log t_r = 5.716 - 3915 \frac{\log \sigma}{T} + 32.60 \frac{U}{T} - 0.007303 U \log \sigma \quad (2)$$

$$\log \dot{\epsilon}_m = 2.765 + 3346 \frac{\log \sigma}{T} - 51.83 \frac{U}{T} + 0.01616 U \log \sigma \quad (3)$$

for σ and U in MPa and T in K.

TABLE 5—Summary of tensile data on Type 304

Test No.	Specimen No.	Condition	Temperature, °C	Proportional Limit	Stress,	
					Yield	
					0.02%	
18248	1871 C3	1065	593	57 (8.2)	20-ppm 87 (12.6)	
18713	1871 C4	1065/1250	593	55 (7.9)	72 (10.4)	
18984	1871 C5	1093	649	42 (6.1)	66 (9.6)	
18751	1872 6	1065	649	52 (7.5)	50-ppm 76 (11.0)	
18763	1873 5	1065	593	41 (5.9)	100-ppm 79 (11.4)	
18758	1873 6	1065	649	56 (8.1)	83 (12.0)	
18764	1874 5	1065	593	35 (5.1)	200-ppm 66 (9.5)	
18759	1874 6	1065	649	56 (8.1)	84 (12.2)	
18755	1875 4	1065	593	66 (9.6)	500-ppm 94 (13.6)	
18756	1875 6	1065	593	63 (9.2)	93 (13.5)	
18249	1875 C3	1065	593	77 (11.2)	101 (14.6)	
18714	1875 C4	1065/1250	593	47 (6.8)	72 (10.4)	
18985	1875 C5	1093	649	48 (6.9)	75 (10.8)	
18250	1876 B6	1065	593	70 (10.2)	700-ppm 101 (14.7)	
18715	1876 B4	1065/1250	593	44 (6.4)	63 (9.1)	
18986	1876 B5	1093	649	62 (9.0)	89 (12.9)	
18251	1877 B3	1065	593	65 (9.4)	1000-ppm 103 (15.0)	
18987	1877 B4	1065	649	57 (8.2)	93 (13.5)	

The predicted values from Eqs 2 and 3 are compared with the data on experimental niobium-containing heats in Figs. 13 and 14. These figures show excellent agreement between the predicted and the experimental values. Furthermore, they provide additional support as to the applicability of previously published [12] relationships between tensile and creep properties in predicting the creep properties of newly developed experimental heats of essentially Type 304 stainless steel.

The use of U in predicting creep properties of experimental heats (Figs. 13 and 14) and the correlation between the creep properties of niobium content (Figs. 5 and 6) require that U and niobium concentration be related. This is shown in Fig. 15. Although there is considerable scatter (possibly due to other factors discussed by Booker and Sikka [5]), the trend is evident that U increases with increasing niobium content. Furthermore, U values on experimental heats from the first melt show excellent agreement with the data on commercial heats. Reasons for higher values of U observed for experimental heats from the second melt (Fig. 15a and

stainless steel containing small niobium additions.

Mpa (ksi)		Elongation		
0.2%	Ultimate	Uniform	Total 25.4 mm	Reduction of area, %
Experimental				
109 (15.8)	409 (59.3)	28.18	37.70	70.14
81 (11.7)	434 (63.0)	29.93	37.85	59.27
98 (14.2)	344 (49.9)	28.51	52.60	65.43
Experimental				
99 (14.3)	297 (43.0)	32.22	63.60	78.06
Experimental				
105 (15.2)	369 (53.5)	35.76	48.65	76.67
100 (14.5)	301 (43.6)	31.76	59.55	79.11
Experimental				
106 (15.3)	376 (54.5)	32.34	46.40	77.17
102 (14.8)	306 (44.3)	32.52	59.90	80.22
Experimental				
106 (15.3)	383 (55.5)	35.35	47.20	75.75
107 (15.5)	380 (55.1)	33.10	44.10	75.52
113 (16.4)	429 (62.2)	27.51	38.50	70.47
81 (11.7)	452 (65.6)	30.06	32.80	55.88
102 (14.8)	368 (53.5)	27.82	44.60	69.40
Experimental				
117 (17.0)	456 (66.1)	27.20	38.00	66.87
84 (12.2)	470 (68.1)	26.03	30.55	48.76
107 (15.5)	393 (57.0)	27.33	41.25	66.29
Experimental				
121 (17.5)	449 (65.1)	28.08	36.15	68.95
117 (16.9)	380 (55.1)	28.20	44.65	70.91

b) are not clear, but the effect of these values was reflected in the creep properties.

Strauss Test and Hot-Cracking Results

Niobium is added to stabilized Type 347 stainless steel to improve its resistance to intergranular attack. However, this steel suffers from cracking [14] in the heat-affected zone on welding thick sections. Thus, when experimental heats are developed, the following points should be considered regarding an optimum niobium yielding improved creep properties:

1. Too little niobium may yield poor intergranular corrosion resistance properties depending upon the intended application.
2. Too much niobium may produce cracking in the heat-affected zone on welding thick sections.

Strauss tests [ASTM Recommended Practices for Detecting Susceptibility to Intergranular Attack in Stainless Steels (A 262-70; Practice E)] [15] were performed on experimental heats with varying niobium content,

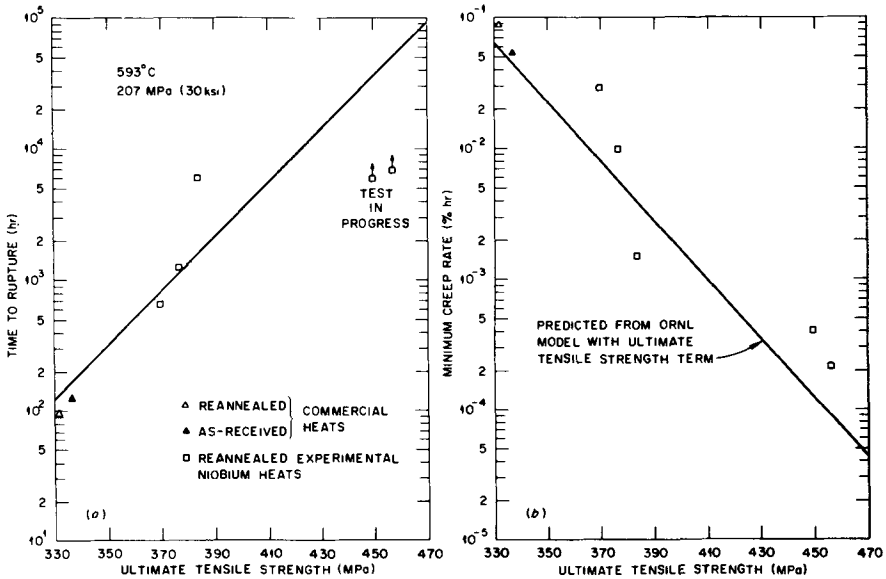


FIG. 13—Plots of creep data on experimental niobium heats at 593°C and 207 MPa as a function of ultimate tensile strength at the creep test temperature. (a) Time to rupture; (b) minimum creep rate. Plots also include predicted curves from ORNL models containing an elevated-temperature ultimate tensile strength term.

a commercial heat of Type 304 containing 200-ppm niobium, and a commercial heat of Type 347 stainless steel. All heats were sensitized for 0.5 h at 677°C. Photomicrographs of the U-bend test specimens and the microstructure taken in the maximum tensile stress region of the U-bends are shown in Fig. 16. The extent of intergranular attack was measured by crack facet length (CFL), which was defined as

$$CFL = n \times d \tag{4}$$

where

- n = number of cracked facets per unit area, and
- d = facet length \approx 1/2 average grain intercept.

The CFL values were calculated from micrographs in Fig. 16 and are plotted as a function of niobium content in Fig. 17. This figure shows that CFL drops sharply with increasing niobium content and its values for 500-ppm heat are only 20 percent of those observed for Type 304.

Moorhead et al [7] performed welding tests using a Tigamajig machine on experimental heats with varying niobium content. They showed that

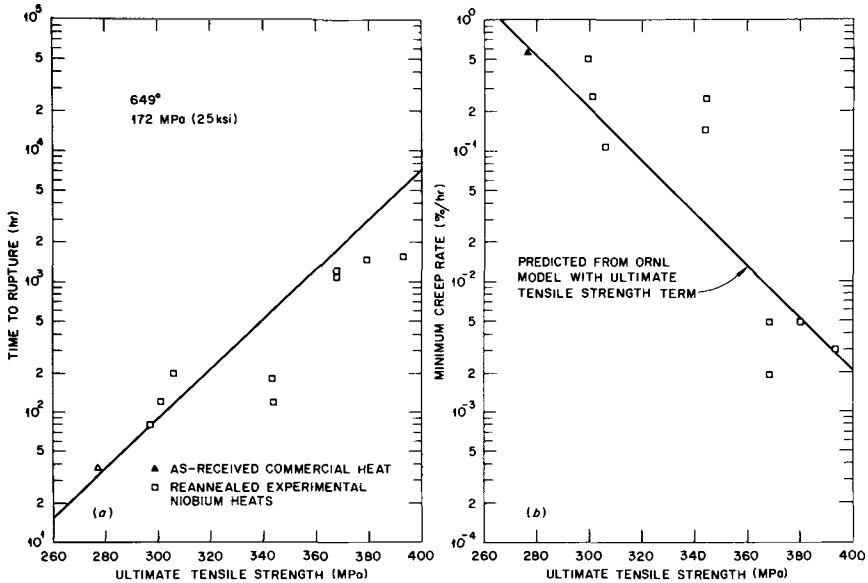


FIG. 14—Plot of creep data on experimental niobium heats at 649°C and 172 MPa as a function of ultimate tensile strength at the creep test temperature. (a) Time to rupture, (b) minimum creep rate. Plots also include predicted curves from ORNL models containing an elevated-temperature ultimate tensile strength term.

heats containing 500 to 1000-ppm niobium were similar in welding behavior to Type 304 in that they retained resistance to cracking in the heat-affected zone compared with extensive cracking observed in Type 347 for the same test conditions. Details of the welding procedure and data analysis are available in the paper by Moorhead et al [7].

Optical and Transmission Electron Microscopy

Optical micrographs for creep specimens tested at 649°C and 172 MPa are shown in Figs. 18 and 19. Micrographs in Fig. 18 are for specimens taken from first melt and those in Fig. 19 are for specimens taken from second melt. Microstructures in Figs. 18 and 19 are for specimens annealed for 0.5 h at 1065°C prior to creep testing. Figure 20 compares micrographs for specimens annealed for 0.5 h at 1150°C. All specimens showed extensive intragranular deformation. Some intergranular cavitation was observed, but fracture appeared to be transgranular. Grain sizes for Melts 1 and 2 showed no significant difference (Figs. 18 and 19). The grain sizes of 20- and 500-ppm heats were essentially the same even after annealing at 1150°C. However, the grain size for the 1150°C anneal was coarser than the 1065°C anneal.

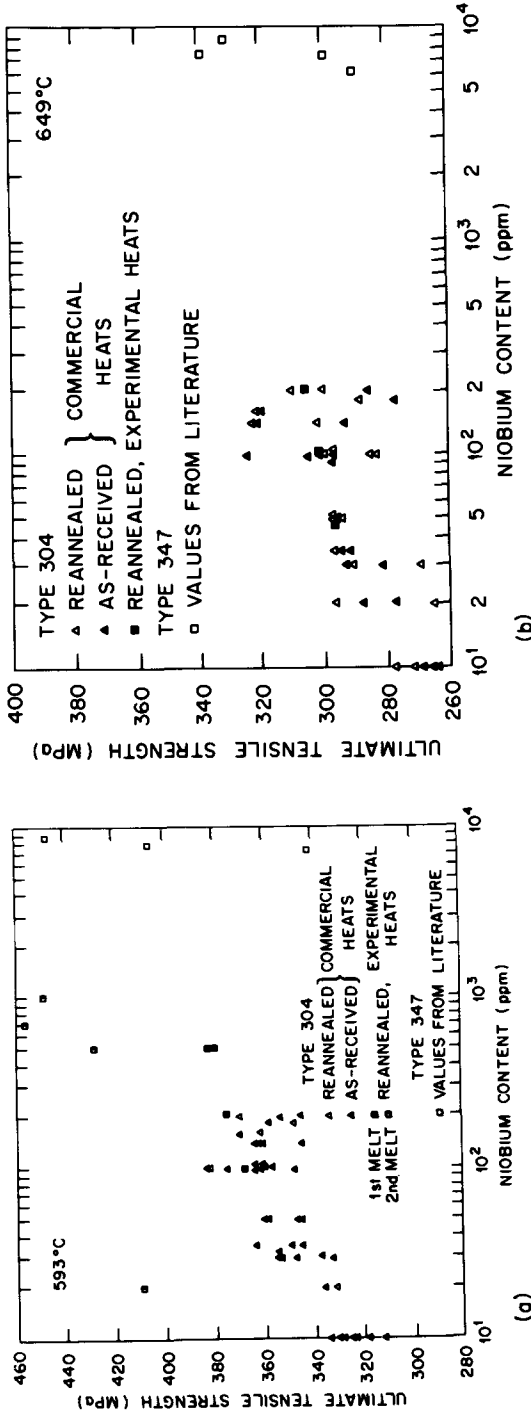


FIG. 15—Plots of ultimate tensile strength as a function of niobium content for commercial and experimental heats of Type 304 and commercial heats of Type 347 stainless steel. (a) 593°C; (b) 649°C.

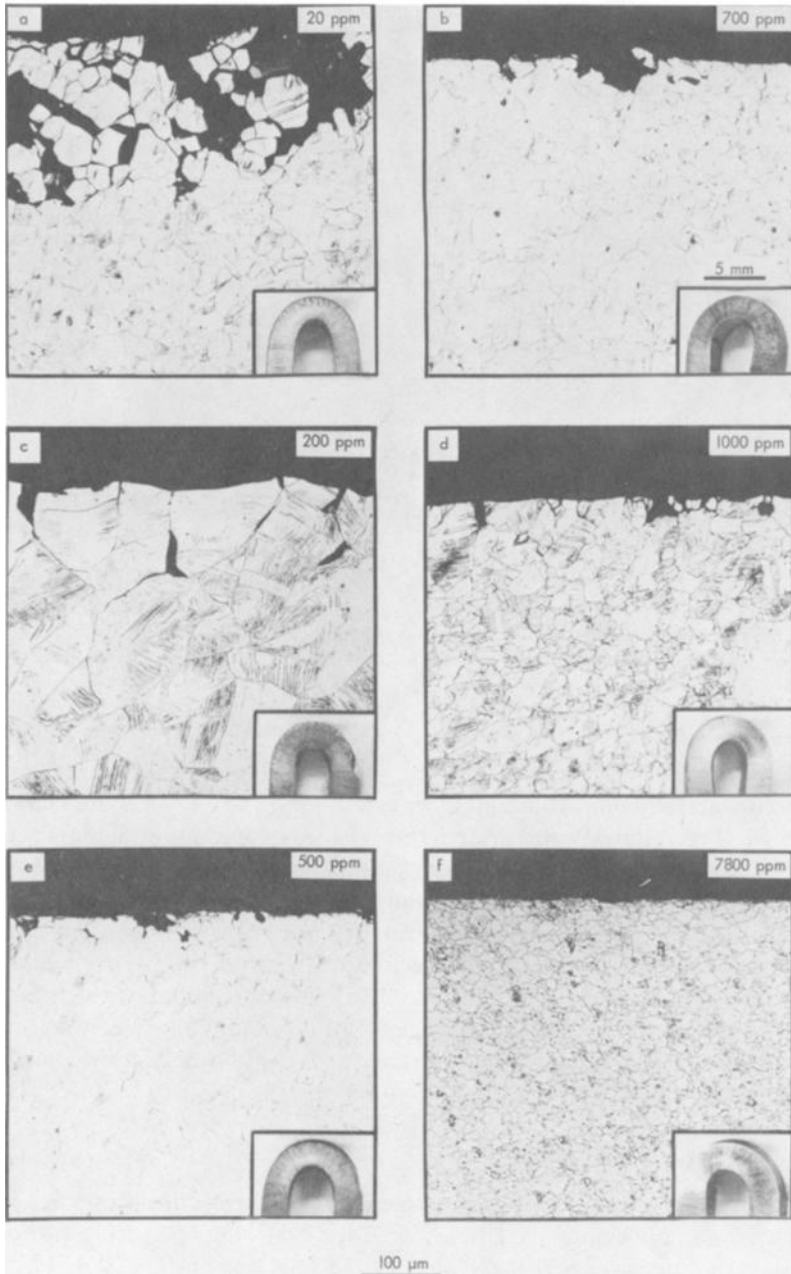


FIG. 16—Micrographs showing improvement in intergranular resistance as a function of increasing niobium (20 to 1000 ppm) in experimental heats of Type 304 stainless steel. For comparison, a micrograph on commercial heats of Type 347 is also included.

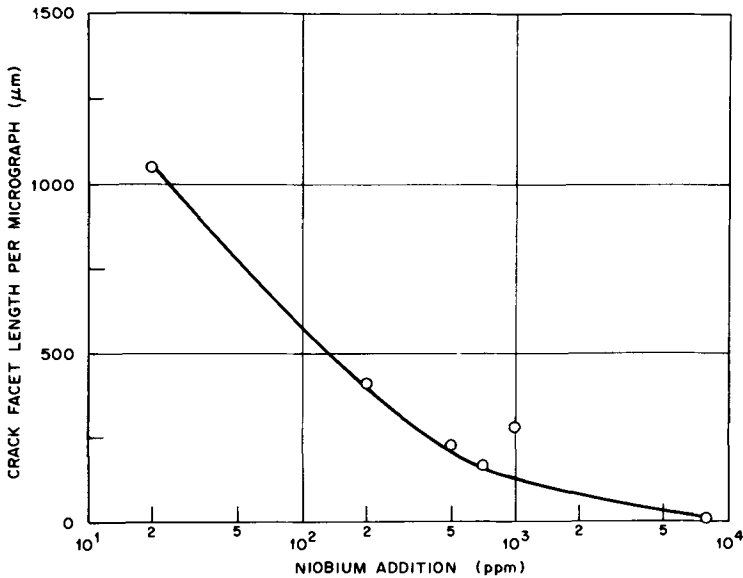


FIG. 17—Plot of crack facet length (CFL) as a function of niobium content for experimental heats of Type 304 stainless steel and a commercial heat of Type 347. The CFL values in this plot are from same size micrographs on each heat.

Transmission electron photomicrographs of the annealed specimens of experimental niobium-containing heats and for Type 347 steel are shown in Fig. 21. Precipitates were observed in all heats containing niobium. However, these precipitates were semicoherent (showed no electron diffraction spots) for niobium content less than 1000 ppm and incoherent for the higher niobium levels. The incoherent precipitates were identified as niobium-carbon type. Most of the precipitates were in the matrix while the grain boundaries were clean. It is probably these precipitates which impart improved creep and other properties by either modifying size, shape, and distribution of $M_{23}C_6$ or changing relative nucleation and growth of these precipitates at grain boundaries and in the matrix.

Summary and Conclusions

Large heat-to-heat variations in creep and creep-rupture properties were observed for 20 commercial heats of Type 304 stainless steel. Although these variations were best correlated by the relationship $(C+N + 10 Nb)/\sqrt{d}$, niobium alone could account for most variations with the exception of a high-nitrogen heat (121) and a coarse-grain heat (796). Experimental heats confirmed the importance of small niobium content in causing

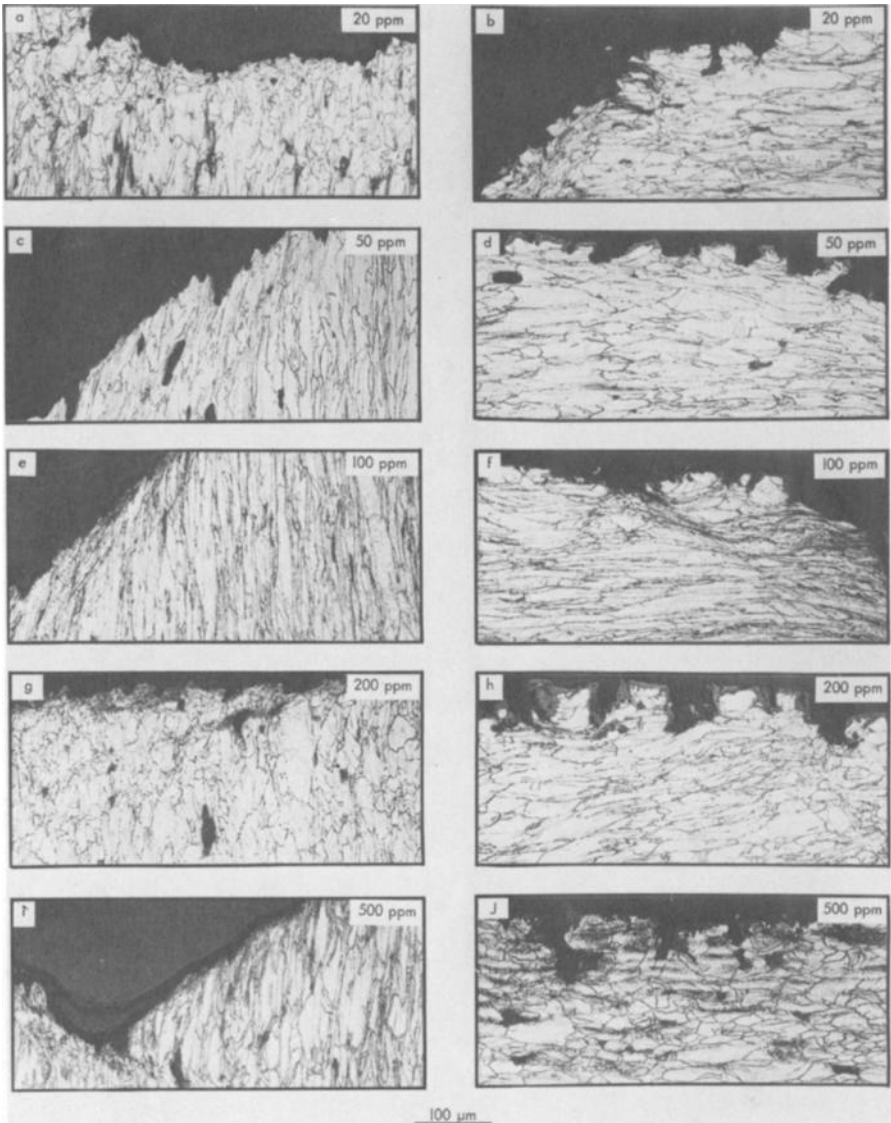


FIG. 18—Micrographs showing fracture and edge near the fracture for specimens creep tested at 649°C and 172 MPa. (a) and (b) 20 ppm; (c) and (d) 50 ppm; (e) and (f) 200 ppm; (g) and (h) 500 ppm. All specimens were annealed at 1065°C for 0.5 h prior to creep testing. Note that there are no significant differences between the fracture of specimens containing various niobium content.

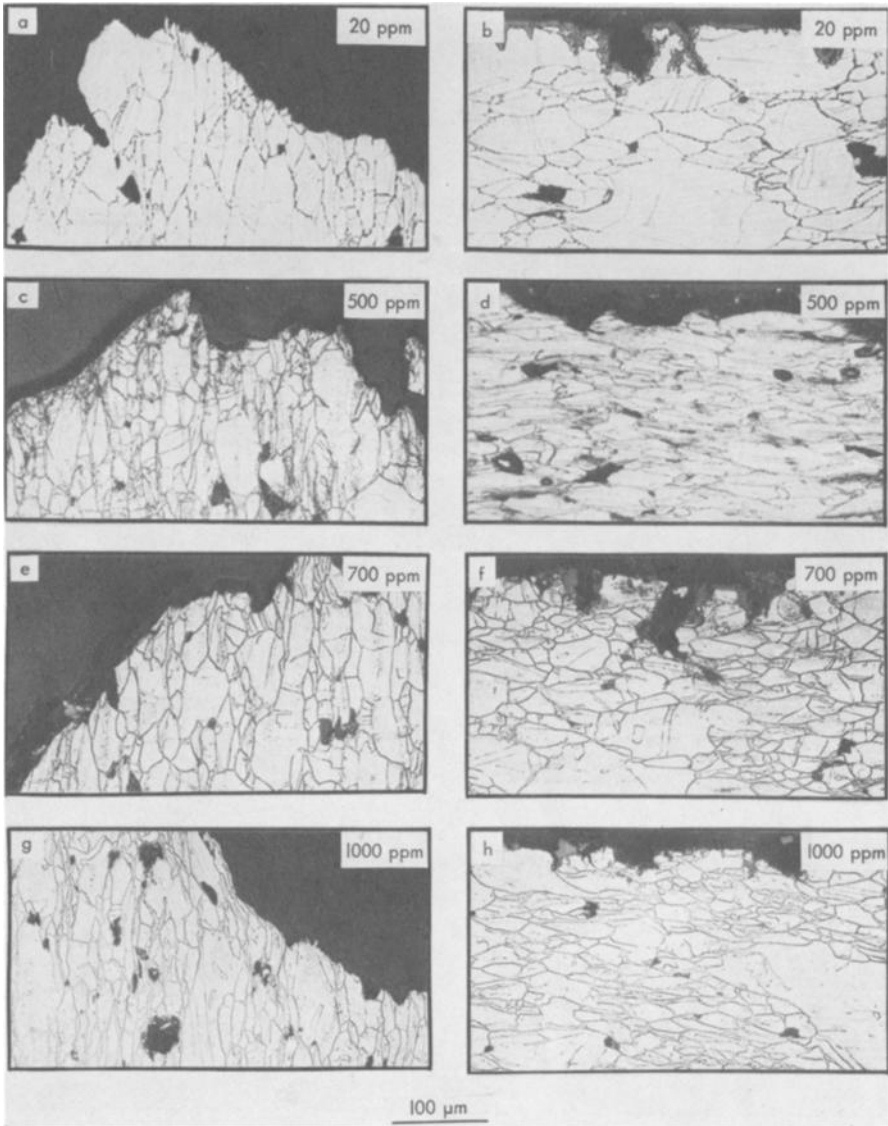


FIG. 19—Micrographs showing fracture and edge near the fracture for specimens creep tested at 649°C and 172 MPa. (a) and (b) 20 ppm; (c) and (d) 500 ppm; (e) and (f) 700 ppm; and (g) and (h) 1000 ppm. All specimens were from second melt and were annealed at 1065°C for 0.5 h prior to creep testing. Note that there are no obvious microstructural differences between the first and second melt.

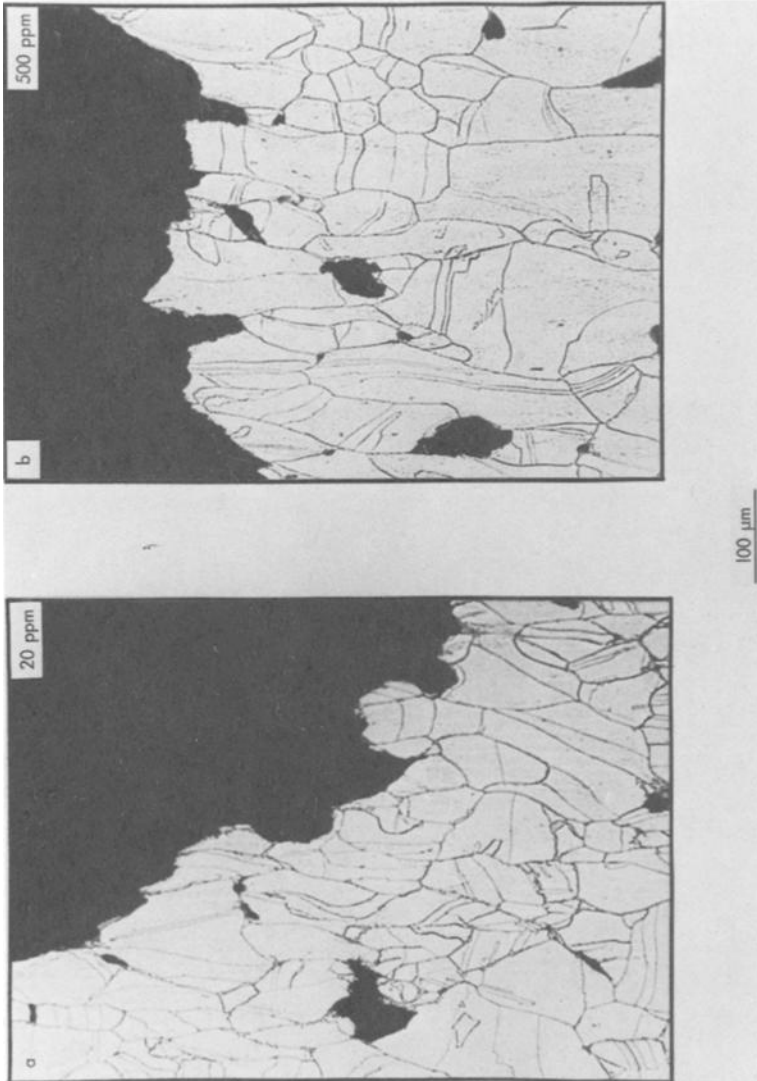


FIG. 20—Micrographs showing fracture for specimens annealed at 1150°C for 0.5 h and creep tested at 649°C and 172 MPa. (a) 20 ppm and (b) 500 ppm. The 1150°C annealed specimens had slightly coarser grain size than observed in Figs. 18 and 19 for the 1065°C annealed specimens.

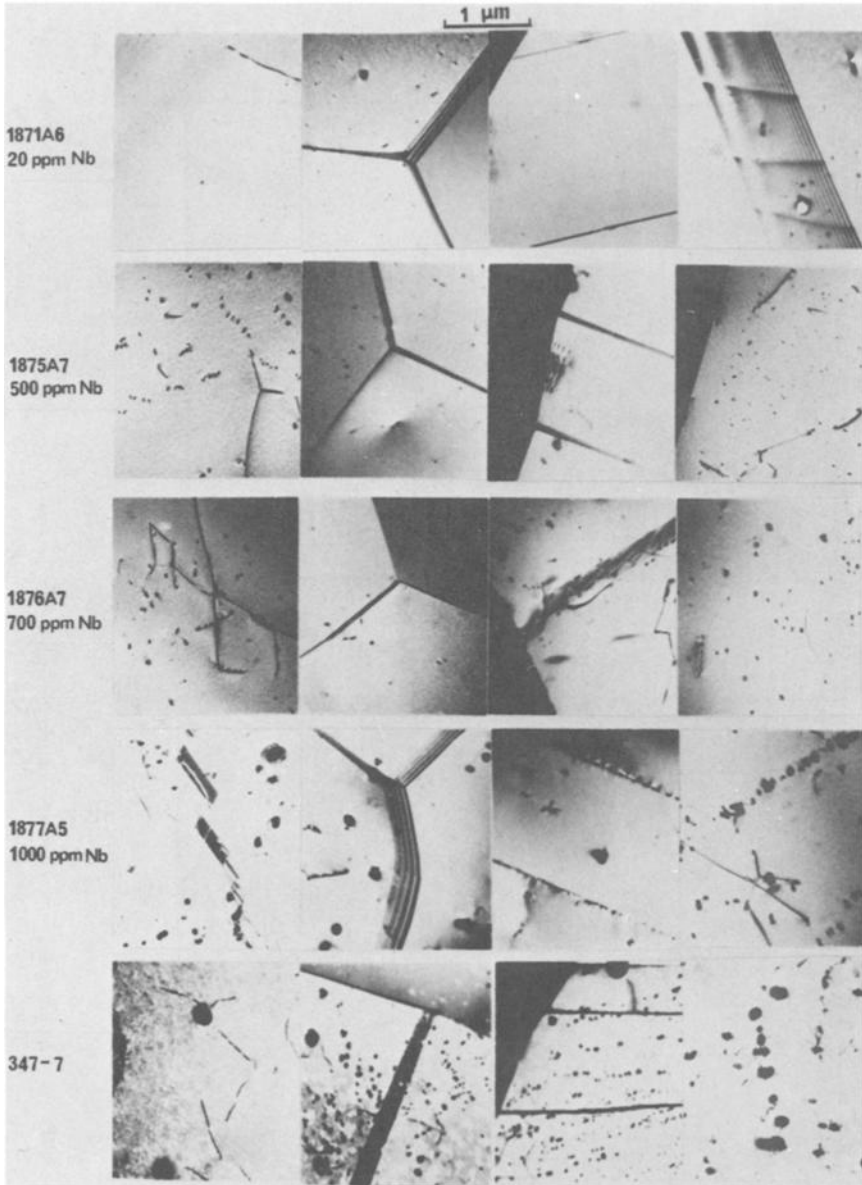


FIG. 21—Transmission electron micrographs for experimental heats of Type 304 containing varying amounts of niobium and on a commercial heat of reannealed Type 37 stainless steel. Note the difference in precipitation with increasing niobium content.

heat-to-heat variations in commercial heats of Type 304 stainless steel. The following are some important conclusions from this work:

1. Time to rupture (t_r) for commercial and experimental heats increased and minimum creep rate ($\dot{\epsilon}_m$) decreased with increasing niobium content, and these properties saturated beyond 500 and 1000 ppm to the 10^4 -ppm level. The saturated values of t_r were higher for high (C+N) content and fine-grain material.

2. Experimental heats of Type 304 stainless steel containing 500-ppm niobium resulted in improved creep and creep-rupture properties at both low (482 and 538°C) and high temperatures (593 and 649°C) investigated.

3. Creep-rupture times and minimum creep rate behavior for experimental heats of varying niobium content could be estimated from a knowledge of their elevated-temperature ultimate tensile strength values.

4. The creep-rupture strength for experimental heats of Type 304 stainless steel containing 500-ppm niobium was comparable to that of Type 347 stainless steel, but with significantly higher ductility.

5. Type 304 stainless steel containing 500-ppm niobium offers superior creep and creep-rupture properties with improved ductility, a factor of approximately 5 better corrosion resistance, and still retains welding response similar to Type 304 stainless steel [7]. It should be noted, however, that the effect of niobium on the creep-rupture properties of Type 304 stainless steel weldments is unknown.

Acknowledgments

We gratefully acknowledge R. L. Hendricks for making the experimental heats, L. T. Ratcliff for performing tension tests, R. H. Baldwin and C. O. Stevens for performing creep tests, J. C. Griess, Jr. for helping in corrosion testing, A. J. Moorhead for performing the welding tests, C. W. Houck for metallography, and H. Jang and J. Moteff (University of Cincinnati) for performing the transmission electron microscopy. We are also thankful to J. R. DiStefano and J. R. Keiser for reviewing, G. M. Slaughter and P. Patriarca for approving, and Linda Croff for typing the manuscript.

References

- [1] Sikka, V. K., McCoy, H. E., Booker, M. K., and Brinkman, C. R., *Journal of Pressure Vessel Technology*, Vol. 97, 1975, pp. 243-251.
- [2] McCoy, H. E., "Tensile and Creep Properties of Several Heats of Type 304 Stainless Steel," ORNL/TM-4709, Oak Ridge National Laboratory, Oak Ridge, Tenn., November 1974.
- [3] Brinkman, C. R. and Korth, G. E., *Journal of Nuclear Technology*, Vol. 48, 1973, pp. 293-306.
- [4] Diercks, D. R. and Raske, D. T., "Elevated Temperature Strain Controlled Fatigue Data of Type 304 Stainless Steel—A Compilation, Multiple Linear Regression Model

- and Statistical Analysis," ANL-76-95, Argonne National Laboratory, Argonne, Ill., 1976.
- [5] Booker, M. K. and Sikka, V. K., "Effect of Composition Variables on the Tensile Properties of Type 304 Stainless Steel," ASTM Symposium on The Effect of Carbon, Nitrogen, and Residual Elements on the Austenitic Stainless Steels and Their Weldments, American Society for Testing and Materials, Atlanta, Ga., 14-15 Nov. 1977.
- [6] James, L. A., this publication, pp. 3-16.
- [7] Moorhead, A. J., Sikka, V. K., and Reed, R. W., this publication, p. 103-123.
- [8] *Annual Book of ASTM Standards*, Part 31, American Society for Testing and Materials, 1971, pp. 470-483.
- [9] Heger, J. J. and Smith, G. V., *Elevated Temperature Properties as Influenced by Nitrogen Additions to Types 304 and 316 Austenitic Stainless Steel*, ASTM STP 522, American Society for Testing and Materials, 1968, pp. 000-000.
- [10] Simmons, W. F. and van Echo, A. J., "The Elevated Temperature Tensile Properties of Stainless Steel," ASTM Data Series D55S1, American Society for Testing and Materials, 1965.
- [11] Sikka, V. K. and Booker, M. K., *Journal of Pressure Vessel Technology*, Vol. 99, 1977, pp. 298-313.
- [12] Booker, M. K. and Sikka, V. K., *Nuclear Technology*, Vol. 30, 1976, pp. 52-64.
- [13] Sikka, V. K., Booker, M. K., and Brinkman, C. R., "Use of Ultimate Tensile Strength to Correlate and Estimate Creep and Creep-Rupture Behavior of Types 304 and 316 Stainless Steel," ORNL-5285, Oak Ridge National Laboratory, Oak Ridge, Tenn., Oct. 1977.
- [14] Woodford, D. A. and Goldhoff, R. M., *Material Science Engineering*, Vol. 5, 1969/70, pp. 303-324.
- [15] *Annual Book of ASTM Standards*, Part 10, American Society of Testing and Materials, 1976, pp. 1-27.

A. J. Moorhead,¹ V. K. Sikka,¹ and R. W. Reed¹

Effect of Small Additions of Niobium on the Welding Behavior of an Austenitic Stainless Steel*

REFERENCE: Moorhead, A. J., Sikka, V. K., and Reed, R. W., "Effect of Small Additions of Niobium on the Welding Behavior of an Austenitic Stainless Steel," *Properties of Austenitic Stainless Steels and Their Weld Metals (Influence of Slight Chemistry Variations)*, ASTM STP 679, C. R. Brinkman and H. W. Garvin, Eds., American Society for Testing and Materials, 1979, pp. 103–123.

ABSTRACT: The mechanical property data for Type 304 stainless steel show large variations in tensile, creep, and creep-fatigue properties. Previous researchers have attributed these differences to variations either in carbon and nitrogen content or in grain size, but we have found some heats which are stronger than can be explained by these factors and attribute this apparent anomaly to the strengthening effect of niobium. To systematically study the effect of niobium on the behavior of Type 304 stainless steel, a low-niobium commercial heat was remelted with varying niobium additions—up to 1000 ppm. A standardized weldability test, the Spot Vareststraint, was used to compare the propensity of various heats for hot-cracking. We found that the fusion and heat-affected zone cracking behavior of the experimental heats was similar to that of a heat of commercial Type 304, and much superior to that of a commercial heat of Type 347 stainless steel. The superior resistance to fusion zone cracking was attributed to the presence of a small amount of delta ferrite in the microstructure of the weld nugget in the experimental materials. The outstanding heat-affected zone cracking behavior was at least partly attributable to backfilling of grain boundary separations in the experimental heats, as well as in the commercial Type 304. We hypothesize that a relatively wide partially melted zone prevents backfilling of heat-affected zone cracks in the Type 347 steels.

KEY WORDS: stainless steel, weldability, hot-cracking, residual element, Spot Vareststraint

Significant variations in mechanical properties and welding behavior have been observed between heats of austenitic stainless steels even when these materials have been purchased to tightly controlled ASTM or Reactor

*Work performed under U.S. DOE/RRT 189a OHO24, Joining Technology Development.

¹Metallurgist, Welding and Brazing Group, metallurgist, Mechanical Properties Group, and senior engineering technician, Welding and Brazing Group, respectively, Oak Ridge National Laboratory, Oak Ridge, Tenn. 37830.

Development and Technology (RDT) specifications. These variations have often been attributed to the effects of minor alloying or residual elements [1-3].² Sikka et al [4] have found that small quantities of niobium—in addition to the previously reported carbon and nitrogen [5]—strongly affect the time to rupture and minimum creep rate of commercial Type 304 stainless steel. The effect of sizable additions of niobium on the welding behavior of austenitic materials—such as the niobium-stabilized stainless steels like Type 347—has been well documented [6,7]. As summarized in this paper, our study evaluated the effect of small niobium additions on the weldability of austenitic materials and specifically of Type 304 stainless steel. The results of the mechanical properties portion of this work are included elsewhere in this publication [4].

Materials

This study used four heats of commercial material. The product form, grain size, and compositions are given in Tables 1 and 2. Portions of two Type 304 stainless steel plates, Heats 9T2796 and 8043813, were machined into 3.18 by 25 by 25-mm (0.125 by 1 by 1-in.) blanks with the 25 by 25-mm (1 by 1-in.) dimension parallel to the original surface of the plate. The 3.61-mm-thick (0.142-in.) Type 347 stainless steel sheet was purchased according to the ASTM Specification for Stainless and Heat-Resisting Chromium-Nickel Steel Plate, Sheet, and Strip (A 167-74) in that thickness in the hot-rolled, annealed, and pickled condition. A third heat of Type 304 was used as the melting stock in the fabrication of four experimental heats with the same nominal composition, but with varying niobium content. The fabrication sequence for these experimental 0.5-kg (1.1 lb) heats was as follows:

1. Melt six times using a nonconsumable tungsten electrode in an evacuated chamber backfilled with a partial pressure of argon.
2. Drop-cast into a 19.0-mm-diameter (0.75 in.) water-cooled copper mold.
3. Hot swage at 1000°C (1832°F) to 12.7-mm-diameter (0.50-in.) rod.
4. Forge a portion of the rod to flats at 1000°C (1832°F).
5. Cold roll the flats to 3.0-mm-thick (0.12 in.) strip.
6. Anneal in vacuum for 1.8 ks (0.5 h) at 1065°C (1949°F).

The chemical analyses of the experimental heats—one of Heat 187 remelted and three with niobium additions to produce ingots with 0.05, 0.07, and 0.1 weight percent niobium—which were evaluated in this welding behavior study are given in Table 3. Note that in all cases the chemical compositions of the experimental heats fall within the range specified by the ASTM Specification for Heat-Resisting Chromium and Chromium-

²The italic numbers in brackets refer to the list of references appended to this paper.

TABLE 1—Product form and grain size of three commercial heats of Type 304, one heat of Type 347, and four experimental heats of stainless steel.

Heat	Heat Symbol	Vendor	As-Received Form	Thickness		Grain Size ^a			
				mm	in.	As Received		Reannealed	
						ASTM	μm	ASTM	μm
Commercial Heats									
Type 304									
8043813	813	Republic	plate	25.4	1.00	3.8	84	4	78
9T2796	796	USS ^c	plate	50.8	2.00	0.26	280	0.26	280
337187	187	Allegheny Ludlum	plate	38.1	1.50	2.1	150	2.3	140
Type 347									
347	sheet	3.6	0.14	6-7 ^b	...
Experimental Heats									
187-1	187-1	ORNL ^d	strip	3	0.12	4-5 ^b	...
187-5	187-5	ORNL	strip	3	0.12	4-5 ^b	...
187-6	187-6	ORNL	strip	3	0.12	5-6 ^b	...
187-7	187-7	ORNL	strip	3	0.12	4-5 ^b	...

^a Method of Hillard, J. E., *Metallurgical Progress*, Vol. 85, No. 5, May 1964, pp. 92-102.

^b Determined by comparison with ASTM Standard Grain Size Charts.

^c United States Steel.

^d Oak Ridge National Laboratory.

TABLE 2—Chemical composition of three commercial heats of Type 304 and one commercial heat of Type 347 stainless steel.

Heat Symbol	Composition, %															
	C	Mn	P	S	Si	Ni	Cr	Mo	Y	Nb	Ti	Co	Cu	Al	B	N
813 ^a	0.062	1.87	0.044	0.004	0.48	8.95	17.8	0.32	0.022	0.020	0.002	0.033
796 ^a	0.047	1.22	0.029	0.012	0.47	9.58	18.5	0.10	0.037	0.008	0.003	0.05	0.10	0.031
187 ^a	0.068	0.83	0.018	0.008	0.59	9.43	18.2	0.07	0.060	0.002	0.003	0.06	0.15	0.031
347 ^b	0.07	1.53	0.04	0.006	0.68	11.50	17.05	0.41	0.03	0.78	<0.01	0.12	0.20	0.01	0.001	0.039

^a Analysis by Oak Ridge National Laboratory of heat before fabricating into Spot Vareststraint specimens.

^b Analysis by outside laboratory of Spot Vareststraint specimen after testing.

TABLE 3—Chemical composition of four heats of Type 304 stainless steel remelted at ORNL, three of which had niobium additions. ^a

Heat Symbol	Composition, %															
	C	Mn	P	S	Si	Ni	Cr	Mo	Y	Nb	Ti	Co	Cu	Al	B	N
187-1	0.052	0.96	0.029	0.009	0.44	9.48	18.22	0.14	0.06	<0.01	<0.01	0.10	0.12	0.01	0.001	0.029
187-5	0.049	0.94	0.028	0.009	0.43	9.53	18.13	0.14	0.06	0.05	<0.01	0.10	0.12	0.01	0.001	0.030
187-6	0.050	0.96	0.029	0.009	0.44	9.57	18.18	0.15	0.06	0.07	<0.01	0.10	0.12	0.01	0.001	0.028
187-7	0.051	0.95	0.029	0.009	0.43	9.51	18.10	0.14	0.06	0.10	<0.01	0.10	0.12	0.01	0.001	0.029

^a Analysis by outside laboratory of Spot Vareststraint specimen after testing.

Nickel Stainless Steel Plate, Sheet, and Strip, for Fusion-Welded Unfired Pressure Vessels (A 240-75a) for Type 304 stainless steel plate.

Experimental Procedure

In order to compare the welding behavior of two commercial heats of Type 304, one commercial heat of Type 347, and four experimental heats, a standardized weld cracking test known as the Spot Varestraint or Tigamajig test was used. The apparatus is pictured in Fig. 1 and shown schematically in Fig. 2. In this test a 25 by 152-mm (1 by 6-in.) coupon containing a solidifying gas tungsten-arc weld nugget is bent by a pneumatic ram around one of a set of radiused die blocks. The arc time is controlled by a timer for reproducibility, while a time-delay relay is used to regulate the time at which the ram is activated. In all our tests the ram was forced into the coupon just as the arc was extinguished. The bending of the specimen around a radius generates reproducible amounts of augmented strain in the fusion and heat-affected zones of the weld. Since strain, one of the factors responsible for weld hot-cracking, is then controlled, the effect of other factors such as composition can be determined. The original Varestraint (variable restraint) test was developed by Savage and Lundin [8] as a *reproducible means for augmenting the normal shrinkage strains in a weldment, thereby simulating the large shrinkage strains characteristic of a highly restrained weldment*, as in heavy sections, in a laboratory specimen. The number and length of cracks developed during this test are related to the weldability of the material. The Spot Varestraint device was developed by Goodwin [9] to incorporate most of the desirable features of the Varestraint test and have the advantage of a smaller specimen size—that is, 25.4 by 152.4 mm (1.0 by 6.0 in.) for the Spot Varestraint as opposed to 50.8 by 304.8 mm (2.0 by 12.0 in.) for the standard Varestraint test.

In our study the scarcity of material available for testing made a modified or “compound” test specimen necessary. This compound specimen is shown in Fig. 3. It requires only enough of the material to be tested to fabricate five or six [3-mm (0.12 in.) minimum thickness by 25.4 by 25.4 mm (1.0 by 1.0 in.)] coupons to which 25.4 by 64-mm (1.0 by 2.52 in.) pieces of a commercial material are attached by electron beam welding. This specimen also has the advantage of allowing testing of small heats of experimental wrought metals. In conventional specimens small quantities of experimental materials can be tested, but the material is deposited in a series of weld beads on a commercial material and the tests are, therefore, on cast rather than on wrought microstructure.

Each heat of material was tested at four levels of strain—0.6, 0.9, 1.3, and 1.9 percent—with the following arc spot parameters:

Arc current	73 A dcsp
Arc time	15 s

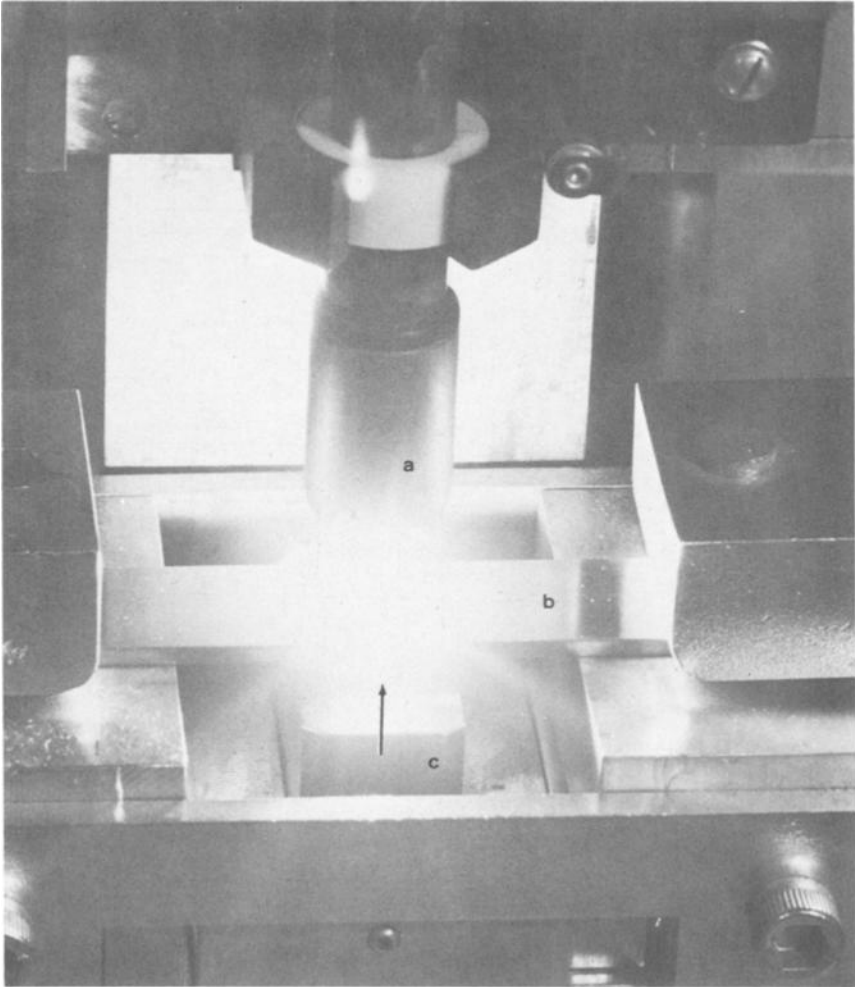


FIG. 1—Spot Varcstraint test in progress, showing: (a) gas tungsten-arc torch, (b) test specimen secured by hold-down blocks, and (c) a die block. The motion of the die block to strain the specimen is indicated by an arrow.

Arc gap	2.29 mm (0.090 in.) measured cold
Electrode	1.58-mm-diameter (0.062 in.), 2 percent thori- ated W, 60-deg included angle with 0.25- mm-diameter (0.010 in.) flat

Postarc time delay	none
Shield gas	argon
Spot size	about 5.1 mm (0.20 in.)

After testing, the specimens were held under load in the fixture for 60 s before removal. The cracking data were obtained from the specimen sur-

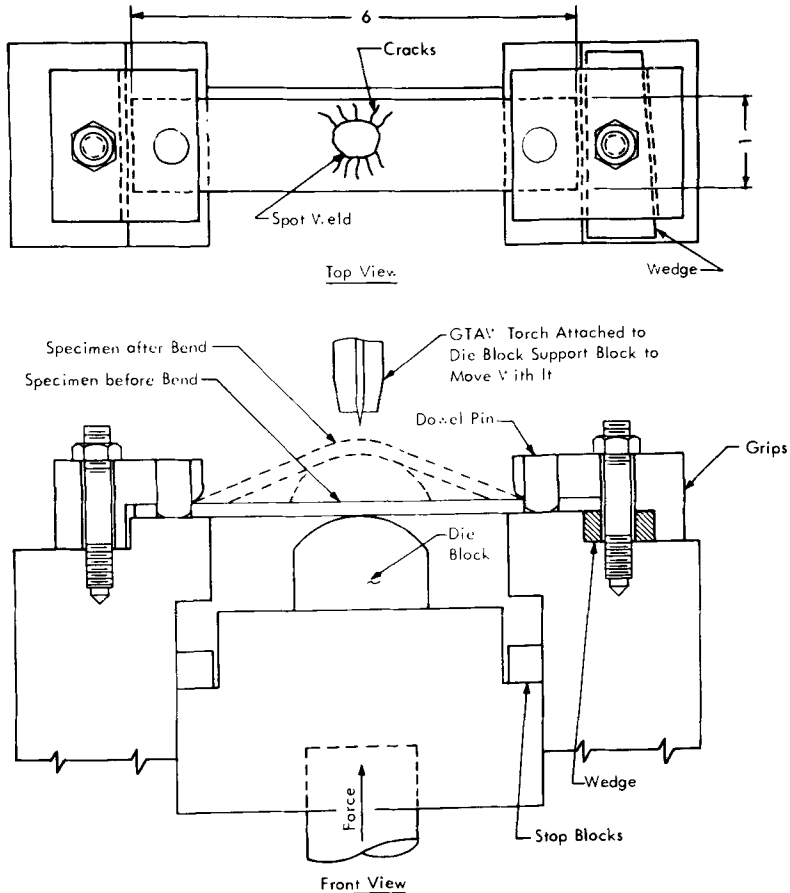


FIG. 2—Schematic of the Spot Varcstraint weldability test apparatus.

face at a magnification of $\times 50$ by a toolmaker's microscope with a digital output. The only cracks measured were those which lay in the partially melted or heat-affected zones (HAZ). Cracks that occurred in the fusion zone were not measured, but their presence or absence is important to weldability; therefore they were noted and are discussed in the following section.

From analysis of the data for each specimen, the following indices of cracking sensitivity were obtained.

1. Cracking threshold—the minimum augmented strain required to cause cracking with a given set of welding parameters.

2. Maximum crack length—the maximum-length crack near a given spot and a function of the width of the cracking-temperature range for a given set of welding parameters and a particular level of augmented strain.

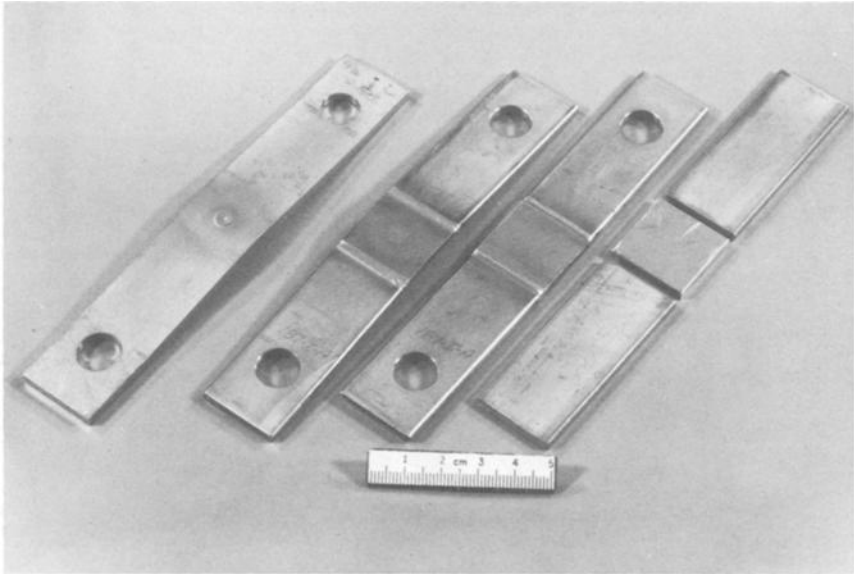


FIG. 3—Spot V restraint test specimens. Standard specimen is at left with compound specimen shown (right to left) before assembly, after electron beam welding, and after testing.

3. Total crack length—the sum of the lengths of all cracks measured in a specimen.

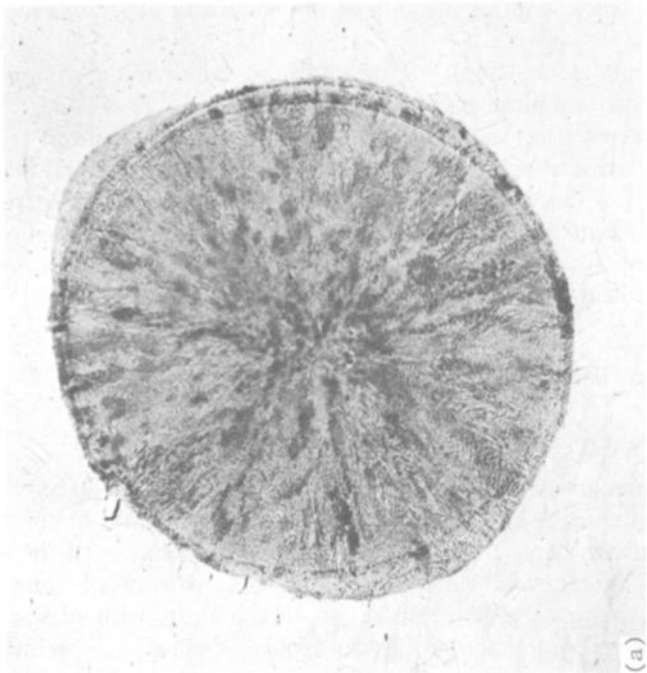
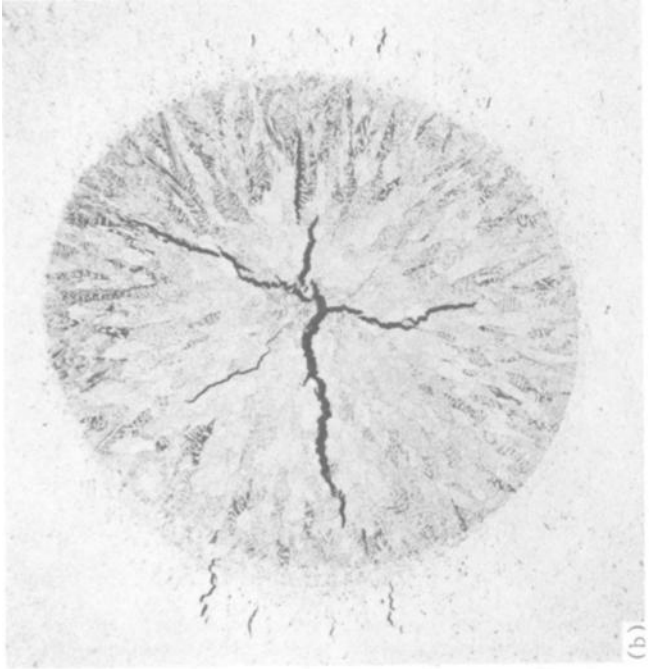
4. Average crack length—a mean found by dividing the total crack length by the total number of cracks.

After the cracking indices had been tabulated, one central test section from each series of specimens was removed for chemical analysis to verify heat identification. A second specimen was mounted for metallographic examination with the surface of the coupon and weld spot being polished. A third coupon from each heat was mounted such that a transverse section of the weldment could be examined.

Results and Discussion

Fusion-Zone Cracking Behavior

Photomicrographs of some of the arc spots after metallographic preparation are shown in Fig. 4. Only two of the experimental niobium-bearing heats are shown here (187-6 and 187-7), but the behavior of the other two heats was similar, and we would expect that if a fusion-zone cracking problem were to arise it would do so in the heats with higher niobium content. These photomicrographs are typical of all of the specimens tested in that extensive fusion-zone cracking occurred in the Type 347 stainless



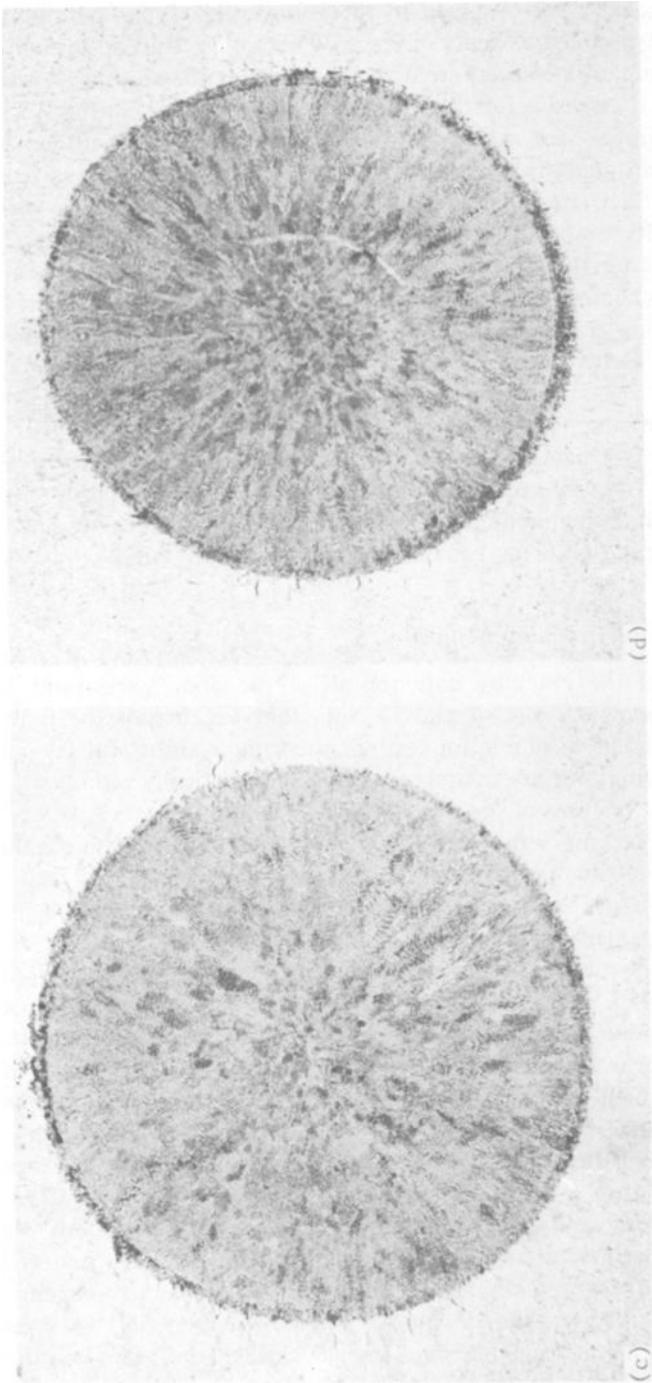


FIG. 4—Polished and etched surfaces of Spot Varestraint test gas tungsten-arc weld nuggets in two commercial and two experimental heats of austenitic stainless steel. (a) Heat 796: 0.008 percent niobium, commercial Type 304 stainless steel; (b) Heat 347: 0.78 percent niobium, commercial Type 347 stainless steel; (c) Heat 187-6: 0.07 percent niobium, commercial Type 304 stainless steel with addition; (d) Heat 187-7: 0.10 percent niobium, commercial Type 304 stainless steel with addition. Etchant: 50 HCl-10 HNO₃ (×15).

steel, but no cracks were observed in the commercial Type 304 stainless steel or in the experimental heats of Type 304 stainless steel with niobium additions. Examination of these welds at higher magnification as shown in Fig. 5 revealed the reason for this difference in cracking behavior: All of the Type 304 stainless steel materials—both commercial and experimental—contained a small amount of delta ferrite in their microstructures. It is a well-established fact [10,11] that the presence of this phase in the fusion zones of austenitic stainless steels greatly reduces weld hot-cracking. The presence of delta ferrite was confirmed by magnetic permeability measurements using a Magne-gage instrument and test procedures specified by the American Welding Society Standard for Calibrating Magnetic Instruments to Measure the Delta Ferrite Content of Austenitic Stainless Steel Weld Metal (AWS A4.2-74). All the Type 304 stainless steel welds had a Ferrite Number (FN) of about 3, whereas the Type 347 stainless steel had no measurable ferrite (that is, FN = 0). The presence or absence of this beneficial phase is a well-established function of chemical composition [12] and a less well-known function of weld energy input, but exactly how its presence reduces hot-cracking has only been hypothesized [13].

Heat-Affected Zone Cracking Behavior

A summary of the cracking data for all of the Spot Varcstraint test specimens is given in Tables 4 and 5. Note that because of the limited amounts of materials available for testing, these data are useful for comparison or screening, but are not purported to be statistically valid.

The significant features of these results are as follows:

1. The HAZ cracking behavior of Type 304 stainless steels with niobium additions (up to 1000 ppm) was similar to that of a commercial heat of Type 304 stainless steel and much superior to that of a commercial heat of Type 347 stainless steel, as illustrated in Fig. 6.

2. The cracking threshold for all of the Type 304 stainless steel materials—commercial and experimental—was greater than 0.6 percent augmented strain but was less than 0.6 percent for Type 347 stainless steel.

3. The data for average crack length and maximum crack length do not correlate well with either niobium content or with percent augmented strain within a type of steel.

Metallographic examination of the test specimens at high magnification reveals an interesting and evidently significant difference in heat-affected zone cracking behavior between the Type 304 stainless steel (both commercial and experimental) and the Type 347 stainless steel materials. When the specimens were etched with boiling Murakami's reagent to selectively reveal the delta-ferrite phase, it was observed that in several instances molten metal from the weld pool backfilled the grain-boundary separations in the HAZ of the Type 304 stainless steel materials. These

TABLE 4—Total crack length data for Spot Varestraint weldability tests conducted on commercial and experimental austenitic stainless steels.

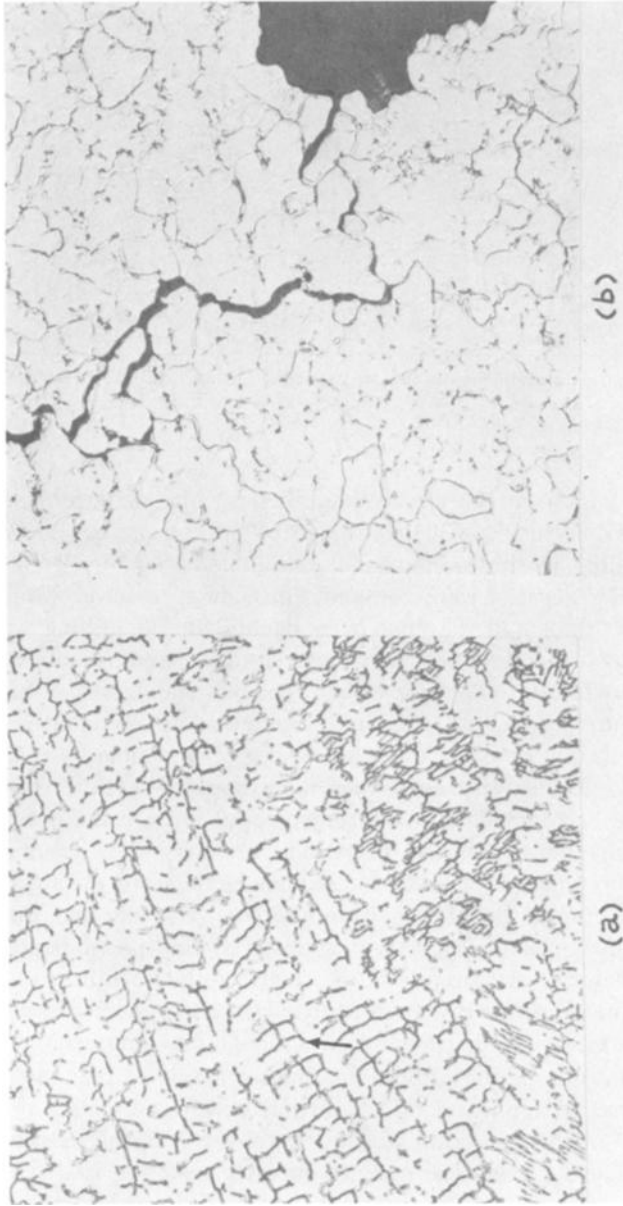
Heat Symbol	Composition (weight %)		Total Crack Length ^a (mm) ^b at % Augmented Strain of:			
	C	Nb	0.6%	0.9%	1.3%	1.9%
Commercial Heats						
813	0.062	0.02	0	0.19	0.25	0.36
796	0.047	0.008	0	0.09	0.34	2.15
347	0.07	0.78	0.29	4.27	8.02	10.56
Experimental Heats						
187-1	0.052	<0.01	0	0.42	0.57	1.06
187-5	0.049	0.05	0	0.28	0.51	2.41
187-6	0.050	0.07	0	0.34	0.82	3.03
187-7	0.051	0.10	0	0.26	1.03	1.48

^aCrack length measurements on as-tested specimen using toolmaker's microscope at $\times 50$ magnification.

^b1 mm = 0.04 in.

backfilled cracks can be clearly identified by the delta-ferrite extending into the HAZ in the Type 304 stainless steel specimens, as shown in Fig. 7. The backfilling of these separations eliminated them from consideration when the HAZ cracks were counted, thus giving a lower value for total crack length than had they not been backfilled. Backfilling was not observed in any of the Type 347 specimens studied metallographically and we attribute this to the following causes. Type 347 stainless steel has a rather wide [0.30-mm (0.012 in.)] partially melted zone (as shown in Fig. 8) between the fusion zone and the HAZ. In Type 304 stainless steels, however, this region is either very narrow or nonexistent. We think this partially melted zone accommodates the strains produced by bending and solidification so that this region does not crack. Cracking does occur in the true HAZ, but, as there is no path for molten metal from the fusion zone to reach these cracks, backfilling cannot occur. This observation has been confirmed by Lundin [14], who has observed this phenomenon in other classes of material. Apparently HAZ cracks can be backfilled only in those systems containing a very narrow partially melted zone. Thus, wide partially melted zones are detrimental to weldment cracking behavior.

Although a number of authors [6,15] have indicated that the base metal grain size has a significant effect on the tendency for HAZ cracking (in general, the smaller the grain size, the lower the cracking tendency), we do not think that our results are greatly in error resulting from variations in grain size. First, five out of the seven heats tested had very similar grain sizes (ASTM 4-5). Second, the one alloy that displayed the greatest hot-cracking tendency (the heat of Type 347) also was the material that had the smallest grain size (ASTM 6-7), and we would anticipate that if heat-



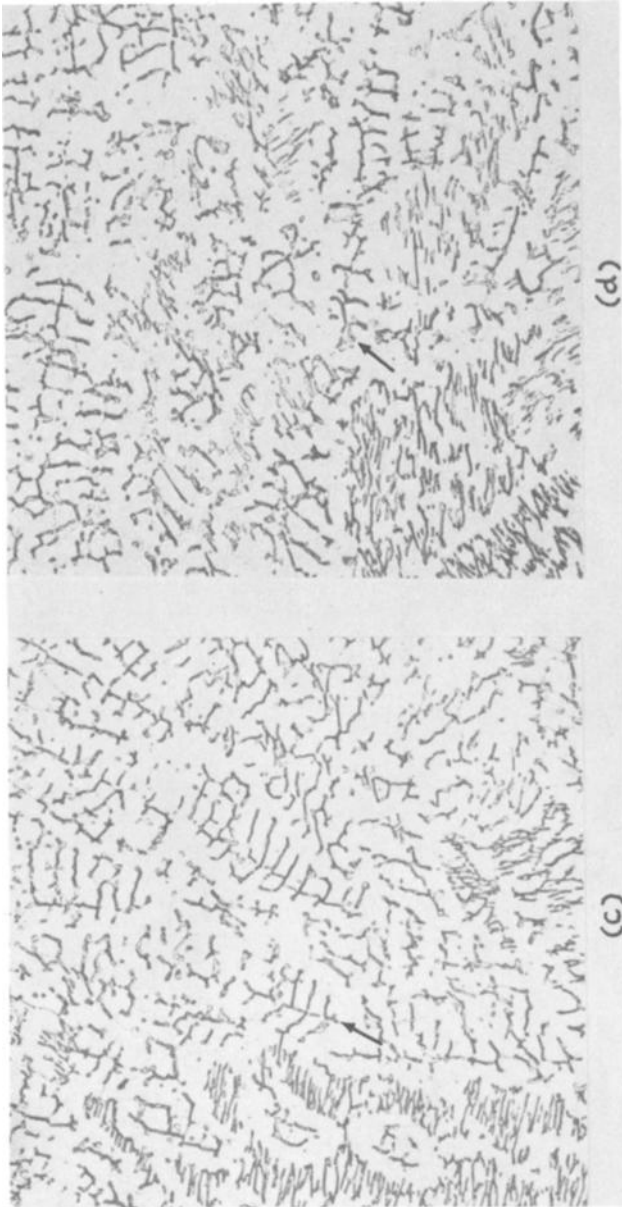


FIG. 5—Fusion zones of Spot Varestraint test welds in two commercial and two experimental heats of austenitic stainless steel. Note that the etched microstructure of each of the Type 304 stainless steel materials contains delta ferrite (arrows), whereas that of the Type 347 stainless steel does not. (a) Commercial heat 796; (b) Commercial heat 347; (c) Experimental heat 187-5; (d) Experimental heat 187-6. Etchant: 50 HCl-10 HNO₃ (×500).

TABLE 5—Maximum and average crack length data for Spot Varestraint weldability tests conducted on commercial and experimental austenitic stainless steels.

Heat Symbol	Composition (weight, %)		Total Crack Length (mm) ^b at % Augmented Strain of:											
			0.6%			0.9%			1.3%			1.9%		
			max	avg	max	avg	max	avg	max	avg	max	avg		
813	0.062	0.02	0	...	0.10	0.09	0.14	0.12	0.20	0.18	Commercial Heats			
796	0.047	0.008	0	...	0.09	^a	0.21	0.17	0.23					
347	0.07	0.78	0.29	^a	0.54	0.28	0.65	0.33	0.51	0.34				
187-1	0.052	0.01	0	...	0.24	0.21	0.21	0.19	0.25	0.15	Experimental Heats			
187-5	0.049	0.05	0	...	0.16	0.14	0.18	0.13	0.29					
187-6	0.050	0.07	0	...	0.17	0.17	0.24	0.20	0.31	0.23				
187-7	0.051	0.10	0	...	0.14	0.13	0.37	0.21	0.29	0.21				

^aSpecimen had a single crack.

^b1 mm = 0.04 in.

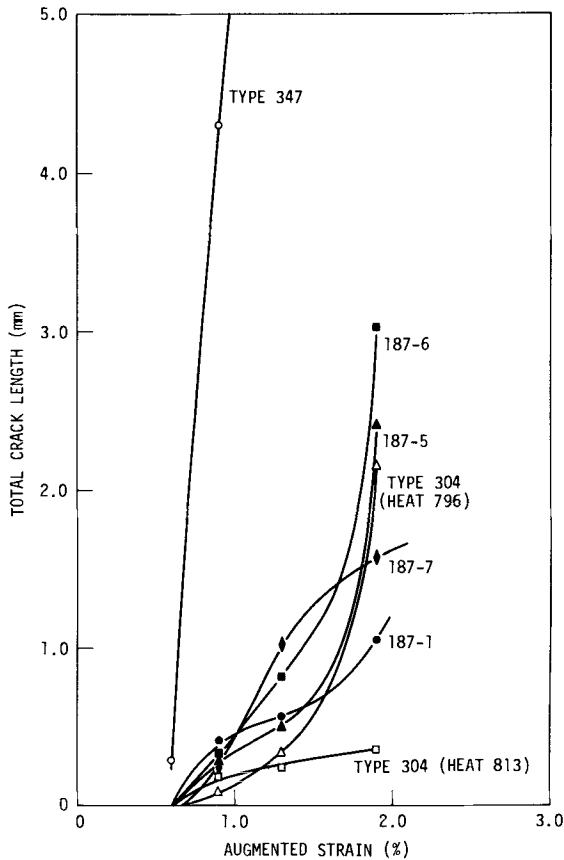


FIG. 6—Total crack length of various heats of commercial and experimental austenitic stainless steels as a function of augmented strain in Spot Varestraint weldability tests.

treated to a larger grain size its HAZ cracking propensity would be even greater.

Conclusions

From our study of the effect of niobium additions on the welding behavior of some austenitic stainless steels, we draw the following conclusions.

1. The compound Spot Varestraint specimen allows us to evaluate the welding behavior of small quantities of wrought base metals.

2. The fusion-zone cracking behavior of Type 304 stainless steel with niobium additions up to 1000 ppm was similar to that of commercial Type 304 stainless steel—as no fissures were detected in either material in this

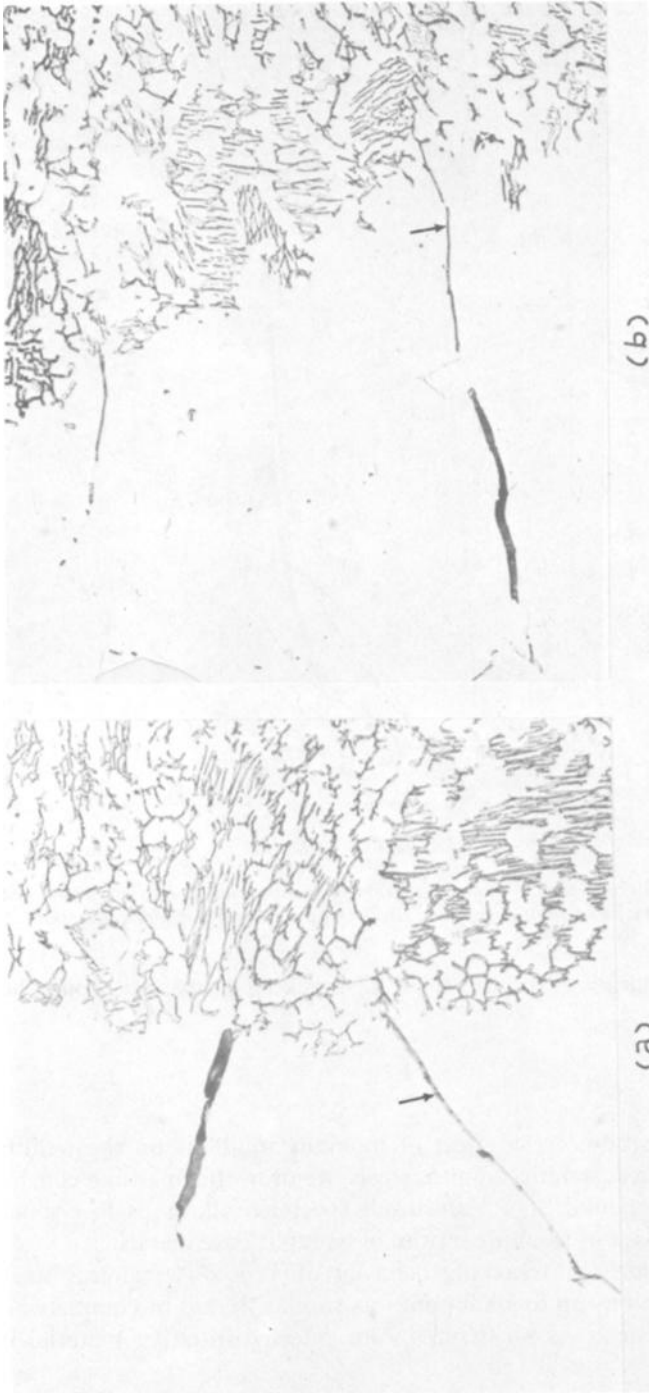


FIG. 7—Typical backfilled grain boundary separations (arrows) in the heat-affected zones of two Type 304 stainless steel materials. (a) Commercial Type 304 stainless steel (Heat 796); (b) Experimental heat 187-6 (0.07 weight percent niobium). Etchant: 50 HCl-10 HNO₃ (×392).

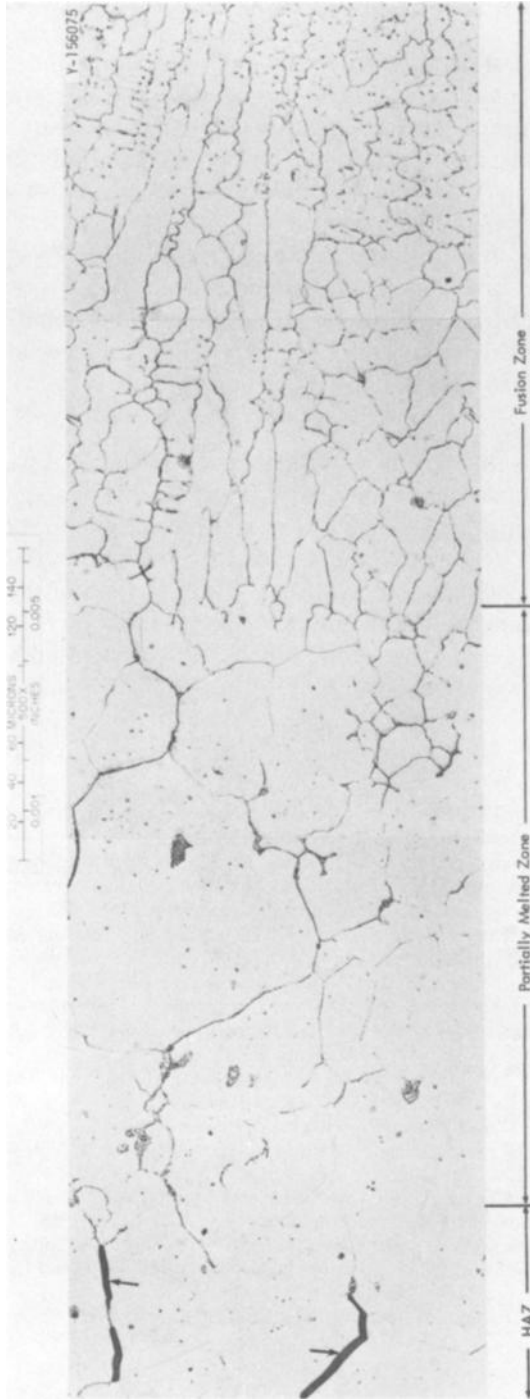


FIG. 8—Spot Varestraint weldment in commercial Type 347 stainless steel showing the extensive partially melted zone which prevents backfilling of heat-affected zone cracks (arrows) by molten metal from the arc spot. Etchant: 50 HCl-10 HNO₃.

study—and was greatly superior to that of a commercial heat of Type 347 stainless steel.

3. The presence of delta ferrite in the weld nugget minimizes fusion-zone cracking in the commercial and experimental Type 304 stainless steels.

4. The heat-affected zone cracking of experimental heats of Type 304 stainless steel with niobium additions up to 1000 ppm was similar to that of commercial Type 304 stainless steel but was much less than that of commercial Type 347 stainless steel.

5. Fewer cracks were observed in the weld HAZ in the Type 304 stainless steel materials because some grain boundary separations were “backfilled” with molten metal from the fusion zone. On the other hand, there was a wide partially melted zone in the Type 347 stainless steel weldments which apparently prevented backfilling of HAZ cracks.

Acknowledgments

The authors would like to express their appreciation to the following individuals who made significant contributions to this paper: R. G. Shooster of the Administrative Services Group was responsible for the machining of specimens; J. W. Nave of the General Metallography Group was responsible for the photographic work, and C. P. Haltom of the same group was the metallographer. The manuscript was reviewed by S. A. David and T. G. Godfrey. The report was edited by N. W. Richards and prepared for reproduction by S. G. Frykman.

References

- [1] *Effects of Residual Elements on Properties of Austenitic Stainless Steels*, ASTM STP 418, American Society for Testing and Materials, 1967.
- [2] King, R. T., Steigler, J. O., and Goodwin, G. M., “Creep Properties of a Type 308 Stainless Steel Pressure Vessel Weld with Controlled Residual Element,” ORNL/TM-4131, Oak Ridge National Laboratory, Oak Ridge, Tenn., May 1973.
- [3] Binkley, N. C., Berggren, R. G., and Goodwin, G. M., *Welding Journal* (Miami), Vol. 53, No. 2, Feb. 1974, pp. 91s-95s.
- [4] Sikka, V. K., Moorhead, A. J., and Brinkman, C. R., this publication, pp. 69-102.
- [5] Heger, J. J. and Smith, G. V., *Elevated Temperature Properties as Influenced by Nitrogen Additions to Types 304 and 316 Austenitic Stainless Steels*, ASTM STP 522, American Society for Testing and Materials, 1968.
- [6] Linnert, G. E., “Welding Type 347 Stainless Steel Piping and Tubing,” Welding Research Council Bulletin 43, New York, Oct. 1958.
- [7] Christoffel, R. J., *Welding Journal* (New York), Vol. 41, No. 6, June 1962, pp. 251s-256s.
- [8] Savage, W. F. and Lundin, C. D., *Welding Journal* (New York), Vol. 44, No. 10, Oct. 1965, pp. 433s-442s.
- [9] Goodwin, G. M., “The Effect of Minor Elements on the Hot Cracking of Inconel 600,” Ph.D. thesis, Rensselaer Polytechnic Institute, Troy, N. Y., June 1968.
- [10] Hull, F. C., *Welding Journal* (New York), Vol. 46, No. 9, Sept. 1967, pp. 399s-409s.
- [11] Lundin, C. D., DeLong, W. T., and Spond, D. F., *Welding Journal* (Miami), Vol. 54, No. 8, Aug. 1975, pp. 241s-246s.
- [12] Long, C. J. and DeLong, W. T., *Welding Journal* (Miami), Vol. 52, No. 7, July 1973, pp. 281s-297s.

- [13] Borland, J. C. and Younger, R. W., *British Welding Journal*, Vol. 46, No. 9, Sept. 1967, pp. 399-409.
- [14] Lundin, C. D., private communication, University of Tennessee, Knoxville, Tenn., 10 Nov. 1977.
- [15] Puzak, P. P. Apblett, W. R., and Pellini, W. S., *Welding Journal* (Miami), Vol. 35, No. 1, Jan. 1956, pp. 9s-17s.

Development of Austenitic Stainless Steels with Controlled Residual Nitrogen Content; Application to Nuclear Energy

REFERENCE: Rabbe, P. and Heritier, J., “Development of Austenitic Stainless Steels with Controlled Residual Nitrogen Content; Application to Nuclear Energy,” *Properties of Austenitic Stainless Steels and Their Weld Metals (Influence of Slight Chemistry Variations)*, ASTM STP 679, C. R. Brinkman and H. W. Garvin, Eds., American Society for Testing and Materials, 1979, pp. 124–141.

ABSTRACT: We have developed AISI 304 and 316 grade steels which exhibit, in addition to their good mechanical properties, intergranular corrosion resistance of the 304L and 316L grades. This development of what we shall call “optimized” steels has been made possible essentially by a detailed knowledge of the respective influences of carbon and nitrogen on the mechanical properties and intergranular corrosion resistance. The method by which such optimized steels are specified, as well as the comparison of their mechanical properties with the ASME Code data, is described. It is obvious that such grades are particularly useful for nuclear applications.

KEY WORDS: carbon content, nitrogen content, mechanical properties, intergranular corrosion resistance, nuclear steels

It is well known that light-water reactors undergo severe loadings, and care should be taken to do away with all the causes of initiation of cracks which would possibly propagate during reactor life, either through low-cycle fatigue or through fatigue from a great number of cycles. Consideration of the possible damage during implementation or transient periods has led, for components in contact with fluid, to selecting only austenitic stainless steels, which resist intergranular corrosion and so limit the risks of initiation of cracks.

A distinction can be made between three families of steels meeting this requirement:

1. stabilized grades,

¹Materials engineers, Department of Mechanics, Creusot-Loire, Centre de Recherches d’Unieux, Firminy, France.

2. grades with very low carbon contents, and
3. optimized grades, which will be discussed at greater length.

The stabilized grades have the reputation of not being as easy to weld as steels in AISI 304 and 316 families.

The weldability of grades with very low carbon contents of Type 304L or 316L is excellent, and these grades have a good intergranular corrosion resistance. Their drawback stems from the fact that, at room temperature or at the operating temperatures, their mechanical properties are lower than those of Grades 316 and 304. These low properties are at the origin of a double handicap for these grades:

1. An economic handicap, since their use would lead to increasing the thicknesses of the parts made.

2. A technological handicap. The construction codes generally used are based on experiments which are not only quite thorough but also very long and costly. Now then, these codes take into account guaranteed mechanical properties of Types 304 and 316 steels. The choice of a material having lower mechanical properties would lead to depriving oneself of all the experience gained and quantified in these codes.

Under the impetus from Electricité de France, every effort was made to develop austenitic stainless steels which

1. cross-check with the composition specifications of AISI Steels 304 or 316,

2. have the stipulated mechanical properties of AISI Steels 304 or 316, and

3. have the same intergranular corrosion resistance as AISI Steels 304L or 316L.

A solution to the last two requirements only might have consisted in selecting steels belonging to the families of Types 304LN and 316LN. These steels, which have carbon contents below 0.030 percent and nitrogen contents between 0.1 and 0.15 percent, have intergranular corrosion resistance and mechanical strength properties which, in the first analysis, would be suitable.

This solution was not chosen since it would have entailed the use of a new material which is not yet retained by current codes, and of which industrial experience is limited.

Furthermore, high nitrogen contents may cause the following difficulties:

1. Difficult welding and in consequence a decrease in reliability of the welded components.

2. Difficult hot-working and the higher risk of processing defects.

Damage Mechanisms of Stainless Steels in Light-Water Reactors

A distinction can be made between three major types of damage:

1. intergranular stress corrosion,

2. damage from fabrication, and
3. damage from fatigue corrosion.

Intergranular Corrosion

Intergranular cracking in a water medium can affect austenitic stainless steels at the operating temperatures. Four conditions must be met for this to happen:

1. The steel must have a rather high carbon content,
2. the oxygen content must be relatively high,
3. the material must be sensitized, and
4. the material must be subjected to high static loadings.

Moreover, it is not altogether impossible that dynamic loading combined with moderate static loading can also produce intergranular cracking.

It should be pointed out that, considering the operating temperatures of light-water reactors, sensitizing can probably only result from sensitizing during fabrication, owing to thermal cycles from welding or stress relief.

Damage from Fabrication

The damage processes arising during manufacture of the reactors must be added to the mechanisms of damage by corrosion during operation, which have just been discussed. Considering the very severe operating loads, it is important that no cracks be initiated as a result of operations such as descaling of welded assemblies sensitized by the thermal cycle of welding or a stress relief cycle. It should be noted that a reactor is a pressure vessel which withstands static loading, transient operating conditions, and vibrational loading.

The transient operating conditions always exist, at a greater or lesser frequency. They are due to rather numerous shutdown and restarting operations. They can also be due to changes in the pressure or the thermal conditions. Even though some of these transient conditions create only elastic deformation changes, a certain number of structural elements actually withstand plastic cycling. These materials are submitted to low-cycle fatigue. Any surface defect resulting from a corrosion mechanism prior to operation, for example, can contribute to decreasing the low-cycle fatigue resistance. The same holds true for vibrational conditions which exert fatigue on the material. The service life in the presence of this type of stress depends on whether or not there are any surface defects.

Damage Through Fatigue Corrosion

Finally, it should be pointed out that, regardless of the causes of initia-

tion of fatigue cracks, these cracks propagate in the reactor medium and not in air.

Engineering firms must have a good knowledge of the possible damage through fatigue corrosion, especially for dimensioning the stainless steel parts in direct contact with the primary or secondary water.

Development of the Optimized 304 and 316 Stainless Steels

As mentioned previously, we have aimed to develop AISI 304 and 316 grade steels which possess the following properties:

1. The mechanical properties of the AISI 304 and 316 steels.
2. The intergranular corrosion resistance of the AISI 304L and 316L steels.

To achieve this aim we have proceeded in two stages:

1. Specification of chemical compositions of steels which exhibit the best intergranular corrosion resistance—in particular, compositions with the maximum acceptable carbon level.
2. Specification of the composition balance which, taking into account the maximum carbon content just described, leads to the mechanical properties of the AISI 304 and 316 steels.

Method for Determination of the Intergranular Corrosion Resistance

Previous studies, in particular by Cihal [1],² have shown that the 18-10 or 17-12Mo type steels of equivalent intergranular corrosion resistance satisfy the following relation [2]

$$[\text{Cr}^*] - 100 [\text{C}^*] = k$$

where Cr* is an equivalent chromium content which allows for the improved resistance to intergranular corrosion due to molybdenum and C* is the equivalent carbon content which is corrected for the influence of the nickel content; this element decreases the solubility of carbon in the austenite matrix and favors the intergranular precipitation of chromium carbides.

One generally uses the following formulas, established empirically

$$[\text{Cr}^*] = [\text{Cr}] + \alpha [\text{Mo}]$$

$$[\text{C}^*] = [\text{C}] + 0.002 ([\text{Ni}] - 10)$$

The second equation simply means that we use a 10 percent nickel steel as the base for comparison.

²The italic numbers in brackets refer to the list of references appended to this paper.

The coefficient α is in general taken equal to 1.0 [3], 1.2 [1], and 1.7 [4] according to different workers and the particular tests. This coefficient expresses the influence of molybdenum on the resistance to intergranular corrosion and depends upon the particular environment.

On a $([Cr^*], [C^*])$ composition diagram (Fig. 1), steels of equal resistance to intergranular corrosion have compositions on the lines represented by the equation

$$[Cr^*] - 100 [C^*] = k$$

and the higher the coefficient k , the better the corrosion resistance. The composition ranges of the 304L and 316L steels are represented by rectangular areas in Fig. 1. Their least resistance to intergranular corrosion is characterized by the minimum value of the coefficient k (k_{\min}) of the line

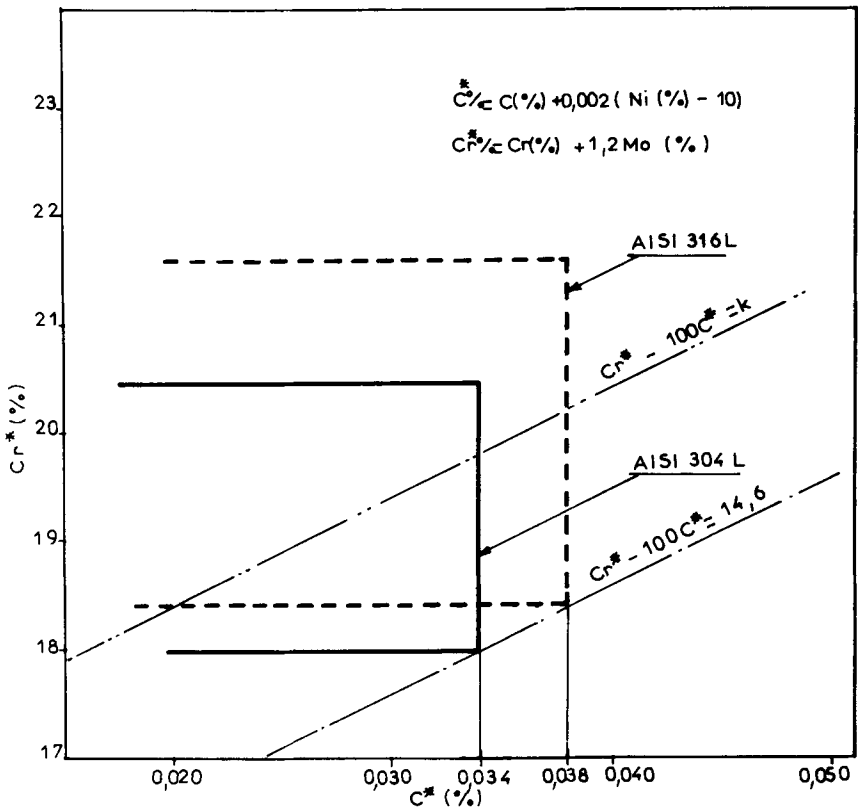


FIG. 1—A Cr^* , C^* composition diagram showing the lines of equal resistance to intergranular corrosion and the composition ranges of the AISI 304L and 316L steels.

$[Cr^*] - 100 [C^*] = k$ which passes by the lower right-hand corner of the composition specification:

If $\alpha = 1.2$

$$k_{\min} = 14.6 \text{ for both grades}$$

and

If $\alpha = 1.7$

$$k_{\min} = 14.6 \text{ for AISI 304L}$$

$$k_{\min} = 15.9 \text{ for AISI 316L}$$

For each service condition it is therefore necessary to determine two parameters:

1. α , which may depend upon the environment and also possibly upon certain microstructural factors (segregations, etc.).
2. The minimum value of k corresponding to a given environment and a given heat treatment (welding, stress relief).

This minimum value of k increases with the severity of the corrosive environment and with a possible loss of chromium during heat treatment.

To choose a steel for use in a given environment after a particular heat treatment, one must choose the specification such that k_{\min} , for the least favorable composition, is always higher than the minimum value of k necessary to pass the particular intergranular corrosion resistance test.

Application to the Specification of an Optimized AISI 304 Steel

The AISI 304L steel is represented in Fig. 2 by a rectangle described by the following limits

Maximum value of $[C^*] = 0.030 \text{ percent} + 0.002 (12 - 10) \text{ percent}$
 $= 0.034 \text{ percent}$

Minimum value of $[C^*]$: unspecified

Maximum value of $[Cr^*] = 20.0 \text{ percent} + 1.2 \times 0.4 \text{ percent}$
 $= 20.5 \text{ percent}$

Assuming that the residual molybdenum content is less than 0.4 percent

Minimum value of $[Cr^*] = 18.0 \text{ percent}$

(the use of $\alpha = 1.2$ being known as giving the best agreement with Autaas 121B test results for grade 304L and 316L steels).

The AISI 304 steel can also be represented by a rectangle which includes

that of the 304L. The horizontal boundaries are the same as those of 304L. Only the right-hand vertical boundary is modified and corresponds to a maximum carbon content

$$[C^*_{\max}] = 0.080 \text{ percent} + 0.002 (10.5 - 10) \text{ percent} = 0.081 \text{ percent}$$

In order to show that two steel grades have the same intergranular corrosion resistance one must check the following

1. The average compositions of the two grades give the same intergranular corrosion resistance.
2. The least favorable composition with respect to the intergranular corrosion resistance of each grade gives the same resistance to intergranular corrosion.

On a diagram such as Fig. 2, two steel grades would have the same resistance to intergranular corrosion if

1. the points representing the average composition of each grade are on the same diagonal, and
2. the lower right-hand corners of each composition rectangle are on the same diagonal,

One can start by specifying various types of 304 grade steel such that for the compositions of maximum C* and minimum Cr* of each type the resistance to intergranular corrosion is the same. Thus a steel having the following composition specification

$$\begin{aligned} 18.5 \text{ percent} < [\text{Cr}] < 20 \text{ percent} \\ & [\text{C}] < 0.035 \text{ percent} \\ 8 \text{ percent} < [\text{Ni}] < 12 \text{ percent} \end{aligned}$$

has the same lower limit to intergranular corrosion resistance as an AISI 304L steel. This is also true for a steel having the composition

$$\begin{aligned} 18.5 \text{ percent} \leq [\text{Cr}] \leq 20 \text{ percent} \\ & [\text{C}] \leq 0.040 \text{ percent} \\ 8 \text{ percent} \leq [\text{Ni}] \leq 10 \text{ percent} \end{aligned}$$

In addition, this steel has composition specifications inside AISI 304 steel chemical requirements.

Such considerations allow one to define the composition limits of the ICL 473 BC steel

$$\left\{ \begin{array}{l} 18.5 \text{ percent} \leq [\text{Cr}] \leq 20.0 \text{ percent} \\ \quad [\text{C}] \leq 0.040 \text{ percent} \\ 9 \text{ percent} \leq [\text{Ni}] \leq 10 \text{ percent} \end{array} \right. \text{ completed by } \left\{ \begin{array}{l} [\text{Mn}] \leq 2 \text{ percent} \\ [\text{Si}] \leq 1 \text{ percent} \\ [\text{P}] \leq 0.035 \text{ percent} \\ [\text{S}] \leq 0.020 \text{ percent} \\ [\text{N}_2] \leq 0.080 \text{ percent} \end{array} \right.$$

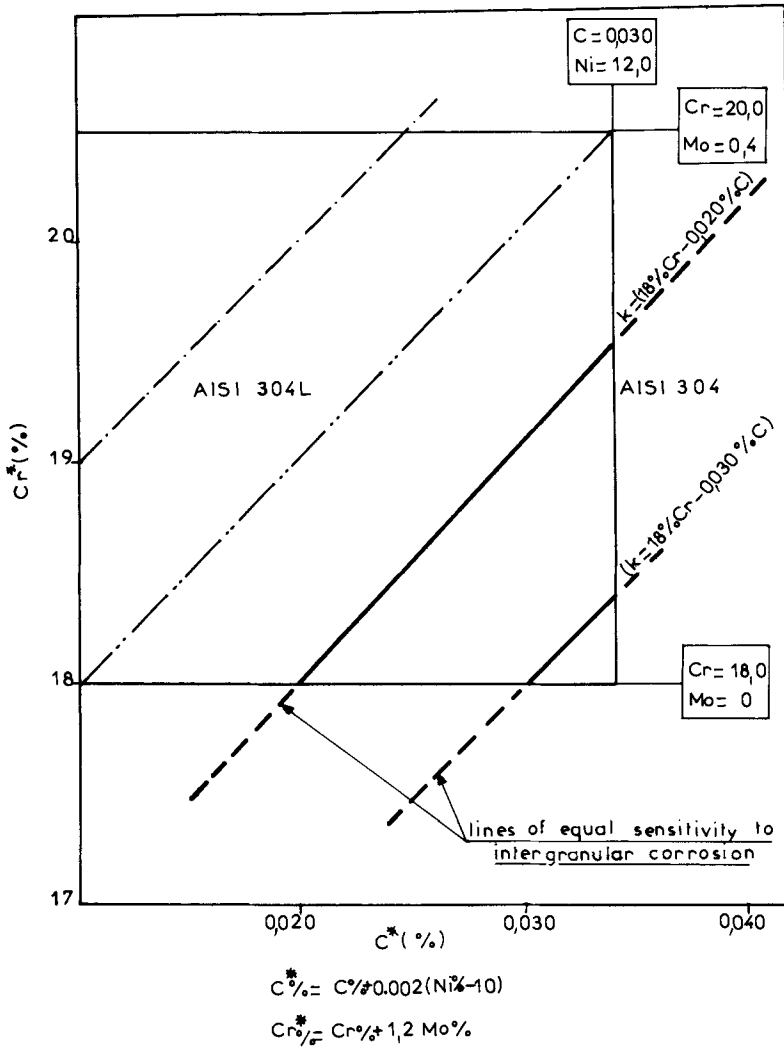


FIG. 2—Cr*, C* composition diagram of the AISI 304L steels.

Using this method, one can see that the ICL 473 BC steel (whose composition is the same as that of an AISI 304 steel) exhibits the same lower limit to intergranular corrosion resistance as the AISI 304L grade.

The average composition of the ICL 473 BC steel has been statistically defined from several hundred industrial melts of 35 tons (30 t)

$[C] = 0.030 \text{ percent}$
 which leads to $[C^*]_{\text{avg}} = 0.029 \text{ percent}$
 $[Ni] = 9.50 \text{ percent}$

$$\begin{aligned}
 [\text{Cr}] &= 19.3 \text{ percent} \\
 &\text{which leads to } [\text{Cr}^*]_{\text{avg}} = 19.50 \text{ percent} \\
 [\text{Mo}] &= 0.15 \text{ percent}
 \end{aligned}$$

The average sensitivity to intergranular corrosion for the ICL 473 BC steel can be defined from the equation

$$k_{\text{avg}} = 19.5 - 2.9 = 16.6$$

The average composition of an AISI 304L steel is not specified. Generally, a good-quality AISI 304L steel has the following average composition

$$\begin{aligned}
 [\text{C}] &= 0.020 \text{ percent} & [\text{C}^*] &= 0.021 \text{ percent} \\
 [\text{Ni}] &= 10.5 \text{ percent} & [\text{Cr}^*] &= 18.7 \text{ percent} \\
 [\text{Cr}] &= 18.5 \text{ percent}
 \end{aligned}$$

assuming that the average molybdenum content equals 0.15 percent.

The average sensitivity of the 304L steel to intergranular corrosion would then be

$$k_{\text{avg}} = 18.7 - 2.1 = 16.6 \text{ percent}$$

Statistically therefore the ICL 473 BC steel has exactly the same resistance to intergranular corrosion as an AISI 304L steel (for the particular environment studied).

Furthermore, the statistical analysis of the mechanical property results on industrial melts shows that the ICL 473 BC steel (of specification chosen according to the foregoing criteria) exhibits the mechanical properties specified for an AISI 304 steel.

Application to the 316 Grade Steels

Using the same method as described above one can specify an optimized AISI 316 grade steel which we call ICL 167 CN. This steel is currently used in France for the construction of primary circuits of P.W.R. nuclear reactors:

$$\left\{ \begin{array}{l}
 [\text{C}] \leq 0.045 \text{ percent} \\
 17.0 \text{ percent} \leq [\text{Cr}] \leq 18.0 \text{ percent} \\
 11.5 \text{ percent} \leq [\text{Ni}] \leq 12.5 \text{ percent} \\
 2.3 \text{ percent} \leq [\text{Mo}] \leq 2.8 \text{ percent}
 \end{array} \right. \text{ completed by } \left\{ \begin{array}{l}
 [\text{Mn}] \leq 2 \text{ percent} \\
 [\text{Si}] \leq 1 \text{ percent} \\
 [\text{P}] \leq 0.035 \text{ percent} \\
 [\text{S}] \leq 0.020 \text{ percent} \\
 [\text{N}_2] \leq 0.080 \text{ percent}
 \end{array} \right.$$

Industrial experience shows that this grade effectively exhibits the same resistance to intergranular corrosion (for a particular milieu) as the AISI 316L grade. In addition, this steel satisfies the mechanical property specifications of the AISI 316 grade.

Specific Role of the Residual Nitrogen Content

According to the melting technique, the residual nitrogen content of the AISI 304 and 316 grades may attain values as high as 0.09 percent and even 0.10 percent. For this reason we decided to limit the maximum nitrogen content of the ICL 473 BC and the ICL 167 CN steels to 0.08 percent. In addition, we have chosen to define a lower limit for the nitrogen content: 0.05 percent.

In this way, the optimized grades contain a controlled nitrogen content which favors good mechanical properties; however, it is very important to note that this nitrogen content stays in the same range as the classical AISI 304 and 316 steels. In particular, the nitrogen content is specifically controlled to be lower than the maximum residual nitrogen contents that are often found in industrial grades of these steels.

It is also noteworthy that, as a security precaution, we have shown that a nitrogen content as high as 0.08 percent does not affect either the resistance to intergranular corrosion or the weldability of this type of steel.

Industrial Applications

The specification tests imposed by the French Electricity Authorities on the stainless steels used for primary circuits in PWR nuclear reactors include an intergranular corrosion test according to the Autaas 121 B standard.

This test consists of a sensitization treatment of 30 mm at 700°C (316 grade) or at 725°C (304 grade), cooling at 60°C per hour to 500°C, followed by air cooling. The test specimens are then held for 72 h in the following boiling reactive

$$\left\{ \begin{array}{l} \text{H}_2\text{SO}_4 (d = 1.83): 10 \text{ percent} \\ \text{SO}_4\text{Cu}, 5\text{H}_2\text{O}: 10 \text{ percent} \\ \text{H}_2\text{O distilled}: 80 \text{ percent} \end{array} \right.$$

The specimens are submitted to a bend test of which the acceptance criterion is that they exhibit no cracks (after a certain bend angle). We should like to insist on the selectivity of this test. Thus a 304L steel having the following composition

$$\left. \begin{array}{l} [\text{Cr}] = 18.0 \text{ percent} \\ \text{Residual molybdenum} \end{array} \right\}$$

$$\left. \begin{array}{l} [\text{C}] = 0.030 \text{ percent} \\ [\text{Ni}] = 10 \text{ percent} \end{array} \right\}$$

and the following $[\text{Cr}^*]$ and $[\text{C}^*]$

$$\left. \begin{array}{l} [\text{Cr}^*] = 18.25 \text{ percent} \\ [\text{C}^*] = 0.03 \text{ percent} \end{array} \right\} [\text{Cr}^*] - 100 [\text{C}^*] \# 15.25 \text{ percent}$$

does not satisfy the Autaas 121 B test.

The modern melting techniques used for the fabrication of the ICL 473 BC grade allow us to regularly obtain, within the composition ranges just indicated, a composition balance such that

$$[\text{Cr}^*] - 100 [\text{C}^*] > 16.2 \text{ percent}$$

Under these conditions, all the ICL 473 BC steel melts pass the Autaas 121 B test. Small cracks may appear if the foregoing condition is not respected (Fig. 3).

These results show the validity of the method of predicting the intergranular corrosion resistance. This current method is also supported by results of the Autaas 121 B test on each industrial ICL 167 CN heat [5]. Thus strict control of the melting technique allows one to choose, within the composition specification area of a particular grade, the region within which one can be sure of the corrosion resistance as measured by the Autaas 121 B test. It is possible, in this way, to produce steels whose average resistance to intergranular corrosion is better than that of the AISI 304L grade. However, this study is based essentially upon the use of the Autaas 121 B test. It is possible that various steel grades would behave differently using other intergranular corrosion tests.

Mechanical Properties of the Optimized Grades—Comparison with the ASME Code Data

Tensile Properties

The 0.2 percent proof stresses (Re) of the ICL 473 BC and ICL 167 CN steels as a function of temperature are plotted in Figs. 4 and 5. We have also presented in these figures curves corresponding to the minimum expected value of Re given by the ASME Code. One observes that the minimum curve (average values less twice the standard deviation) is above

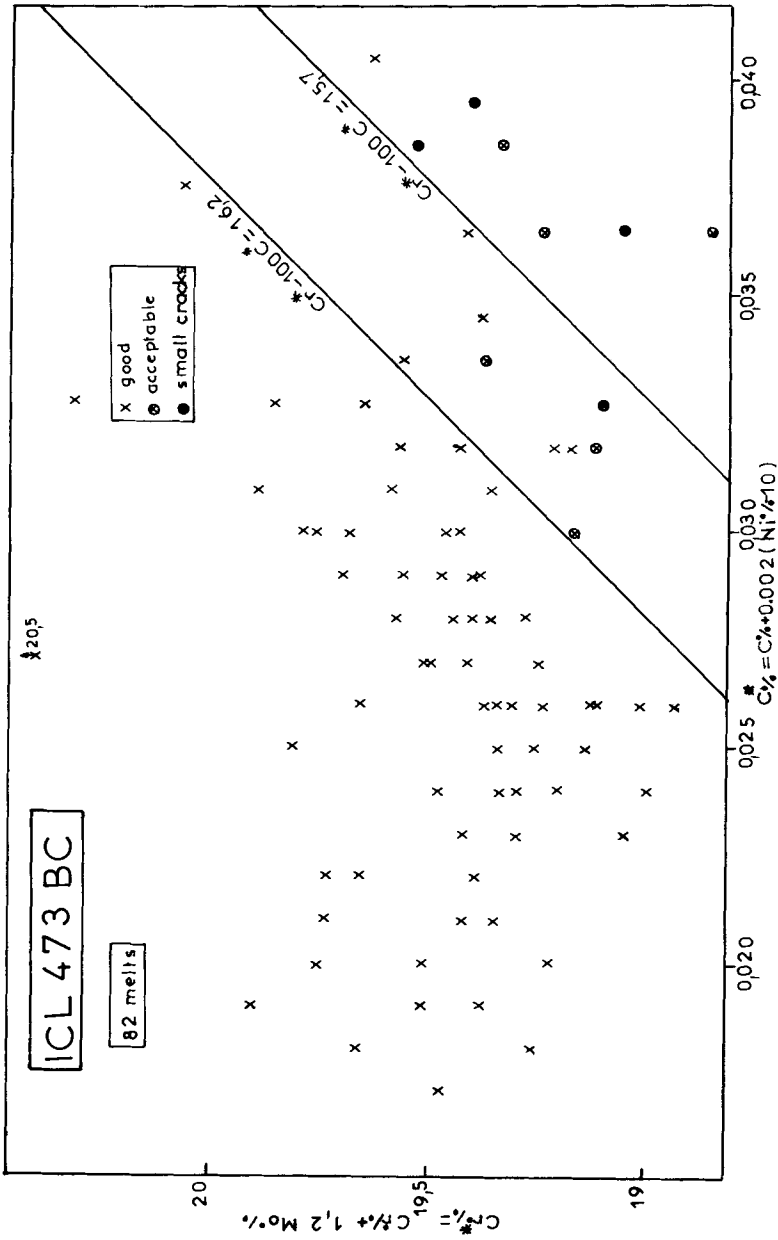


FIG. 3—Intergranular corrosion testing results for industrial melts.

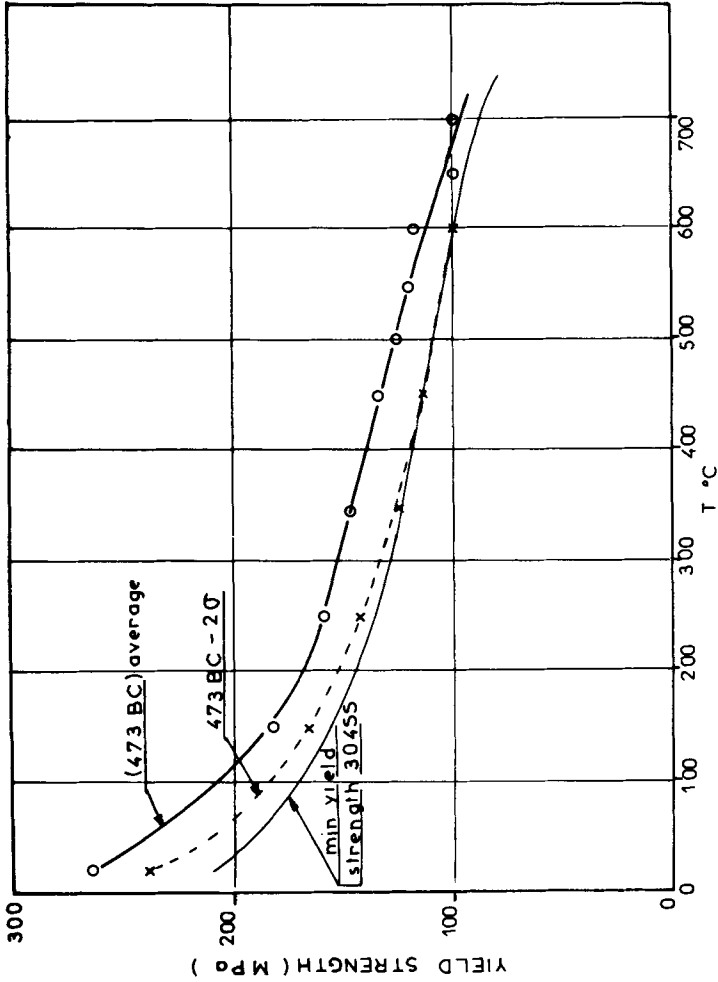


FIG. 4—Variation of the yield strength of the ICL 473 BC as a function of temperature.

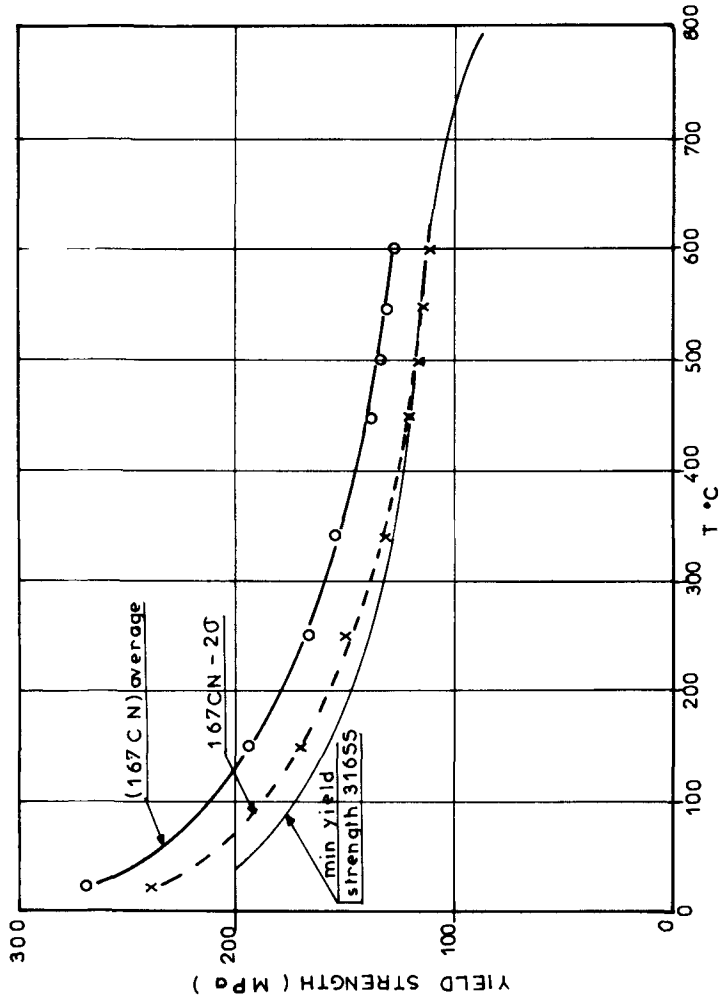


FIG. 5—Variation of the yield strength of the ICL 167 CN as a function of temperature.

the minimum values given by the ASME Code. The results presented are based on several hundreds of tests for 20°C and 343°C, and on about 10 tests (concerning ten different heats) for other temperatures.

Creep Properties

The results of the creep rupture tests carried out on the ICL 473 BC and ICL 167 CN steels are compared with the minimum values of the stress to rupture of Types 304 and 316 steels according to the ASME Code (Figs. 6 and 7). The average stress levels giving for the ICL 473 BC and ICL 167 CN steels a particular time to rupture are roughly 20 percent higher than the corresponding minimum rupture stresses of the 304 and 316 steels.

In Figs. 6 and 7, each point represents one test.

Fatigue Properties

As an example of the fatigue resistance of these steels, Fig. 8 shows the average fatigue curve obtained on five different melts of the ICL 167 CN steel. The results show that this grade exhibits fatigue properties similar to those obtained on the AISI 316 steels. We would also add that good agreement has thus been verified by high-temperature low-cycle fatigue tests and by fatigue-crack propagation measurements at various temperatures [6]. In addition, the good behavior of the ICL 167 CN steel has also been shown by tests in a PWR environment (320°C, 150 bars) [6].

Conclusion

As far as the pressurized light-water nuclear system is concerned, we have shown that an original solution was suggested to make allowance for all the risks of damage. This solution is not a compromise; the materials used are not intermediate ones between Types 304L and 304 or between 316L and 316. By paying particular attention to the composition balance of the different grades and in particular by controlling the carbon and nitrogen contents, we can propose an optimum solution. The materials used actually have the same mechanical strength as Types 304 or 316 steels and successfully pass Autaas intergranular corrosion test 121 B as do low-carbon steels 304L and 316L.

As far as the boiling-water reactor system is concerned, this solution is proposed to the constructors of this type of reactor. Although still under study, this solution should make it possible to improve the intergranular corrosion stress resistance without having to call upon a completely new material and, consequently, without having to question any design codes.

Finally, present melting techniques allow one to produce Grade L stainless steels with the mechanical properties of the AISI 304 or 316 steels in addition to their good intergranular corrosion resistance.

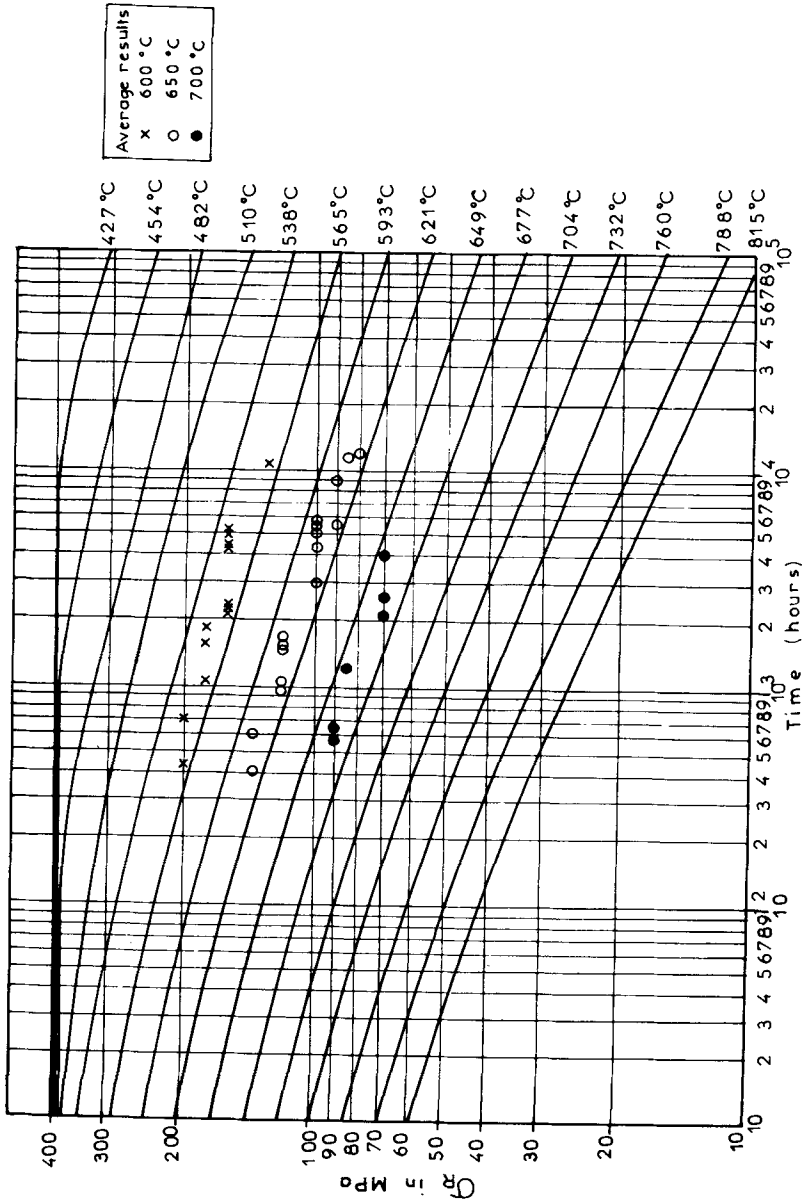


FIG. 6—Stress-rupture test results of the ICL 473 BC steel (a comparison with Code Case 1592 results).

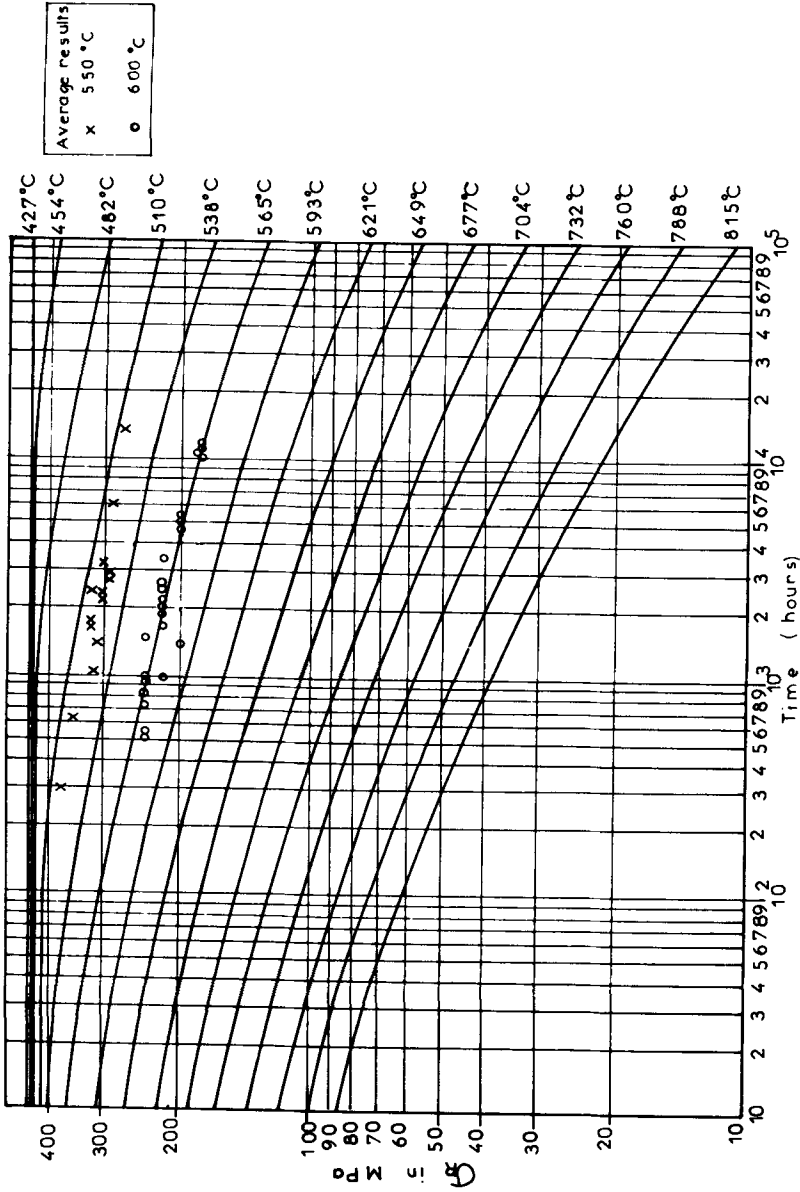


FIG. 7—Stress-rupture test results of the ICL 167 CN steel (a comparison with Code Case 1592 results).

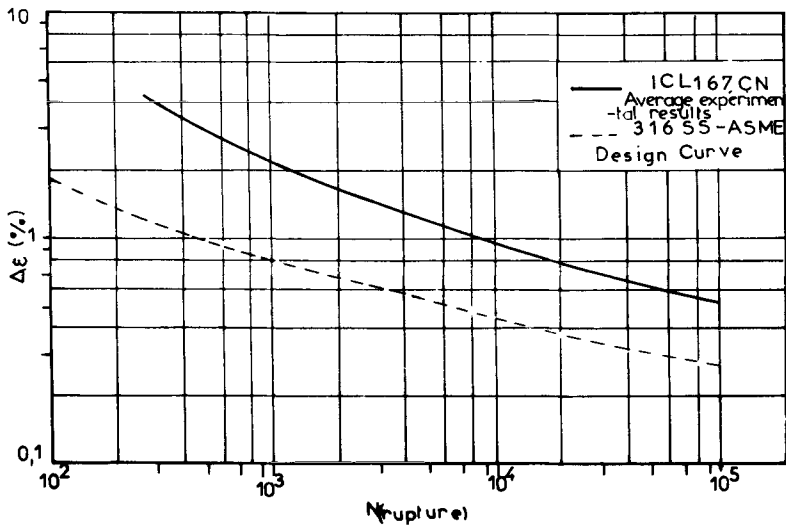


FIG. 8—Low-cycle fatigue life test results at room temperature.

References

- [1] Cihal, V., "La corrosion intergranulaire des aciers inoxydables," Rapport Creusot-Loire DRU N° 953, Nov. 1969.
- [2] Vieillard-Baron, B. and Bonnard, Y., *Revue Française de l'Energie*, 25ème année, 1973, pp. 211-227.
- [3] Gobin, F., *Corrosion et Anticorrosion*, Vol. 9, No. 4, 1961, p. 119.
- [4] Cihal, V., *Corrosion-Traitements-Protection-Finition*, Vol. 18, No. 7, 1970, p. 441.
- [5] F. Leroy, Freycenon, J., and Heritier, J., "Tenue à la corrosion intergranulaire de l'acier inoxydable I.C.L. 167 CN," Creusot-Loire, Report 1285, July 1977.
- [6] Rabbe, P., Amzallag, C., and Raoul, J. P., *17è Colloque de métallurgie de Saclay*, June 1974.

DISCUSSION

*Raymond Cockroft*¹ (written discussion)—What delta-ferrite contents might be expected from the chemistry range quoted for ICL 167 CN, and what strengthening effects are anticipated from the presence of any delta-ferrite?

P. Rabbe and J. Heritier (authors' closure)—Delta-ferrite contents are ≤ 1 percent. Such a ferrite content is an optimum regarding both mechanical, corrosion, and embrittlement properties.

¹Cameron Iron Works, Houston, Tex.

Summary

The papers presented in this symposium dealt primarily with the influence of carbon, nitrogen, and residual element content on the elevated-temperature mechanical properties of Types 304 and 316 stainless steel and associated weld metals. Four of the seven papers were devoted to base material behavior and the remaining three papers to weldability and mechanical properties of as-deposited weld metal.

The Sikka et al paper dealt with the influence of niobium content in the range of 20 to 1000 ppm (weight) on the elevated-temperature mechanical properties of Type 304 stainless steel. These investigators, while studying heat-to-heat variations in creep properties of 20 commercial heats of this material, noticed a strong correlation between creep behavior and residual niobium content over the range from 10 to 200 ppm. Accordingly, a number of small laboratory heats were prepared with varying niobium contents. Small additions of niobium were shown to increase rupture life while decreasing the minimum or secondary creep rate. These changes were also reflected in the results of short-term elevated-temperature ultimate tensile strength measurements. Approximately 500 ppm (weight) of niobium resulted in optimum ductility, creep-rupture strength, and corrosion resistance.

In a sequel to the Sikka et al paper, Moorhead et al used the Spot Varestraint weldability test to compare the propensity for hot-cracking of several laboratory heats (up to 1000 ppm of niobium) of Type 304 stainless steel with commercial heats of Types 304 and 347 stainless steel. They found that the fusion and heat-affected zone cracking resistance of the experimental heats was similar to that of commercial Type 304 and much superior to that of the commercial heat of Type 347 stainless steel.

These two papers clearly demonstrated that small amounts of niobium (about 500 ppm, weight) are beneficial in improving the mechanical properties of Type 304 stainless steel. However, the work done to date was accomplished with small heats. Accordingly, continued development was recommended, using a larger heat so as to permit greater emphasis on fabricability. Thermal aging followed by microstructural and mechanical property studies was also recommended.

Rabbe and Heritier attempted to optimize the compositions of Types 304 and 316 stainless steel within AISI specifications for these materials. This was done to maximize resistance to intergranular stress-corrosion cracking and to maintain optimum mechanical properties and fabricability. The

authors were seeking the best composition specifications for use in PWR's in France. Their objective was achieved by controlling the carbon and nitrogen contents.

Eckenrod and Kovach reported on the beneficial effects of nitrogen additions of up to about 0.16 percent on the properties of the 18Cr-8Ni stainless steels. Such additions retarded intergranular carbide precipitation. Intergranular cracking, pitting, and crevice corrosion resistance were all improved without an adverse effect on weldability.

James investigated the heat-to-heat variability in cyclic crack growth resistance of five heats of Type 304 and three heats of Type 316 stainless steel. The heats of Type 306 stainless had been prepared by three different melting practices. He found no effect of heat-to-heat variability on the continuous cycle or hold-time crack growth behavior of these steels when tested at 538°C.

Edmonds et al studied the influence of various residual elements on the elevated-temperature mechanical properties of Types 308, 316, and 16-8-2 stainless steel weld metals. They found that the optimum residual element contents were nominally 0.05Ti-0.04P-0.006B for shielded metal-arc welds and 0.5Ti-0.04P-0.006B for gas tungsten-arc welds. Submerged-arc welds with 0.2 percent titanium exhibited improved creep strengths.

Thomas noted that the elevated-temperature tensile properties of AISI Type 316 stainless steel weld metal deposited by manual metal-arc welding depend upon the basicity of the electrode coating. Variations in phosphorus level had little effect on subsequent mechanical properties, while boron concentrations of about 60 ppm increased deposit strength without reducing ductility.

C. R. Brinkman

Oak Ridge National Laboratory, Oak Ridge,
Tenn. 37830; symposium chairman and
coeditor.

Index

A

Autaas 121B standard intergranular corrosion test, 133

B

Boron content, 43, 54, 57, 65

C

Carbon content, 21, 57, 78
 Chloride environments, 30
 Coefficient of determination, 11
 Continuous cycling fatigue, 11
 Corrosion fatigue, 126
 Corrosion resistance, 127
 Crack growth (*see* Linear elastic fracture mechanics)

D

Delta-ferrite, 30, 114, 141

F

Fabrication damage, 126
 Fusion-zone cracking, 111

G

Gas tungsten arc weld nuggets, 112
 Grain size, 6, 16, 18, 74, 78, 104, 115

H

Heat-affected zone cracking, 114
 Heat-to-heat variations in mechanical properties
 Crack propagation, 4
 Creep rupture and minimum creep rates, 75
 Hold time, 11
 Hot cracking, 38, 42, 56, 91, 108, 114
 Huey test, 24

I

Intergranular corrosion resistance, 130
 Intergranular corrosion test, 133

L

Light water nuclear reactors, 125
 Linear elastic fracture mechanics, 3

M

Mechanical properties
 ASME codes, 136-139
 Creep, 88
 Fatigue, 3, 138
 Tensile, 88
 Microfissuring, 57
 Murakami's reagent, 114

N

- Niobium content, 11, 16, 70, 79
 - Weldability, 103
- Nitrogen content, 16, 78, 125, 133
 - Mechanical properties, 36
 - Weldability, 37, 41

O

- Olsen cup ductility, 37

P

- Phosphorus content, 43, 55, 57, 65

R

- Rutile coated electrodes, 43

S

- Sensitization, 20, 126
- Sigma phase, 44, 54, 68
- Silicon content, 53
- Specimens
 - Compact tension, 4
- Spot vareststraint test (*see* Tigamajig test)
- Strauss test, 91
- Streicher test, 26
- Stress corrosion, 30
- Sulfur content, 43, 57

T

- Thermal aging, 14
- Tigamajig test (Spot vareststraint test), 93, 108, 114
- Time temperature sensitization diagrams, 22
- Titanium content, 43, 57, 59, 65
- Transmission electron microscopy, 93

U

- U-bend specimens, 92

W

- Welding
 - Gas-tungsten arc process, 25
 - Heat-affect zone (HAZ) sensitization, 25
 - Manual metal-arc welding process, 42
- Weldability, 37, 133
- Weld metal
 - Mechanical properties, 47, 53, 54, 57
 - Oxide metal ratios, 51
 - GTA type 16-8-2, 57, 65
 - GTA type 308, 59, 65
 - GTA type 316, 59, 65
 - SA type 308, 65
 - SA type 316, 65
 - SA type 16-8-2, 65
 - SMA type 308, 57, 65
 - SMA type 316, 57

